UNCLASSIFIED

AD 400 326

Reproduced
by the

ARMED SERVICES TECHNICAL INFORMATION AGENCY
ARLINGTON HALL STATION
ARLINGTON 12, VIRGINIA

UNCLASSIFIED

NOTICE: When government or other drawings, specifications or other data are used for any purpose other than in connection with a definitely related government procurement operation, the U. S. Government thereby incurs no responsibility, nor any obligation whatsoever; and the fact that the Government may have formulated, furnished, or in any way supplied the said drawings, specifications, or other data is not to be regarded by implication or otherwise as in any manner licensing the holder or any other person or corporation, or conveying any rights or permission to manufacture, use or sell any patented invention that may in any way be related thereto.

63-3-1

TECHNICAL INFORMATION SERIES

AD No. 400326
FILE COPY
400 326

R62SD84

EXPERIMENTAL PLANETARY ENTRY RESEARCH FOR MARS AND VENUS — 1962

T.K.PUGMIRE

STIA
APR 9 1963
TISIA

SPACE SCIENCES LABORATORY
GENERAL ELECTRIC
MISSILE AND SPACE VEHICLE DEPARTMENT

$ 9.10

SPACE SCIENCES LABORATORY

ELECTRON PHYSICS SECTION

EXPERIMENTAL PLANETARY ENTRY RESEARCH FOR MARS AND VENUS - 1962*

Project Leader

T. K. Pugmire

*This Study was supported in part by the Jet Propulsion Laboratory, California Institute of Technology, under subcontract 950250 sponsored by the National Aeronautics and Space Administration via contract NAS 7-100, in part by the Air Force Office of Scientific Research under contract AF 49(638)-931, and in part by the General Electric Company under its Contractor's Independent Research and Development Program.

R62SD84 - Class I
October, 1962

MISSILE AND SPACE DIVISION

GENERAL ELECTRIC

Mr. T. K. Pugmire was the Project Engineer for this research. Principal Contributors to the project were: B. B. Cary, N. S. Diaconis, D. G. Flom, J. S. Gruszczynski, R. S. Harner, C. J. Harris, W. C. King, M. J. Linevsky, D. A. Rogers, H. Sadjian, R. A. Sheridan, S. Visvanathan, H. Y. Wachman and W. R. Warren.

TABLE OF CONTENTS

TABLE OF CONTENTS

LIST OF FIGURES

LIST OF FIGURES

LIST OF FIGURES

LIST OF FIGURES

LIST OF FIGURES

I. INTRODUCTION

The program for planetary entry research for Mars and Venus was jointly coordinated between theoretical and experimental studies. The material reported is a final report of the 1962 experimental studies. Some portions of this work were partially supported by other contracts from AFOSR and JPL.

The Martian and Venusian model atmospheres utilized followed those given in a preliminary engineering estimate provided by JPL. As the characteristics of these atmospheres are not known precisely, probable bounds were established. These bounds for the Martian and Venusian atmospheres are tabulated as well as the planetary dynamic data for the two planets. As the Venusian Atmosphere data was given in terms of temperature and pressure, the density was calculated and is plotted as a function of altitude.

TABLE 1-1. MARS ATMOSPHERE*
INDEPENDENTLY DETERMINED PARAMETERS

Symbols	Parameter	Unit	Low	Nominal	High
g_o	Acceleration of Surface Gravity	ft/sec^2	12	12	13
		cm/sec^2	360	375	390
M_m	Surface Mass Pressure	$slug/ft^2$	9.5	16	22
		gm/cm^2	150	250	350
T	Stratosphere Temperature	°R	230	320	410
		°K	130	180	230
T_o	Surface Temperature	°R	380	410	470
		°K	210	230	260
C_p	Specific Heat at Constant Pressure	BTU/slug °R	7.4	7.7	8.1
		cal/gm °K	.23	.24	.25

*Tentative

TABLE 1-2. MARS ATMOSPHERE
PARAMETERS DEPENDENT* ON SELECTED COMPOSITION OF ATMOSPHERE

Symbol	Parameter	Unit	Low ⟵ (g) ⟶ High High ⟵ (M_m) ⟶ Low
C_{c_v}	Concentration of Constituents by Volume	%	
	CO_2		0.7 — 1.9 — 7.2
	A		0.6 — 6.0
	O_2**		0 — --
	N_2		98.7 — 86.8
C_{c_m}	Concentration of Constituents by Mass	%	
	CO_2		1.1 — 3 — 11
	A		0.8 — 8.7

TABLE 1-2. MARS ATMOSPHERE (Cont'd)
PARAMETERS DEPENDENT* ON SELECTED COMPOSITION OF ATMOSPHERE

Symbol	Parameter	Unit	Low ⟵ (g) ⟶ High High ⟵ (M_m) ⟶ Low		
	O_2		0		(2.7)
	N_2		98.1		80.3
M	Average Molecular Weight by Volume		28.2	28.4	29.9
γ	Ratio of Specific Heats		1.42	1.41	1.41
			High ⟵ (g, M_m) ⟶ Low		
P	Surface Pressure	lb/ft^2	284	196	113
		mb.	136	94	54

*Data are consistent within columns
**Conjectural Oxygen not considered in Average Molecular Weight

TABLE 1-3. MARS ATMOSPHERE
DERIVED* PARAMETERS

Symbol	Parameter	Unit	Low ⟵ g, Po, M, M_m ⟶ High High ⟵ T ⟶ Low		
ρ_o	Surface Density	$\frac{slug \times 10^{-4}}{ft^3}$	1.4	2.7	4.3
		$\frac{gm \times 10^{-4}}{cm^3}$	0.75	1.4	2.2
H	Scale Height	$\frac{ft \times 10^3}{Km}$	59 18	41 12.5	29 9
β	Reciprocal of H	$\frac{1 \times 10^{-5}}{FT}$	1.7	2.4	3.4
		$\frac{1 \times 10^{-2}}{Km}$	5.6	8.0	11.0
τ	Dry Adiabatic Lapse Rate	$\frac{^oR \times 10^{-3}}{ft}$	-1.96	-2.04	-2.13
		$\frac{^oK}{Km}$	-3.43	-3.75	-4.10

TABLE 1-3. MARS ATMOSPHERE (Cont'd)
DERIVED* PARAMETERS

Symbol	Parameter	Unit	Low ← g, Po, M, M_m → High High ← T → Low		
a_o	Speed of Sound at Surface	ft/sec	1064	1013	985
		m/sec	325	309	300
s_u	Speed of Sound in Stratosphere	ft/sec	1013	903	765
		m/sec	309	275	233
$\frac{\tau}{T_o}$	Lapse Rate / Surface Temp.	$\frac{1 \times 10^{-6}}{ft}$	-4.17	-4.98	-5.61
		$\frac{1 \times 10^{-2}}{Km}$	-1.32	-1.63	-1.95

* Data are consistent within columns

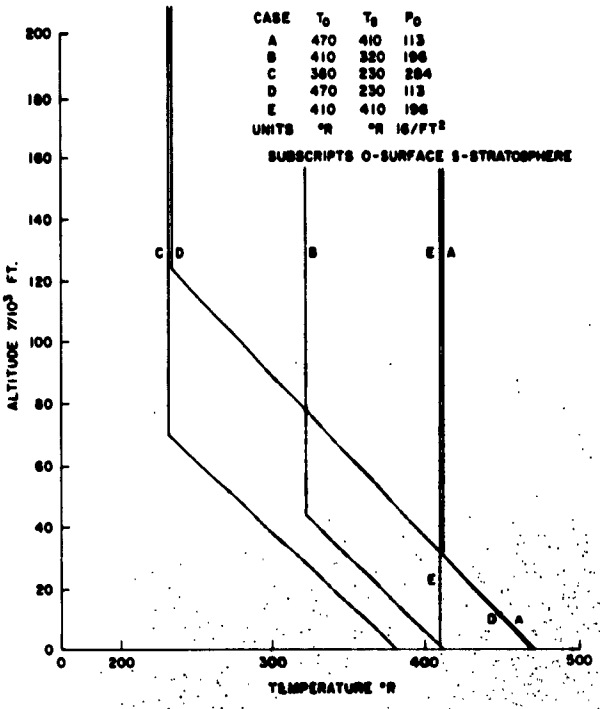

Figure 1.1 Temperature of Mars Atmosphere.

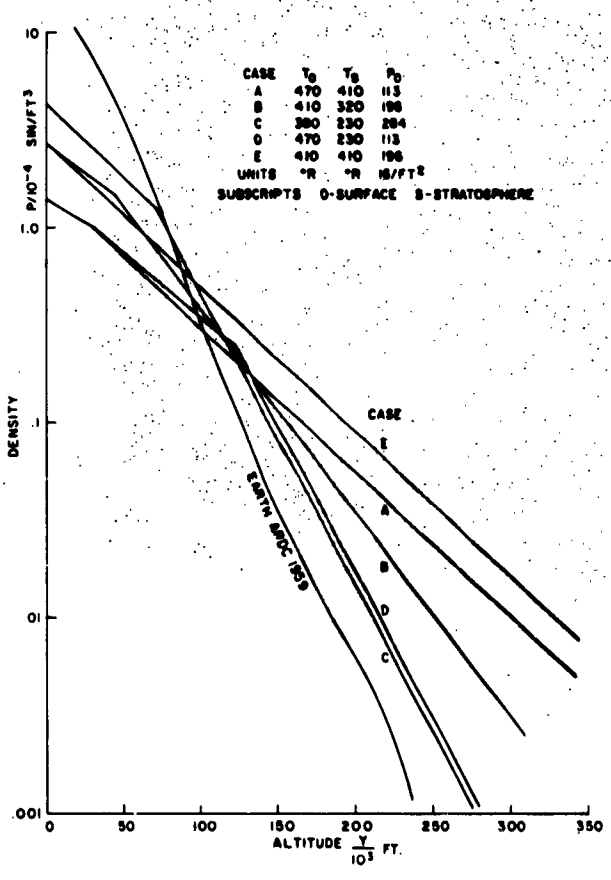

Figure 1.2 Density of Mars Atmosphere.

TABLE 1-4. COMPOSITION OF VENUSIAN ATMOSPHERE

I ("best")	II	III
90% N_2	96% N_2	74% N_2
9% CO_2	3% CO_2	25% CO_2
1% A	1% A	1% A
$\bar{m} = 29.6$	$\bar{m} = 28.6$	$\bar{m} = 32.1$
$\bar{\delta} = 1.39$	$\bar{\delta} = 1.40$	$\bar{\delta} = 1.38$
$\frac{\bar{\delta}}{\bar{\delta}-1} = 3.56$	$\frac{\bar{\delta}}{\bar{\delta}-1} = 3.50$	$\frac{\bar{\delta}}{\bar{\delta}-1} = 3.63$
$\Gamma = -8.5^{\circ}K/km$	$\Gamma = -8.4^{\circ}K/km$	$\Gamma = -8.9^{\circ}K/km$

$\bar{m}$ = mean molecular mass

$\bar{\delta}$ = mean ratio of specific heats*

Γ = dry adiabatic lapse rate*

*These quantities are given for STP. At the temperatures and pressures which appear to be present near the surface of Venus they are badly in error.

TABLE 1-5. VENUSIAN ATMOSPHERE BEST MODEL

Altitude KM	Pressure ATM	Density Earth lbs./ft.^{3}	Temp. ^oK	Molecular Wt.	Sp. Ht. Ratio	Speed of Sound ft/sec.
0	16.6	.6244	600	29.6	1.363	1565
18.8	5.5	.2816	440	29.6	1.39	1367
42.9	0.59	.0565	235	29.6	1.40	1003
110.0	2.76×10^{-6}	3.1111×10^{-7}	200	29.6	1.40	925
122.0	5.72×10^{-7}	0.5605×10^{-7}	230	29.6	1.40	993
133.0	1.68×10^{-7}	1.4555×10^{-8}	260	29.6	1.40	1054
144.0	5.92×10^{-8}	4.3555×10^{-9}	300	29.0	1.405	1149
178.0	4.94×10^{-9}	2.4277×10^{-10}	450	29.0	1.393	1400
235.0	4.94×10^{-10}	1.4555×10^{-11}	700	27.1	1.38	1797
292.0	8.88×10^{-11}	1.6277×10^{-12}	800	19.3	1.506	2379
349.0	3.95×10^{-11}	0.5816×10^{-12}	900	17.4	1.555	2700

TABLE 1-6. VENUSIAN ATMOSPHERE EXTREME MODEL I

Altitude KM	Pressure ATM	Density Earth lbs./ft^3	Temp. ^{o}K	Molecular Wt.	Sp. Ht. Ratio	Speed of Sound ft/sec
0	54	1.6277	750	29.6	1.347	1732
36.5	8	0.41	440	29.6	1.389	1367
60.5	.86	8.27×10^{-2}	235	29.6	1.4	1003
110.0	5.92×10^{-6}	5.1277×10^{-7}	260	29.6	1.4	1058
122.0	1.58×10^{-6}	1.1444×10^{-7}	310	29.6	1.4	1144
133.0	6.02×10^{-7}	3.6666×10^{-8}	370	29.6	1.396	1256
144.0	2.37×10^{-7}	1.1611×10^{-8}	450	29.0	1.392	1394
178.0	4.25×10^{-8}	1.25×10^{-9}	750	29.0	1.352	1777
235.0	8.29×10^{-9}	1.3722×10^{-10}	1250	27.1	1.340	2368
292.0	3.16×10^{-9}	3.1944×10^{-11}	1450	19.3	1.476	3162
349.0	1.58×10^{-9}	1.2611×10^{-11}	1650	17.4	1.532	3691

TABLE 1-7. VENUSIAN ATMOSPHERE EXTREME MODEL II

Altitude KM	Pressure ATM	Density Earth lbs./ft.^{3}	Temp. ^oK	Molecular Wt.	Sp. Ht. Ratio	Speed of Sound ft/sec.
0	6.3	.285	500	29.6	1.381	1447
7.1	4.0	.206	440	29.6	1.39	1367
31.2	0.42	.0404	235	29.6	1.40	1003
41.2	8.38×10^{-2}	1.264×10^{-2}	150	29.6	1.40	796
60.0	1.805×10^{-3}	2.72×10^{-4}	150	29.6	1.40	796
80.0	3.06×10^{-5}	4.61×10^{-6}	150	29.6	1.40	796
100.0	5.13×10^{-7}	7.72×10^{-8}	150	29.6	1.40	796
150.0	1.875×10^{-11}	2.82×10^{-11}	150	29.6	1.40	796
200.0	7.1×10^{-16}	1.07×10^{-16}	150	29.6	1.40	796
250.0	2.66×10^{-20}	4.01×10^{-21}	150	29.6	1.40	796
300.0	9.65×10^{-25}	1.457×10^{-25}	150	29.6	1.40	796

TABLE 1-8. PLANETARY DYNAMIC DATA -- VENUS AND MARS

	Venus	Mars
Radius	0.97 ± 0.01 R_E 6200 ± 100 Km	0.52 R_E 3400 ± 50 Km
Mass	0.82 ± 0.01 Mg 4.90×10^{24} Kg	0.107 Mg 6.40×10^{23} Kg
Density	5.0 ± 0.3 gm/cc	4.0 ± 1 gm/cc
Oblateness	1%	1/192
Surface Gravity	0.88 ± 0.03 g 860 ± 30 cm/sec^2	390 ± 10 cm/sec^2 0.39 g
Orbit Details		
Mean distance to Sun	108.1×10^6 Km	227.8×10^6 Km
Maximum distance to Sun	109.4×10^6 Km	248×10^6 Km
Minimum distance to Sun	106.5×10^6 Km	206×10^6 Km
Eccentricity of Orbit	0.007	0.093
Inclination of orbit to plane of ecliptic	3° 24'	1° 51'
Minimum distance to Earth	42×10^6 Km	1° 51'
Maximum distance to Earth	257×10^6 Km	
Sidereal period	225 days	687 days
Synodic period	584 days	780 days
Mean orbit velocity	35.0 Km/sec	24.2 Km/sec
Semi-major axis	108.21×10^6 Km	227.9×10^6 Km
period of rotation	undetermined	24 hrs 37 min
escape velocity	10.4 Km/sec	5.0 Km/sec
inclination of Equator to orbital plane	undetermined	25° 12'
Satellites	none detected	2

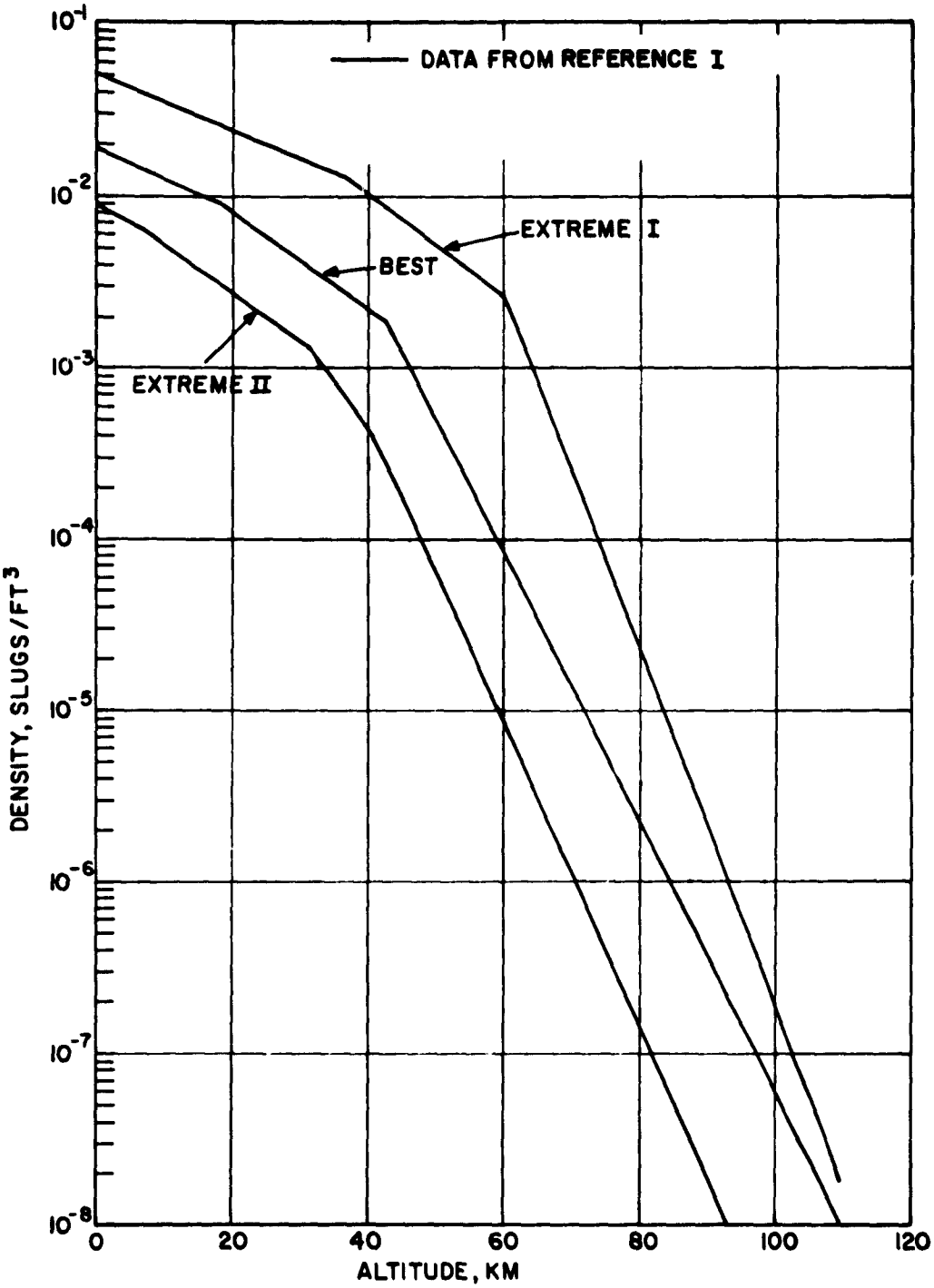

Figure 1.3 Venusian Model Atmospheres.

II. PROGRAM OBJECTIVES

The objective of this comprehensive program of research was to solve the problem of ballistic entry into the atmosphere of Mars and to establish the techniques for its solution for Venusian entry. This requires the theoretical and experimental determination of the heat transfer, the aerodynamic forces, and the behavior of typical thermal protection systems during the ballistic entry of a space probe into the atmosphere of Mars.

The investigators in the Electron Physics Section performed studies in order to:

1. Prepare shock wave data and Mollier tables for Mars and Venus.

2. Experimentally determine dissociation rates typical for the atmosphere of Mars.

3. Construct and investigate the feasibility of using an arc-heated helium driven shock tube-tunnel for the determination of heat transfer and aerodynamic data by evaluating and calibrating a prototype facility, and developing an adequately sized test facility utilizing the prototype results.

4. Determine analytically the shock facility's expected performance with N_2 and CO_2.

5. Develop new transducers and instrumentation concepts for acquiring model data in the high enthalpy shock facility (particularly for obtaining heat transfer).

6. Determine experimentally the aerodynamic heat transfer to the stagnation point of a blunt body during ballistic entry into the atmosphere

of Mars and investigate the heat transfer for similar entry into Venus.

7. Establish the behavior of various ablation shield materials in environments typical of hypervelocity entry into atmosphere of Mars.

8. Determine Venusian ionosphere attenuation effects.

III. STUDY RESULTS

III-1 EQUILIBRIUM THERMOCHEMISTRY*

For both the theoretical and experimental studies of planetary entry it was necessary first to establish the conditions behind the shock wave. This required the determination of the equilibrium gas composition. Two approaches were taken to the problem: first, an older method made use of equilibrium constants to express abundance of certain chosen species in terms of the abundance of other aribtrarily chosen (or more abundant) species. This method, referred to as the Brinkly method (Ref. 3), depends entirely on the solution of chemical equilibrium equations. As a consequence, the program for the Brinkly method must be readjusted for each different set of elemental substances in a mixture, i.e., a (Brinkly) program written for an N, O system is not applicable to an H, O system. However, as the program for such computations was nearly complete and checked out for a number of species and mixtures, it was utilized to obtain early results. This work supported by JPL contract was completed (Refs. 4 and 5) and was used throughout other portions of this and other studies. A second approach to this problem was undertaken as a part of this study. This approach, referred to as the Rand method, makes no distinction among constituent species. It is based on the fact that any n component chemical system is in thermodynamic equilibrium when the free energy of that system (i.e., the Gibbs function) is at a minimum. With this procedure where the free energy equation is linearized, the input required consists of values of

*Principal Investigators: M. J. Linevsky and H. Y. Wachman

the standard molar free energy of each constituent and the quantities of each elemental substance in the mixture. With this approach, four-decimal place accuracy in constituent mole fractions can be obtained. Mole fractions of trace constituents can be calculated by using a simple subroutine which improves the computed mole fractions by substituting them in a set of linearized chemical equilibrium equations. In this case, the chemical equilibrium equations are only used to improve the mole fractions and obtain values for minor constituents. If the elemental substances of the mixture change, the procedure requires only a change in the data input and in the afore mentioned trace element subroutine. The latter change is not required if only major constituents and thermodynamic properties are desired. Simple algebraic forms suffice for expressing the free energy of constituent or mixture, and a variety of computational methods are available.

In addition to the linear programming method, the free energy equation can be minimized using a desk computer by a method of steepest descent. This has already been worked out in a way consistent with the linear programming approach.

In general the Rand method can be readily adapted to constant volume and constant pressure problems; the former which is usually quite complex leads to an even simpler formulation in this case than the latter.

Extention of the method to multiphase systems and to ionic systems was straightforward.

Trace elements can be eliminated or included in computations at will

and this does not hamper the accuracy of the final result. Even if a trace element has been omitted in the original formulation, it can be included by simple calculation.

The method was also modified so that the mole fraction of any constituent can be fixed in advance, and the equilibrium composition and thermodynamic properties of a multicomponent system containing a fixed mole fraction of any constituent are calculable. For example, the method can be used to compute the properties of a chemical system in which a certain ionization level is to be achieved by seeding with a low ionization potential material. The desired ionization level is introduced as an input, and the program is used to calculate the equilibrium composition and the quantity of material required to achieve equilibrium In general, convergence is quite rapid regardless of starting point and thus requires little machine time. The computer program has been completed for a multicomponent chemical system including ionized species and has been augmented to take advantage of the maximum capacity of the IBM 7090 computer. The subroutine for trace constituents was written based on a list of components representative of planetary atmospheres. Subsequent to a check out, this program will be available for fast inexpensive calculations of chemical equilibrium compositions and thermodynamic properties for any perturbation of the still very uncertain planetary atmospheres or test gases used to represent the planetary atmosphere in the ground simulation test facilities.

III-2 DISSOCIATION RATE STUDIES*

Studies of non-equilibrium processes in various gases, especially nitrogen, have been carried out over the past two years in a combustion driven stainless steel 2" x 2" shock tube in which good purity control is maintained (impurities $<$ 20 ppm). Figure 2.1 shows the tube and associated equipment. A Mach-Zehnder interferometer capable of 0.1 micro second time resolution was used to follow the changing density in the dissociation zone. Knowledge of the shock strength together with the hydrodynamic constraint equations plus an assumed kinetic mechanism led to inferred values for the dissociation rate constant. An f-3 time-resolved spectrograph was used to simultaneously examine and record the white and monochromatic fringes of the emitted light from the reaction zone. Successful control of the combustion technique allowed observation of high degrees of dissociation (up to 70%) in relatively rich mixtures at relatively high initial pressures.

The past work accomplished with this facility has been documented in reports to the sponsoring agencies: Ballistic Systems Division and Office of Scientific Research of the U.S.A.F. Measurements of the types which have been conducted are required to assess the importance of non-equilibrium processes in planetary atmospheres.

In the nitrogen study (Ref. 6) two points were stressed. The first point emphasized was an acceptable degree of purity. By actual mass spectrometric analysis of gas samples taken from the tube it was found that

*Principal Investigator: B. B. Cary

impurity levels were less than 20 ppm. The second emphasis was placed on demonstrating that steady, uniform flow fields could be generated by combustion driven shocks, providing great care was taken to match the peak burning pressure of the combustible load to the burst pressure of the diaphragm. Figure 2.2 shows a white light interferogram taken of a Mach 10.3 shock propagating into a 13% N_2 - 87% Ne mixture. The shock arrives at the left at the upstream interferometer beam causing an upward jump of the fringes followed by a further rise in the dissociation zone. The fringes then show only a small decay until the time when the shock arrives at the downstream beam. Here the fringes revert to their original position and show a good bit of mirror symmetry in the dissociation zone. This symmetry attests to the control of the combustion technique. It should be pointed out that a monochromatic interferogram can be simultaneously recorded with the white light picture. Figure 2.3 shows a time-resolved spectrogram of the luminosity emitted behind a M 12 shock in a mixture of 1% H_2 - 99% Ar. The stark broadening of the Hβ line is the most prominent line in the center. It is considerably broadened owing to the high ion densities attained (10^{17} per cc). All other visible lines have been identified as argon lines.

Ten theoretical density profiles have been generated by a program written for the IBM 1620. This program allows the computation of the density profiles behind normal shocks resulting from the bimolecular dissociation of a diatomic gas in a rare gas mixture. The experimentally

determined profiles were fitted to the theoretical profiles in order to find the collision efficiencies of N_2 and N in promoting N_2 dissociation. Additional iteration was undertaken to obtain final values. Experimentally, a perturbation on the N_2 and N system will be made later by operating with nitrogen and small amounts of CO_2. These results will be compared to the nitrogen data to determine the influence of the presence of the small quantities of CO_2 as in the atmosphere of Mars.

The final expression for the rates of nitrogen dissociation as determined in the recent study are:

$$N_2\text{-}N_2\text{: } k_{d_1} = (6.8 \times 10^{22}) \times T^{-1.7} \times \exp\left(\frac{-113,260}{T}\right) \pm 25\% \ \frac{cc}{mol\text{-}sec.}$$

$$(N_2\text{-}N)\text{: } k_{d_2} = (5.5 \times 10^{19}) \times T^{-1.0} \times \exp\left(\frac{-113,260}{T}\right) \pm 40\% \ \frac{cc}{mol\text{-}sec.}$$

$$(N_2\text{-}Ne)\text{: } k_{d_3} = (1.5 \times 10^{19}) \times T^{-1.0} \times \exp\left(\frac{-113,260}{T}\right) \pm 40\% \ \frac{cc}{mol\text{-}sec.}$$

$$(N_2\text{-}A)\text{: } k_{d_4} = (2.1 \times 10^{19}) \times T^{-1.0} \times \exp\left(\frac{-113,260}{T}\right) \pm 40\% \ \frac{cc}{mol\text{-}sec.}$$

At 6,400°K the nitrogen atom is about as efficient as the nitrogen molecule in promoting dissociation. The vibrational and dissociative zones were uncoupled over the temperature and density ranges covered. Photographing the luminosity behind M 14 shocks in pure nitrogen with an f-3 spectrograph failed to reveal the 1^- band system of N_2^+.

Table 3.1 gives a comparison of the inferred recombination rates of this study with previous results by other investigators.

Table 3-1

INFRARED RECOMBINATION RATES $\frac{k_r \text{ cm}^6}{\text{mole}^2 - \text{sec}}$

Source	Third Body	300°K	6,000°K
This paper	N_2	$1.6\ 10^{17}$	$4.2\ 10^{14}$
	N	$2.0\ 10^{16}$	$4.7\ 10^{14}$
	Ne	$5.4\ 10^{15}$	$1.3\ 10^{14}$
	A	$8.0\ 10^{15}$	$1.9\ 10^{14}$
Byron[7]	N_2	$8.6\ 10^{16}$	$4.4\ 10^{14}$
	N	$1.9\ 10^{16}$	$2.0\ 10^{15}$
	A	$1.5\ 10^{15}$	$1.6\ 10^{14}$
Eckerman[8]	Xe	$5.1\ 10^{17}$	$2.7\ 10^{15}$
Camm[9]	N_2	--------	$1.1\ 10^{15}$
	N	--------	$8.7\ 10^{15}$
Allen[10]	N	--------	$6.5\ 10^{15}$
Herron[11]	N_2	$5.7\ 10^{15}$ (297°K)	--------
	A	$3.3\ 10^{15}$ (297°K)	--------
Wentinck[12]	N_2	$1.2\ 10^{16}$	--------
Harteck[13]	N_2	$6.1\ 10^{15}$	--------
	A	$6.1\ 10^{15}$	--------

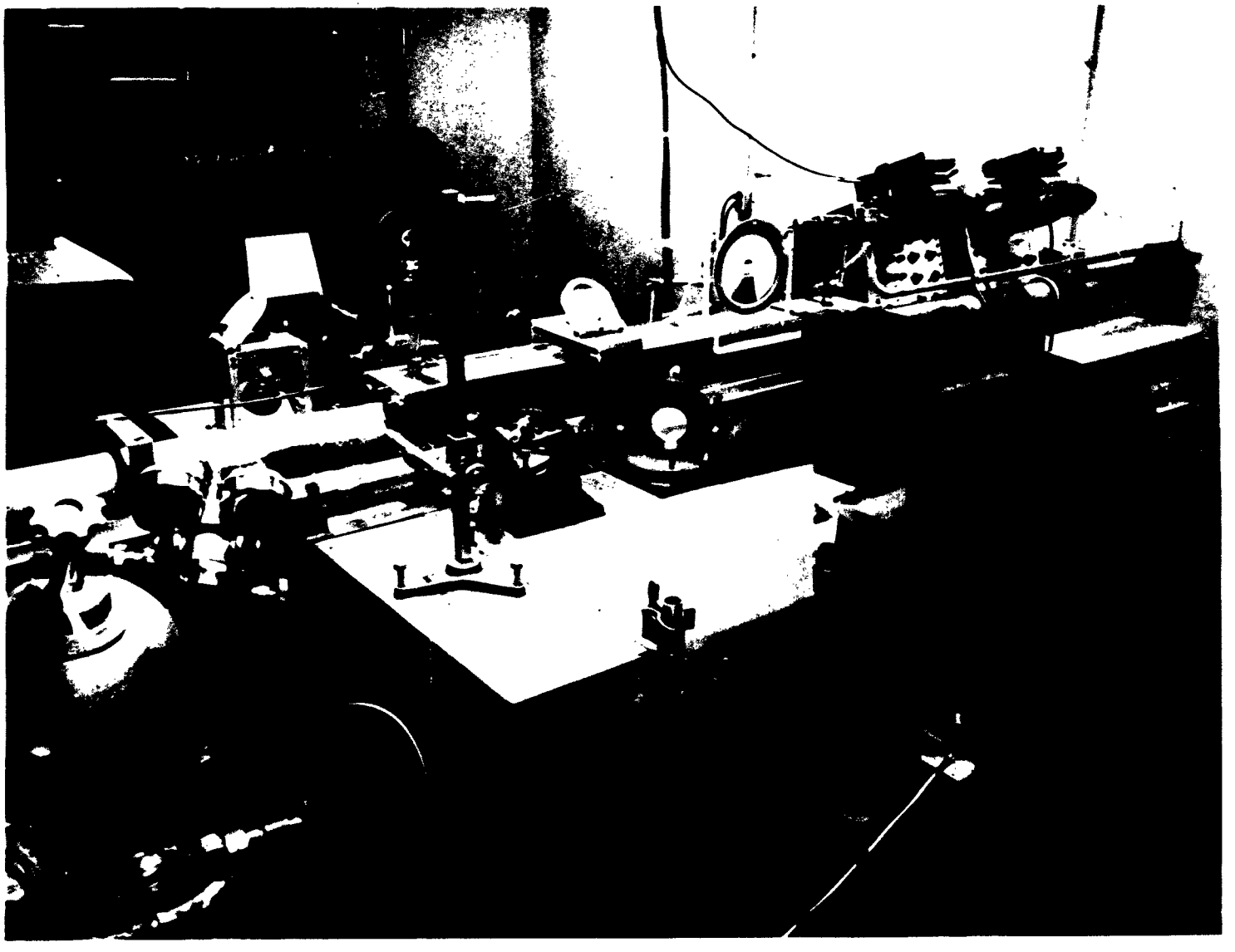

Figure 2.1 Shock Tube and Associated Instrumentation .

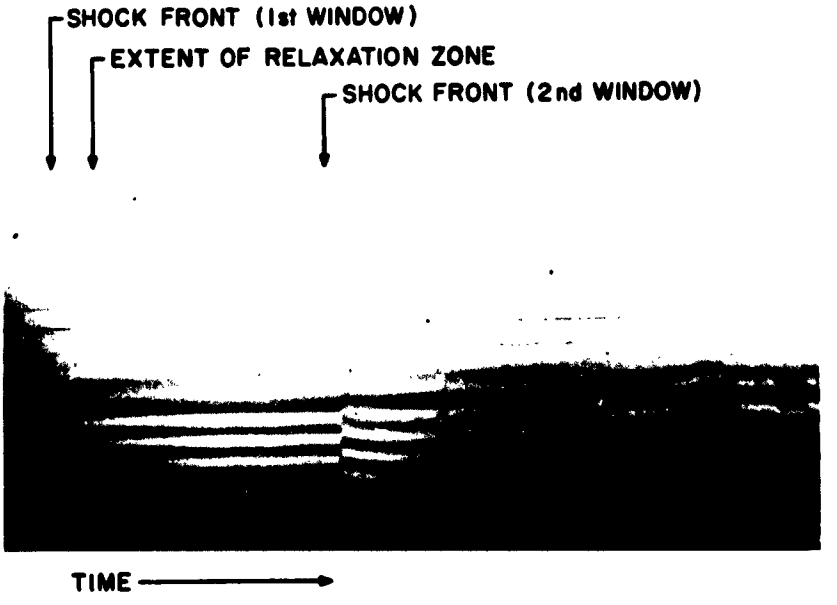

Figure 2.2 White Light Interferogram of a M 10.3 Shock Wave.

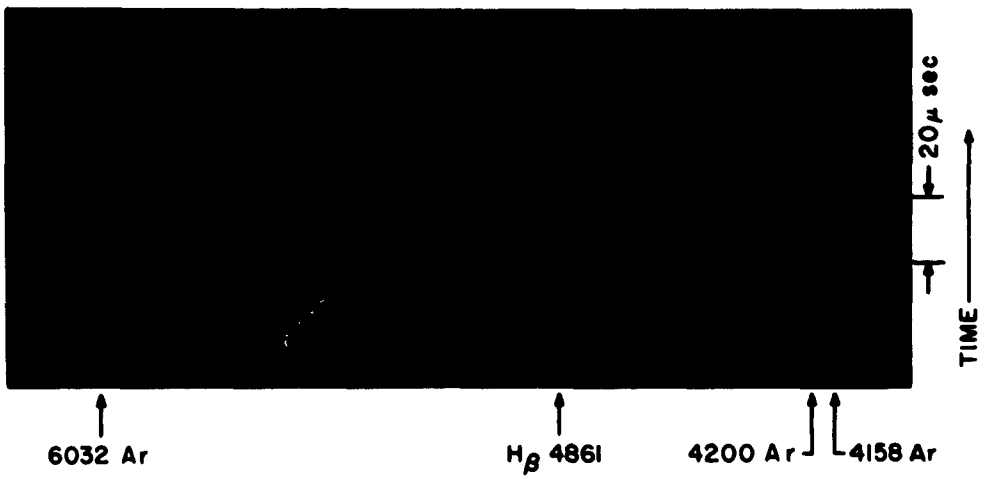

Figure 2.3 Time Resolved Spectrogram.

III-3 EXPERIMENTAL HEAT TRANSFER STUDIES *

3.1 Introduction

One of the many problems connected with space flight is the intense heating experienced by the vehicle during its entry into the planetary atmosphere. During the flight at relatively low altitudes a shock wave forms ahead of the body. The free stream gas passes through this shock wave and undergoes a large increase in internal energy which is sufficient to cause dissociation of molecules and even partial ionization of the gas. This hot, chemically reacting gas flows around the vehicle and heat is transferred to its surface. Two modes of heat transfer can be distinguished. One is the aerodynamic heat transfer process which includes conduction, convection and diffusion of molecules, atoms, ions and electrons across the boundary layer; the other is the radiation from the hot gas cap (shock layer) surrounding the forward section of the vehicle.

The purpose of this experimental study was to investigate the aerodynamic heat transfer to the stagnation point of a blunt body in a hypersonic flow of simulated atmospheres of Venus. Besides supporting the available analytical studies, the results of this work provide heat transfer data for a range of flight conditions beyond the scope of the present analyses.

It can be shown that at the stagnation point of a blunt body in hypersonic flight the aerodynamic heating is accurately simulated if the conditions at the edge of the boundary layer including the pressure distribution and wall conditions are correctly reproduced.

*Principal Investigators: J. S. Gruszczynski, C. J. Harris and W. R. Warren

The experiments were carried out in the newly developed arc-heated 2" shock tube which is capable of producing in the laboratory the environmental conditions encountered by the entry vehicle. The correct conditions of enthalpy and stagnation pressure were simulated in two assumed composition models of Venusian atmosphere for flight velocities up to about 40,000 ft/sec.

Preliminary analytical work involved the calculations of shock tube performance for both test gas mixtures corresponding to the specified atmosphere of Venus. Thermodynamic properties behind incident and normal shocks, and at the stagnation point of the hemispherical body were computed. An estimation of the radiation heat flux was also made to assess the magnitude of radiant heating sensed by the stagnation point heat gage. To confirm theoretical calculations an attempt has been made to measure the radiant heating using a new type of a total radiation gage. The primary objective of these radiation measurements was to demonstrate that the radiative contribution to the measured heating results was small, that is, they are used to verify that the measured heat transfer rates are essentially caused by the convective or boundary layer heat transfer mechanism.

3.2 Test Facility

The shock tube has been used for many years in experiments for the generation of aerodynamic data in flows of high energy and high stagnation pressure (Refs. 14, 15 and 16). The demand for an experimental facility in the area of simulation of orbital or even super-orbital enthalpies and pressures forced further development of its performance. It was obvious that this was beyond the capability of a conventional combustion driven shock

tube. The arc-heated shock tube used for the present experiments was developed specifically for that purpose (Ref. 17). It was originally designed as a prototype of a large facility but has been used successfully in experimental investigations. Numerous heat transfer tests were run with air, CO_2 and N_2 as the test gas and some of the data were reported in Reference 16.

Figure 3.1 shows schematically the design details of the whole shock tube assembly. The driven section is 2 in. in diameter and it is 135.5 in. long. The driver is 17 in. inside length with 2 1/4 in. internal diameter. A Lexan cylindrical sleeve with 1/4 in. wall thickness fits inside the driver tube. It is used to provide electrical insulation along the arc path; that is, it insures that the arc discharge is contained within the driver gas and that the energy is uniformly distributed axially along the driver. A thin wire is used to initiate the arc discharge. This is located on axis so that the wall losses will be uniform in the axial direction.

The high voltage electrode which is insulated from the driver end flange by a Lexan bushing is in the form of a hollow copper cylinder with a 3/8 in. diameter. A 1/8 in. diameter brass rod insulated by teflon tubing and held in position by a tapered steel washer and a nut is inserted through the center of the main electrode. A 5 mil tungsten wire is attached to the spider electrode at the diaphragm end of the driver and by about 1 in. cotton thread to the copper main electrode. The position of the brass rod relative to the main electrode determines the breakdown voltage. This adjustment is made with the main capacitors bank disconnected, using a small capacitor to prevent breaking of the wire.

The electrical circuit for the driver heating system is shown in Figure 3.2.a. The energy for the arc discharge is stored in forty-seven capacitors, each rated at 5 microfarads and 20,000 volts.

Figure 3.2.b shows a typical current wave form. It indicates that the circuit is critically damped and that the energy is completely dissipated in about 50 microseconds, and before the diaphragm opens which occurs about 150 microseconds later. Full description of the considerations entering into the design of this test facility is presented by Warren, et al (Ref. 17).

Helium is used as the gas heated in the driver. The diaphragm separating the driver and the driven section of the shock tube is made of stainless steel. It is scribed to a controlled depth (generally 20% - 40% of the thickness) along two diametrical cross lines. The required conditions of a given test run dictate the proper selection of the diaphragm. The diaphragm is found to open cleanly with a negligible loss of material.

As indicated in Ref. 17 , an extensive research program was necessary before a satisfactory operation of this facility was achieved. A photograph of the complete test facility including the power supply, vacuum pumps, etc., is shown in Figure 3.3. The performance of the tube in air is shown in Figure 3.4 where the attainable shock velocity is plotted as a function of initial pressure and energy input. The experimental data indicate that shock velocity up to 30,000 ft/sec can be obtained with 1 mm Hg driven tube initial pressure and full energy in the capacitors. With a lower initial pressure, shock velocity up to 36,000 ft/sec can be reached. Superimposed is a curve depicting the performance of a combustion driver facility. The limitation of the latter is self-evident.

3.3 Experimental Technique

Large amounts of carbon-like residue are normally found to cover the driver tube walls and models after each test. The origin of this is the Lexan sleeve used to insulate the driver. It appears that during the electrical discharge the inner wall surface of the sleeve decomposes slightly and particles of carbon so formed are carried along the driven tube by the expanding driver gas.

To insure a low degree of contamination of the test gas several steps were taken after each test run and before a new run was made. The driven tube was thoroughly wiped with alcohol until no trace of carbon could be noticed on the inner walls. The same applies to the test model, which was also carefully cleaned, and the gage surface brought to approximately the same degree of reflectivity as in the previous run. The tube was then evacuated down to about 10 - 20 microns pressure. The leak rate was then measured. If the rate did not exceed 10 microns per minute, the tube was considered to be in satisfactory condition.

Next the tube was filled with the test gas to the required test pressure P_1 (normally either 1 mm or 5 mm Hg). To further minimize the contamination of the test gas by impurities due to outgassing of the walls, the test gas mixture was allowed to flow through the tube at a rate of approximately 20 tube volumes per minute for about 20 - 30 minutes. The initial pressure in the driven tube was measured with a McLeod gage.

The driven section of the 2" shock tube is equipped with six port

holes equally spaced at 11" apart as shown in Figure 3.5. The model normally is located about 1/8 in. behind position 6. The signal from the piezoelectric pressure gage located at position 1 was used to trigger the scopes displaying heat transfer gage output.

Shock velocity was monitored by measuring the elapsed time for the incident shock wave to travel between positions 3-5, 4-5 and 5-6. Pressure gages were used as time of arrival sensors. The last two intervals were used to determine the shock velocity for the particular test run. The scatter between data for these two intervals is invariably within the reading accuracy of the wave transit time for one interval ($\pm$ 1-1/2%). This indicates the existence of only small incident shock wave attenuation effects (if any). A two color pyrometer was used to monitor the luminosity behind the incident shock wave. The violet range extended between 3500 - 4500 $\mathring{A}$, while the red region response was between 6000 - 8000 $\mathring{A}$. The history of the pressure behind the incident shock wave was also observed by displaying the output of a pressure gage from position 5. The output was filtered to eliminate the ringing of the gage whose natural frequency lies around 40 kc.

The heat transfer rate was determined with a calorimeter gage mounted at the stagnation point of the hemispherical model 1/2 in. in diameter (Figure 3.6). The design dimensions of the gage were 1/16 in. wide by 3/16 in. long. The gage element itself was made of 0.004 in. thick Hytemco (iron-nickel) alloy. The leads were brought out from the gage through the internal cavity of the model and its supporting sting and were connected in

a circuit shown schematically in Figure 3.7. One of the features (Ref. 17) of the circuit is the grounding of the instrument circuit in common with the driver circuit and the connection of the gage leads across a balanced differential amplifier. These steps allow extraneous electrical effects observed earlier in the experiments to be reduced to a level such that they do not preclude the observation of the heat transfer signal.

The output of the heat transfer gage was displayed and photographed on four oscilloscopes in parallel, each with a different sweep rate. The rates were 20, 10, 5 and 2 μsec/cm. Since the region of interest (corresponding to the steady flow conditions) lies approximately within the first 20 μ sec from the moment of the bow shock formation, either the five or two μsec/cm records were used to read off the heat transfer rate.

The relation between the heat rate and the change of the voltage with time across the gage is expressed by the simple expression

$$\dot{q} = K \frac{1}{E_o} \frac{dT}{dt}$$

and

$$K = \frac{\rho C L}{\alpha}$$

where

ρ = density of gage material

C = specific heat of gage

L = gage thickness.

α = temperature coefficient of resistivity

E_o = initial voltage across gage

Since the bulk properties of the gage material are well known, the coefficient K can be easily calculated and the gage response established without an extensive calibration procedure. The temperature coefficient of resistivity, α, has been checked experimentally, however, in previous studies.

Stagnation point radiant heat energy flux has been measured by means of a newly devised technique which involves the use of a cavity gage as shown in Figure 3.8. Depending on the proper design of the entrance and the location of the cavity gage within the hemispherical model, almost all of the radiant energy originating from a known volume of the highly heated gas cap and incident upon the cavity entrance slit is absorbed within the internal walls of the gage. In addition, the electrons generated by high energy photons will be prevented from escaping. The energy entering the cavity gage will be absorbed by the thin (about 0.2 μ) platinum film deposited on its internal surfaces. By segmenting the gage as shown in Figure 3.8 the one-dimensionality of its operation is preserved and its sensitivity thereby increased considerably. Due to limited size of the model for this study (as dictated by the blockage effect in the 2" internal diameter shock tube) the test configuration allowed only the measurement of radiation along the stagnation streamline with a gage arrangement shown in Figure 3.9.

3.4 Shock Tube Parameters

Using the equilibrium thermodynamic properties computed by Browne (Ref. 5) for the established two gas mixtures, one with the nominal

content of 9% CO_2, 90% N_2 and 1% A and the other with 25% CO_2, 74% N_2 and 1% A, various gas dynamic properties associated with traveling and stationary shock fronts were calculated and charted as functions of shock velocity and the driven tube initial pressures.

The tabulated values of the equilibrium thermodynamic properties were plotted and the solution of the Rankine-Hugoniot shock relations obtained. All calculations were made for three initial driven tube pressures of P_1 = mm, 5 mm and 25 mm of Hg. The initial driven tube temperature, T_1, was taken to be 294°K. The range of shock velocities, U_s, between 10,000 ft/sec and 30,000 ft/sec was covered. However, due to the limited range of the available thermodynamic properties which extended only up to 15,000°K some of the shock tube parameters could not be calculated for all velocities.

a. Incident Shock

The state of the gas on both sides of a normal shock is related by three basic equations corresponding to the physical principles of the conservation of mass. momentum and energy. These are:

$$u_2 = u_s \left(1 - \frac{\rho_1}{\rho_2}\right)$$

$$P_2 - P_1 = \rho_1 u_s^2 \left(1 - \frac{\rho_1}{\rho_2}\right)$$

$$h_2 - h_1 = \frac{1}{2} u_s^2 \left[1 - \left(\frac{\rho_1}{\rho_2}\right)^2\right]$$

where h = enthalpy

p = pressure

u = velocity

ρ = density

and subscripts 1 and 2 refer to regions ahead and behind the incident shock. The simultaneous solution of these equations together with the available tabulation of the equilibrium state produces results which are plotted in Figures 3.10, 3.13, 3.16, 3.19 and 3.21 for the 9% CO_2 mixture and in Figures 3.22, 3.25, 3.28, 3.31 and 3.33 for the 25% CO_2 mixture.

b. Stationary Normal Shock (Laboratory Coordinates)

After the passing of the incident shock the model finds itself in a supersonic quasi-steady flow with the properties of region 2 ahead of the model bow shock wave. The flow close to the axis of symmetry is decelerated to subsonic velocity. The state of the gas along the stagnation streamline on both sides of the bow shock is governed by the same three conservation laws.

$$\rho_2 u_2 = \rho_3 u_3$$

$$P_3 - P_2 = \rho_2 u_2^2 \left(1 - \frac{\rho_2}{\rho_3}\right)$$

$$h_3 - h_2 = \frac{1}{2} u_s^2 \left[1 - \left(\frac{\rho_2}{\rho_3}\right)^2\right]$$

where subscript 3 refers to the region behind the bow shock. The calculation produced the results which are presented in Figures 3.11, 3.14, 3.17, 3.20 for the 9% CO_2 mixture and in Figures 3.23, 3.26, 3.29 and 3.32 for the 25% CO_2 mixture.

c. Stagnation Region

The flow along the stagnation streamline in region 3 is decelerated to a stop at the body. The stagnation conditions are found as follows: The enthalpy is given directly by $h_s = h_3 + 1/2\ U_3^2$. The stagnation pressure is computed approximately by assuming incompressible flow $P_s = P_3 + 1/2\ \rho_3\ U_3^2$. Both the stagnation temperature and the corresponding density are read off directly from the thermodynamic state charts and plotted in Figures 3.12, 3.15 and 3.18 for 9% CO_2 mixture and in Figures 3.24, 3.27 and 3.30 for the 25% CO_2 gas.

d. Composition of Stagnation Region Gas

The equilibrium concentration of the various species appearing in the dissociated and ionized gas when heated to the enthalpy level corresponding to the stagnation point had also been obtained and plotted as a function of shock velocity. These are shown in Figures 3.34 through 3.37 for both the 9% and 25% CO_2 mixtures and for the two test cases of P_1 = 1 and 5 mm Hg. Electron concentration for pure CO_2 and pure N_2 are also included in Figures 3.38 and 3.39 respectively.

e. Radiant Heat Flux to the Stagnation Point

The radiation heat flux to the stagnation point of the 1/2 in. diameter model was calculated using appropriate emissivities obtained for the heated atmospheres of Venus (Ref. 18). The stagnation point region was replaced by an infinite slab at a uniform temperature, T_s, and density, ρ_s, whose thickness, δ, is the shock stand off distance given by

$$\frac{\delta}{R_N} = \frac{2/3}{\frac{\rho_3}{\rho_2} - 1}$$

where R_N = radius of the hemispherical model.

The calculations were done for both atmospheric models and for three driven tube initial pressures. The results are presented in Figures 3.40 and 3.41.

3.5 Results and Discussion

In the simulation of hypersonic flight situations at the stagnation point of a model in the shock tube the corresponding stagnation enthalpy and pressure are produced in a different manner than in the flight case. The test gas is first compressed and accelerated by the incident shock wave generated when the diaphragm dividing the driver and the driven tube is ruptured. The flow behind the shock front, although moving with high velocity, is only slightly supersonic due to the high temperature or high sonic velocity in the gas processed by the advancing incident shock wave. This gas will now flow around our model. Since a blunt body is being investigated, a detached bow wave will be established. The gas along the stagnation streamline will undergo compression essentially across a normal shock and finally will be stagnated at the surface of the body.

As long as the boundary layer thickness is small in comparison with the shock layer whose measure at the stagnation point is the detachment distance, the boundary layer problem can be considered separately from the inviscid flow field and hence independently of the Reynolds number. The

only requirements for accurate simulation are the stagnation enthalpy, the velocity gradient at the stagnation point, and gas equilibrium in the various flow processes. For the hemispherical body the Newtonian approximation predicts that the velocity gradient is independent of Mach number. This has been confirmed experimentally. The correlation for the heat transfer rate through the laminar boundary layer at the stagnation point can be written

$$\dot{q}\sqrt{\frac{R_N}{P_s}} = f(h_s - h_w)$$

where R_N is body nose radius

h_w is wall enthalpy

Thus, the environment created in a shock tube can be directly applied to the solution of the stagnation point heating problem.

The performance of the shock tube in the mixtures of CO_2, N_2 and A does not differ appreciably from its performance in air. Maximum shock velocities obtained during this experimental program for P_1 values of 5 mm and 1 mm Hg were approximately 24,500 ft/sec and 30,200 ft/sec. In both cases maximum capacitor energy (about 50,000 joules) was discharged in the driver for heating the helium.

The constituent concentrations of the mixtures tested differed slightly from the nominal values listed earlier.

Nominal	Actual
1. 9% CO_2, 90% N_2, 1% A	1. 8.80% CO_2, 89.98% N_2, 1.22% A
2. 25% CO_2, 74% N_2, 1% A	2. 25.10% CO_2, 73.78% N_2, 1.12% A

The test gas mixtures were considered to be sufficiently close to the specified values to satisfy the objectives of the study.

During each run, wall pressures histories behind the incident shock wave were recorded. A typical oscillogram of signal from a pressure gage located at position five is shown in Figure 3.42, corresponding to a shock velocity U_s = 20,300 ft/sec and initial tube pressure of 5 mm Hg. The effect of boundary layer growth behind the incident wave is indicated by the side wall pressure rise with time. Note that this rise is small during the passage of the test gas, however. Pressure forces of the type shown in Figure 3.42 are complicated by large oscillations caused by the response of the gage and associated electronic circuits. They are used primarily to verify the test pressure level and to qualitatively interpret the phenomena occurring in the tube process (arrival of expansion wave - not seen in Figure 3.42 - and boundary layer effect on pressure level, for example).

The heat transfer measurements were made at the stagnation point of a 0.5 in. diameter hemisphere-cylinder model using a calorimeter heat transfer gage (Ref. 19). The gage material used for the 0.5 in. diameter model was .004 in. thick Hytemco. A few experiments were performed with a 0.75 in. diameter model and the gage used 0.003 in. thick platinum. According to the analytical results of Ref. 19, these thicknesses can only introduce the order of 1% error in the measured heating results. Their use is, therefore, justified by practical considerations. The oscillogram of the signals from both type gages are shown in Figures 3.44a and 3.44b

respectively. The conditions of both tests were very similar. The shock velocities were 29,200 and 29,600 ft/sec, and the initial pressures 1 mm Hg in both cases. The first test was in 25% CO_2 mixture; the second, in air. Although in this particular case the noise level of the response of either gage seems to be of the same magnitude, closer examination of the traces will prove that the platinum gage response is cleaner. This was also observed in other runs. The initial jump of the DC level with the Hytemco gage was also observed to occur with the platinum gage. Lack of similarity of the precursor response during the two or three microseconds before shock arrival cannot be explained at present.

The oscillogram from a calorimeter heat gage at the stagnation point of the 0.5 in. model is shown in Figure 3.43. The instantaneous rate of change of the output together with the known properties of the Hytemco alloy gives the unknown heat rate for a given time interval. A corresponding trace of the optical pyrometer sensing the radiation across the incident shock of station 5 is also shown. Taking the time interval during which the intensity of radiation is level and allowing for the formation of the bow shock (2 to 3 μs), the useful test time was arrived at and the slope of the gage signal during that period was measured, giving the unknown heat transfer rate.

The experimental study involved a series of runs in the 9% and 25% CO_2 mixtures over a wide shock velocity range (note that U_s does not equal U_f), simulating hypersonic entry at altitudes between 240,000 and 260,000

ft. of the atmospheric model I. The results are shown in Figure 3.45. Points marked by circles and triangles are from tests in 9% and 25% CO_2 mixtures, respectively. In addition, some data obtained in pure CO_2 and N_2 are included. The limited results in CO_2 heat transfer measurements of Rutowski and Chan (Ref. 20) at low enthalpies are also entered.

The theoretical curves representing Scala's calculation of equilibrium boundary layer for dissociated and ionized nitrogen are drawn together with his early estimated region of uncertainty for partially ionized carbon dioxide. At $(h_s - h_w)$ values below 24,000 BTU/lb the experimental data follow the theoretical curve. At higher enthalpies the present data give heat transfer rates somewhat lower than the ionized theory for N_2. The pyrometer records indicate that the simulation of flight velocities below 35,000 ft/sec gives valid data with sufficient test time. The results corresponding to higher flight velocities may have insufficient test time for accurate readings. This limitation is more likely to exist for the CO_2 mixtures than for air and nitrogen because of the apparent long relaxation times for the non-equilibrium process behind the incident shock wave (see Figure 3.43). Such an effect could cause the observation of values lower than actually exist and is, therefore, quite important. This possible restriction on the results is imposed by the present 2" test facility and will be remedied by the installation of the 6" shock tube scheduled for operation shortly.

It is interesting here to note that the electron densities of the stagnation point as calculated for 9% and 25% CO_2 mixtures, pure N_2 and pure CO_2

differ little from each other; this can be seen in Figures 3.34 through 3.37.

The contribution of radiation to the measured heat transfer rate was calculated and, in the case of both gas mixtures, its magnitude is less than 8% assuming complete absorption by the gage surface. This is the theoretical upper limit of possible radiative error in the measured boundary layer heating. Figure 3.46 shows the response of the cavity radiation gage during a test run in the 25% CO_2 mixture. It is pointed out that the sensing element in the cavity gage is a thin film surface temperature resistance thermometer so that its response is different from that of a calorimeter gage. For example, for a constant heating pulse applied in a step function at t = 0, the thin film response will be proportional to $\sqrt{t}$ while the calorimeter response will be proportioned to t. The signal shown exhibits some electronic noise just prior to shock arrival over a time period similar to that observed with the calorimeter gage traces. Again, this is undoubtedly due to rapid charge equilibration about the model in the ionized flow. The physical mechanisms causing these early signals are not clear; however, it again appears that they become unimportant soon after the shock wave reaches the model. The relatively clean response of the gage during approximately the 10μsec following the shock wave arrival indicates that this is the time for passage of the shocked test gas. The subsequent fall and rise are responses to the irregular driver gas flow that then impinges on the model. Note that a drop in response is an indication of suddenly reduced heating rate. The radiative heating rate at the stagnation point corresponding to

the gage signal shown in Figure 3.46 has not yet been reduced accurately. However, an approximate reduction shows it to be within 30% of the calculated value. Therefore, the conclusion is drawn that the radiation contribution to measured heating rate values is small (10% or less). This conclusion is now based upon both experimental and theoretical grounds.

3.6 Conclusions

The experimental program of stagnation point heat transfer rates measurement on a blunt body in two simulated atmospheres of Venus supplied data which indicate that within the experimental accuracy no discernible difference between the heat transfer rate in 9% CO_2 mixture and in the 25% CO_2 mixture can be observed. For conditions corresponding to flight velocities below 35,000 ft/sec the experimental data agree well with theory. For higher values of $(h_s - h_w)$ or corresponding flight velocities the test results may suffer due to short test time caused by slow approach to equilibrium of reaction processes behind the normal shock. The new 6" shock tube now in process of installation will increase considerably the available test time. Calculation of the upper limit of equilibrium radiation from the shock layer to the stagnation point indicates that its contribution to the measured rates is small. Measurement of the radiation by the newly developed total radiation gage gives values close to the theoretical prediction.

Further studies of equilibrium and non-equilibrium radiation and the influence of non-equilibrium flows on the convective heat transfer rate are recommended. The behavior of the laminar and turbulent boundary layers and the transition phenomena should also be studied in the hypervelocity shock tube facility.

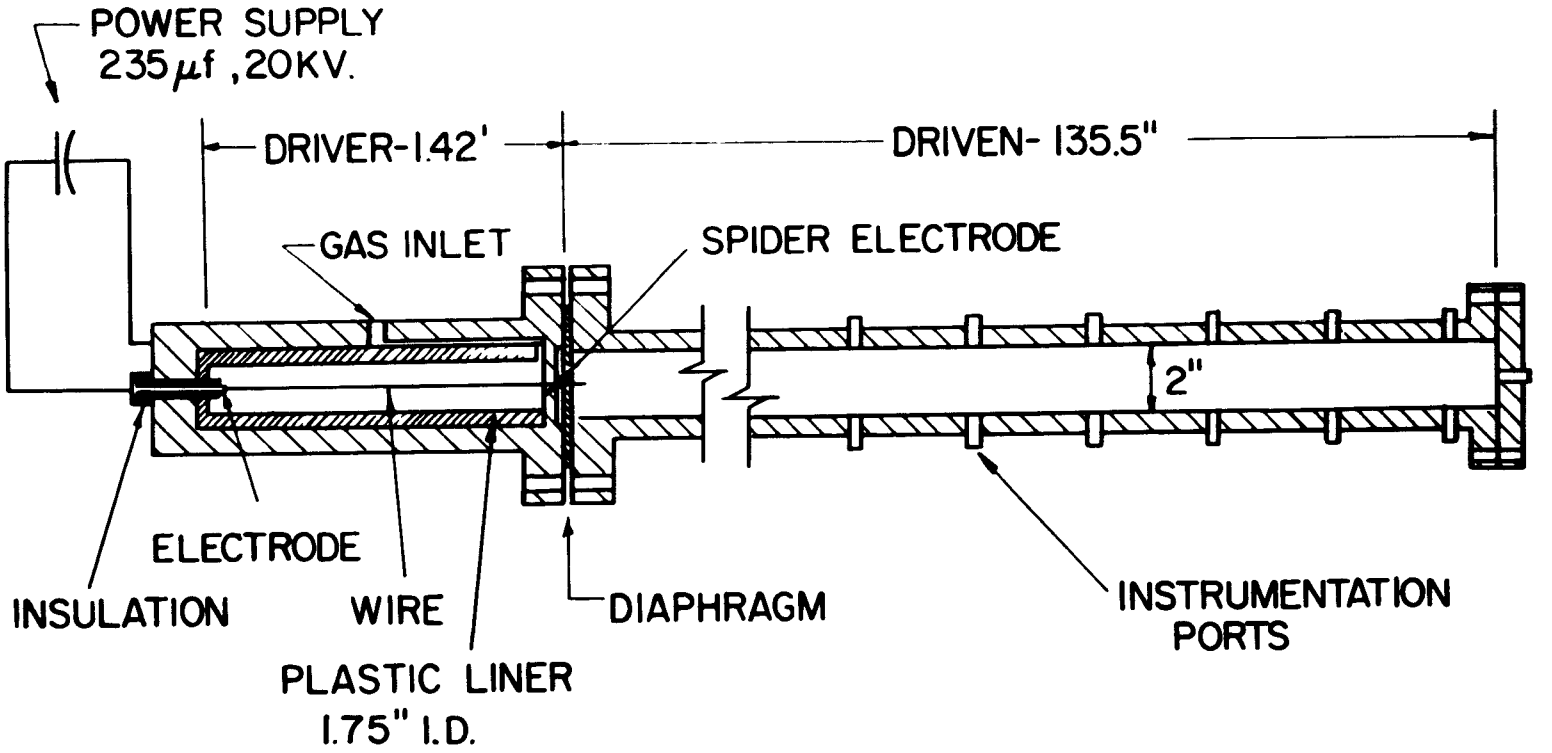

Figure 3.1 Design of Arc Heated Shock Tube.

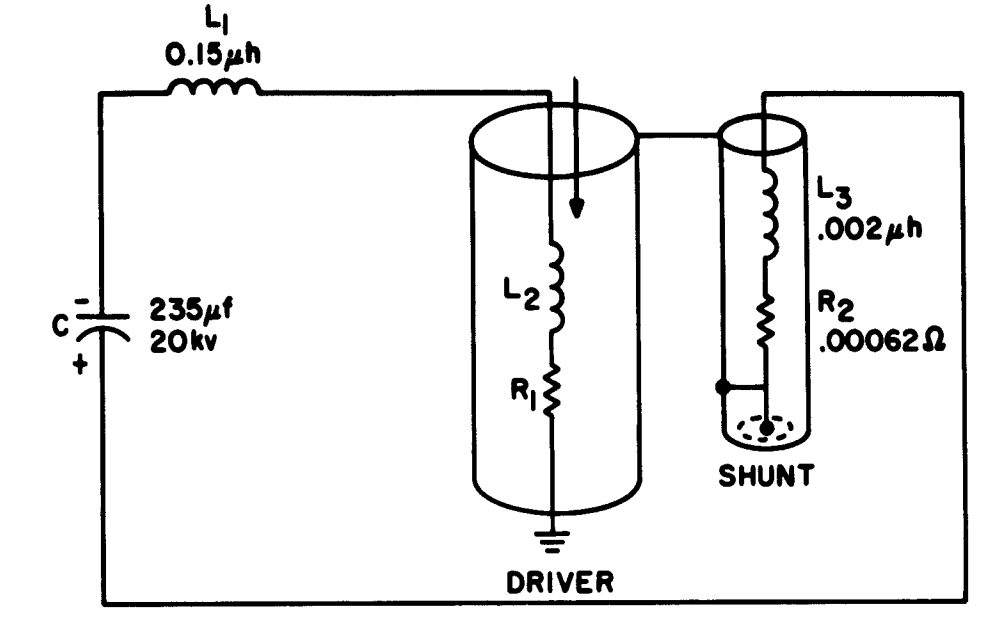

(a) CIRCUIT DIAGRAM

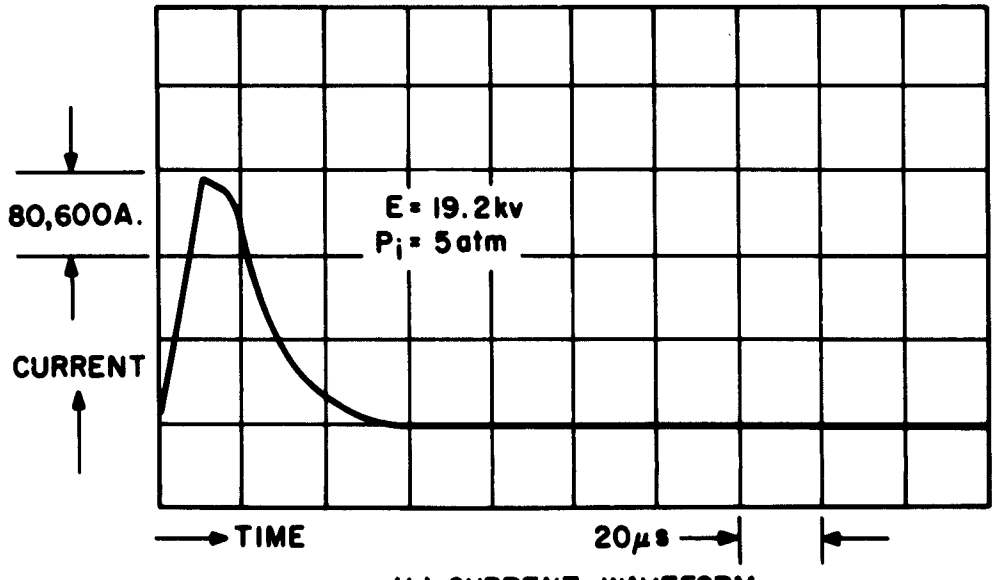

(b) CURRENT WAVEFORM

Figure 3.2 Typical Electrical Characteristics of Prototype Shock Tube

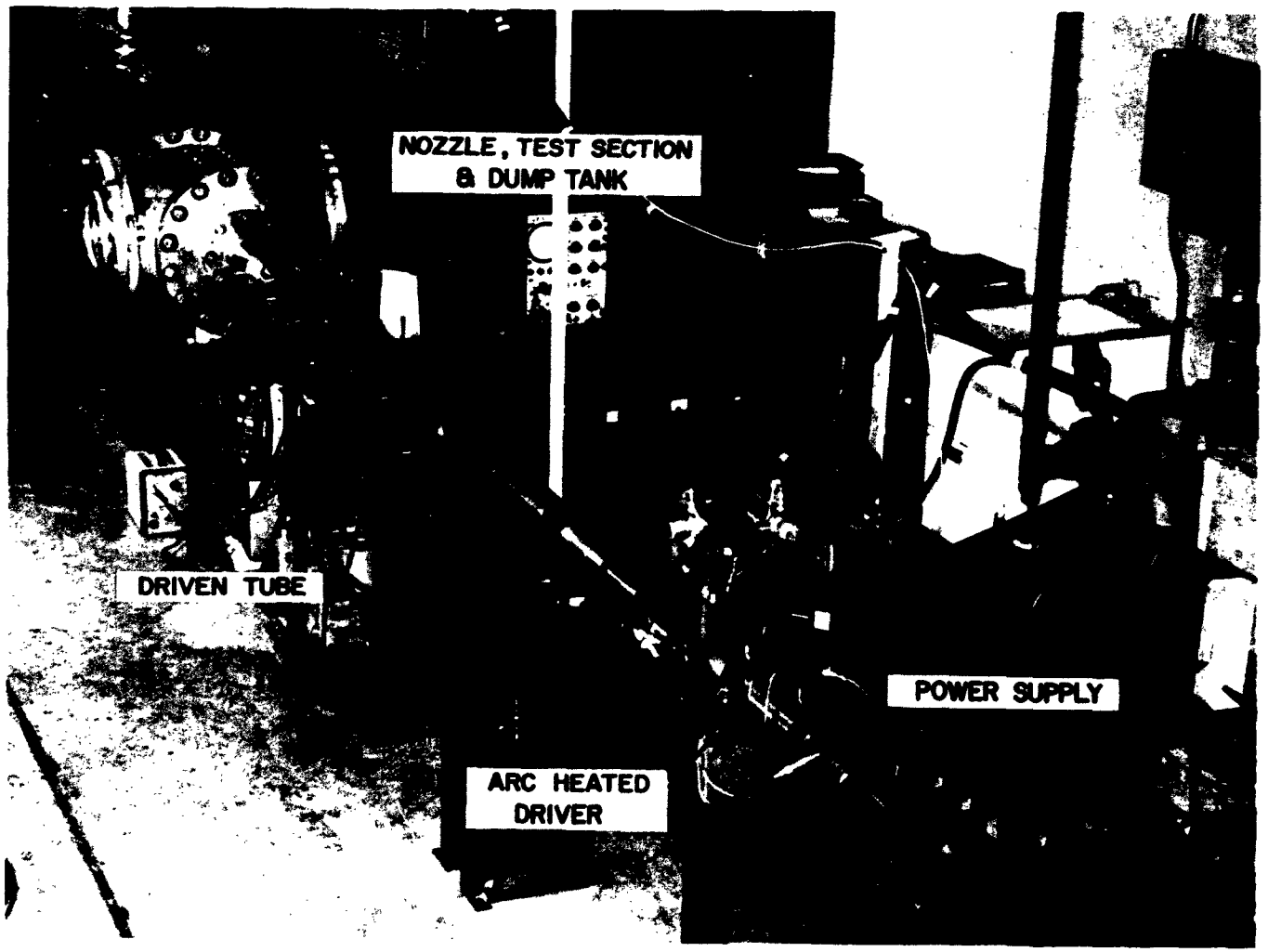

Figure 3.3 High Enthalpy Shock Tube Facility

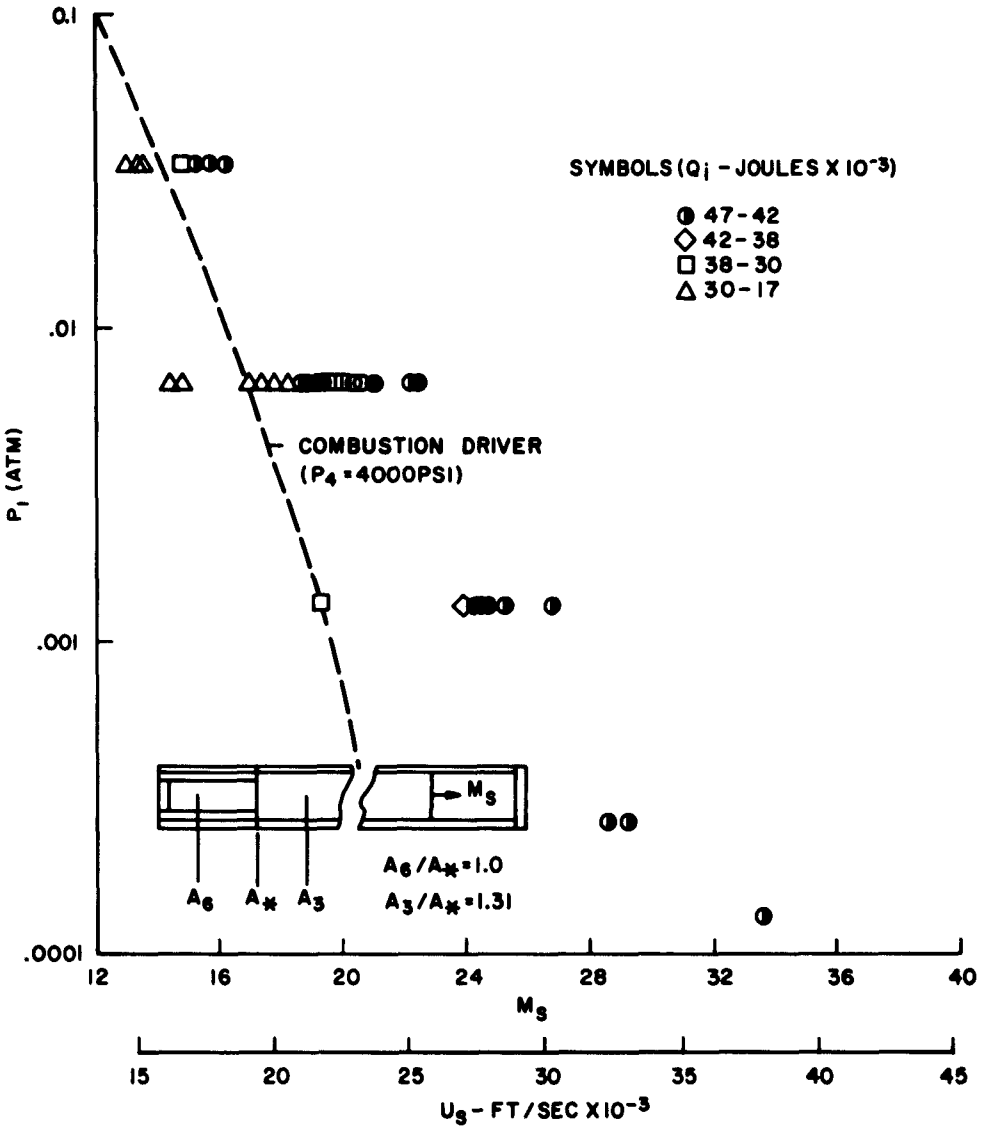

Figure 3.4 Arc Heated Helium Driver Shock Tube, M_S vs. P_1

(2" Shock Tube - Max. Available Energy: 47,000 Joules)

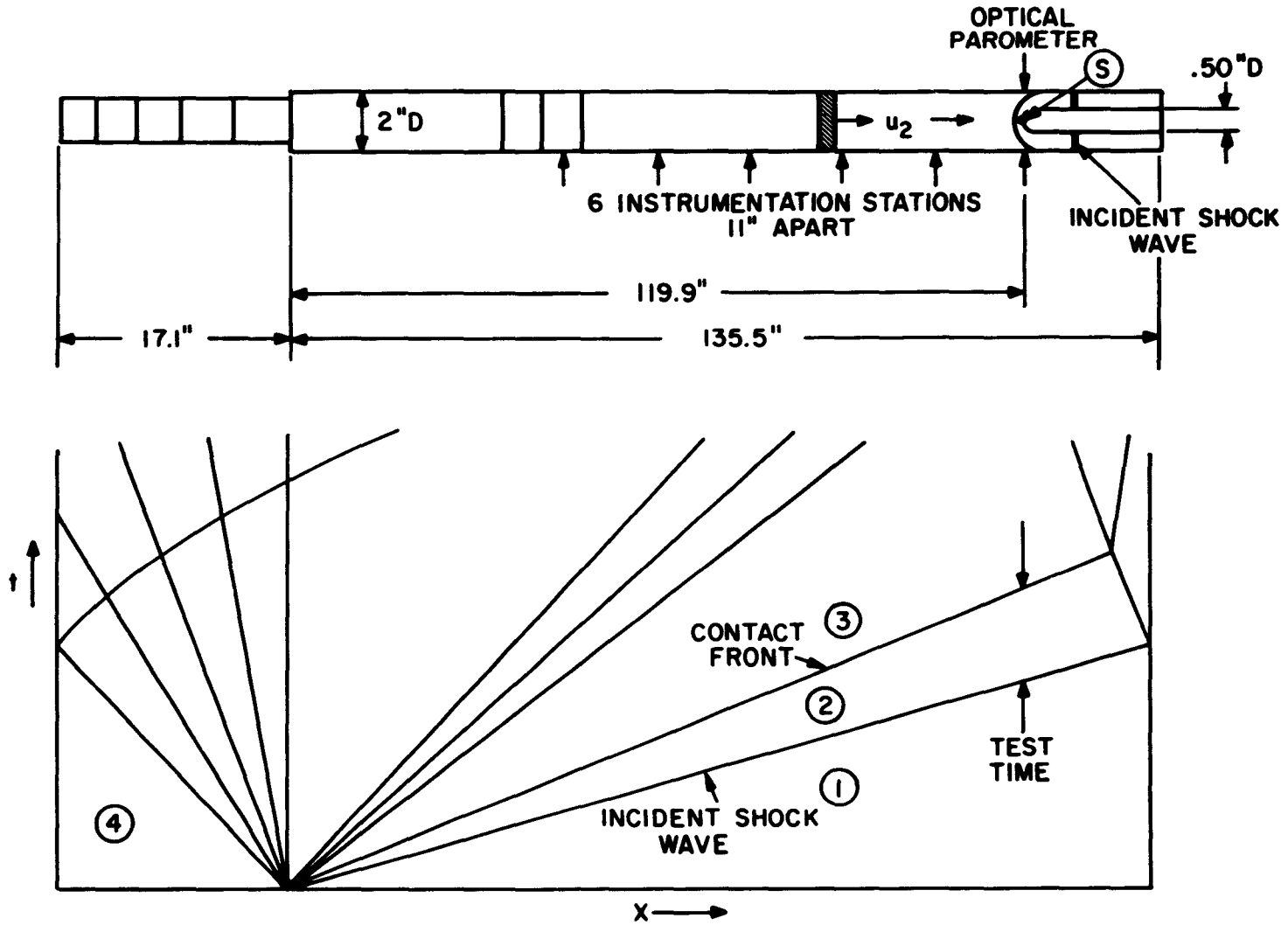

Figure 3.5 Straight Tube Test Configuration Model. Heat Transfer Measurements.

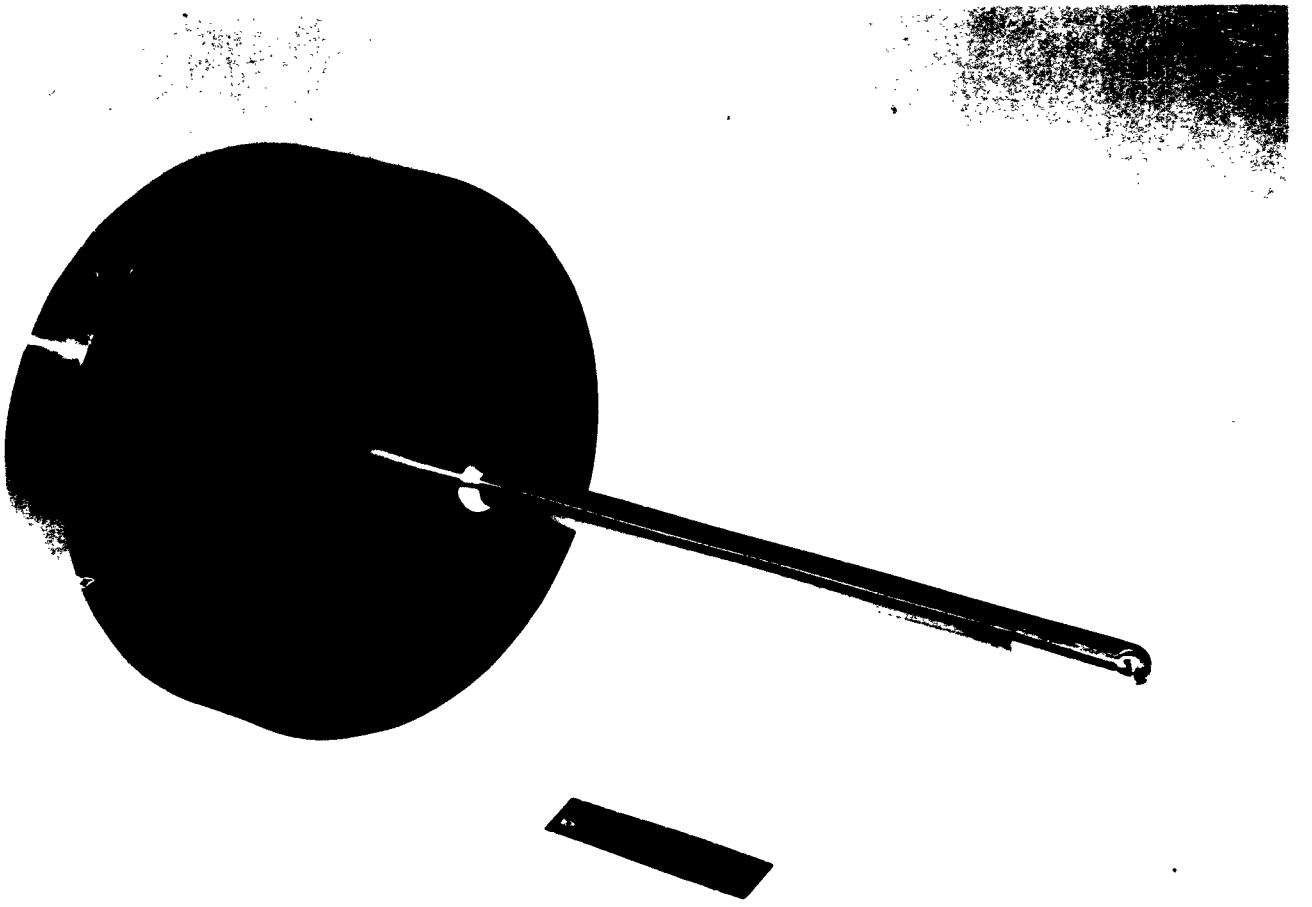

Figure 3.6 Half-inch Model with Heat Transfer Gage

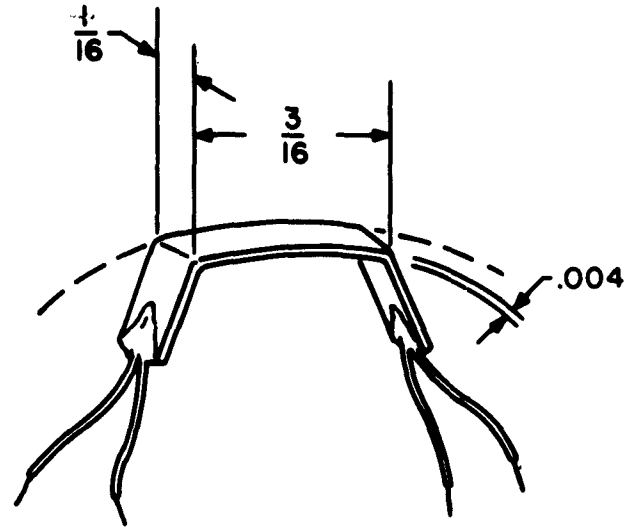

a. CALORIMETER GAUGE

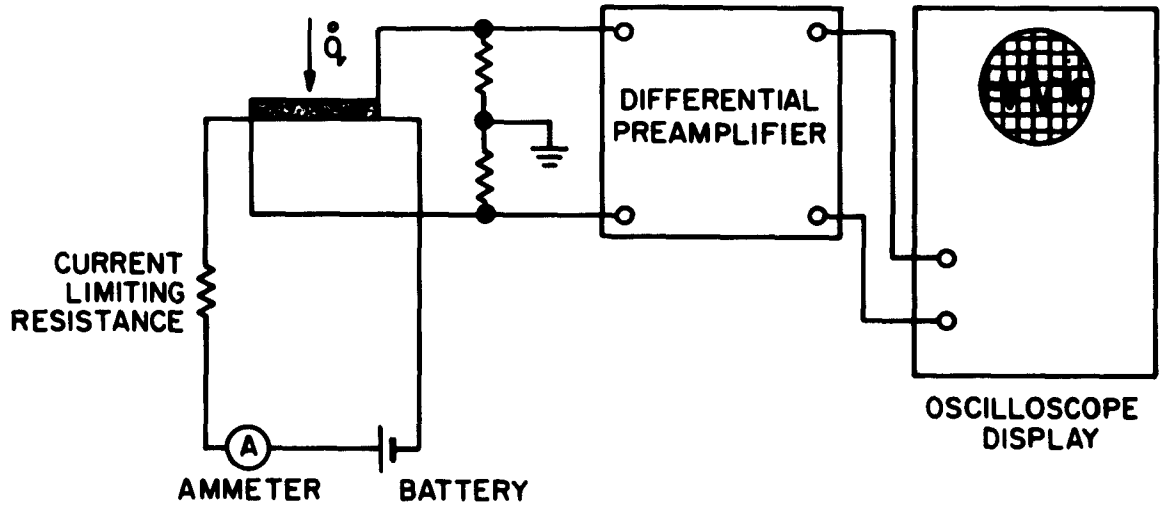

b. SCHEMATIC OF GAUGE CIRCUIT

Figure 3.7 Heat Transfer Rate Measurement Set-up.

ADVANTAGES:

1. WINDOWLESS AND NO SURFACE EFFECT UNCERTAINTY. ACCEPTS AND MEASURES ALL INCIDENT RADIATION

2. COLLIMATION ALLOWS MEASUREMENT OF TOTAL EMISSION FROM LOCAL AREAS OF HEATED GAS WITH μs RESOLUTION.

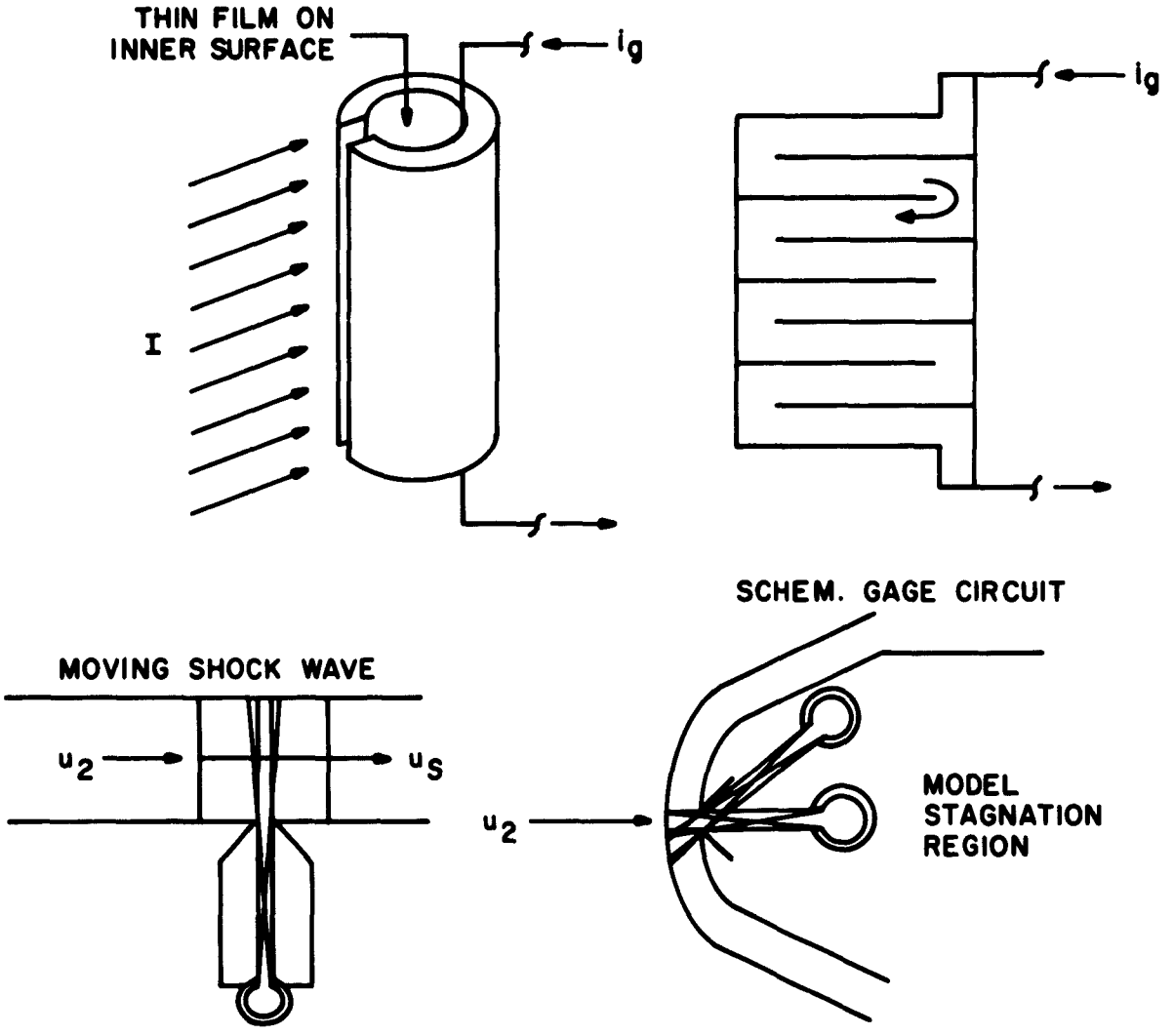

Figure 3.8 Cavity Gage for Total Radiative Heat Transfer Measurements

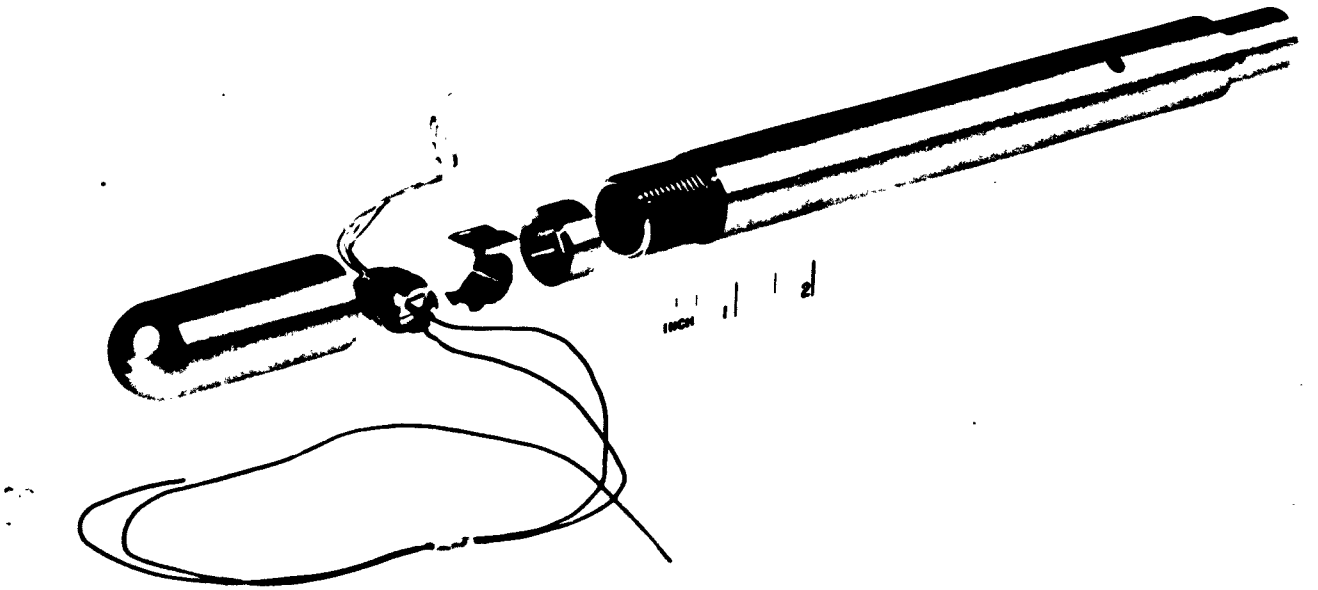

Figure 3.9 Total Radiation Gage

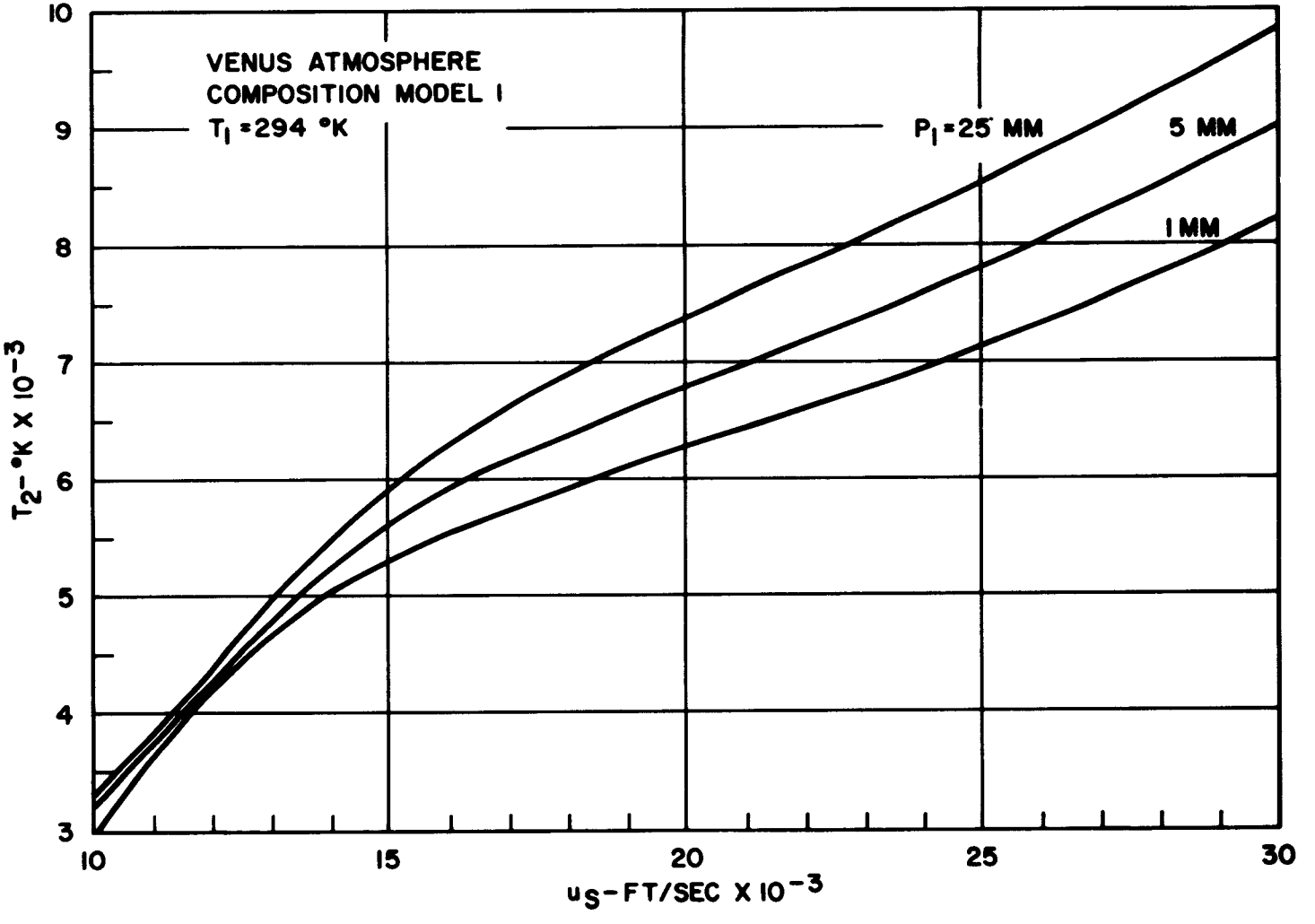

Figure 3.10 Temperature Behind Incident Shock

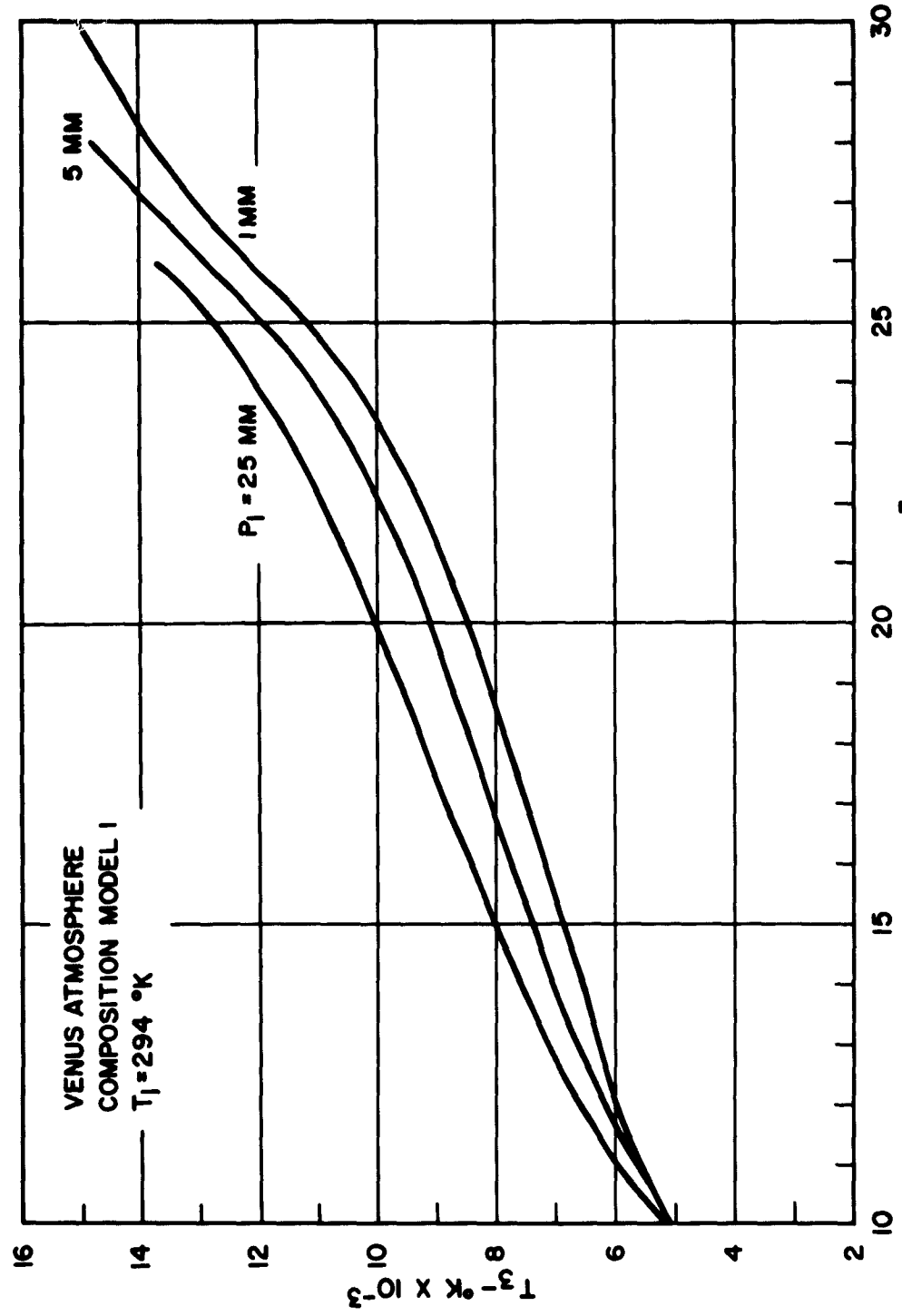

Figure 3.11 Temperature Behind Normal Shock

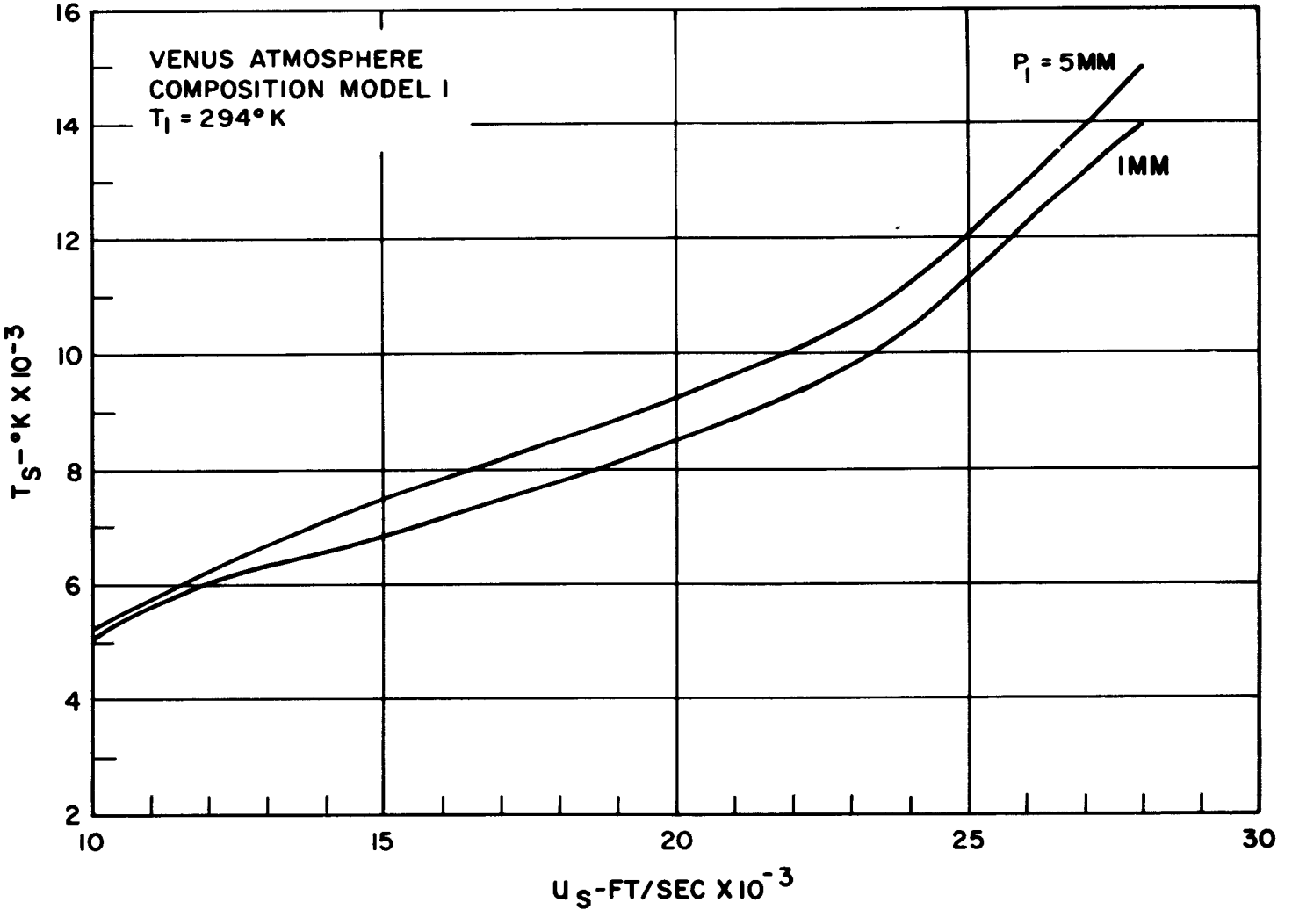

Figure 3.12 Stagnation Temperature

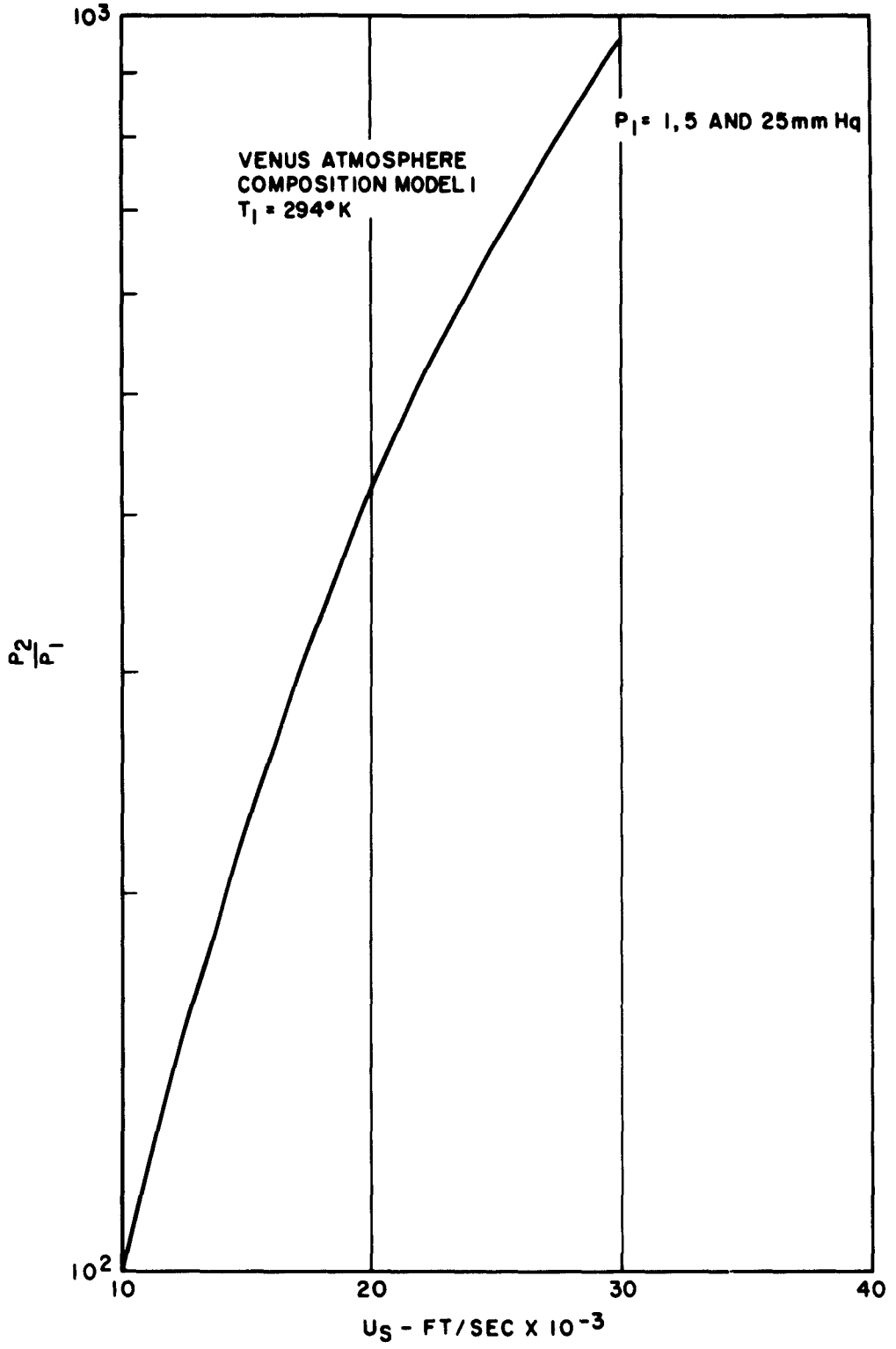

Figure 3.13 Pressure Behind Incident Shock

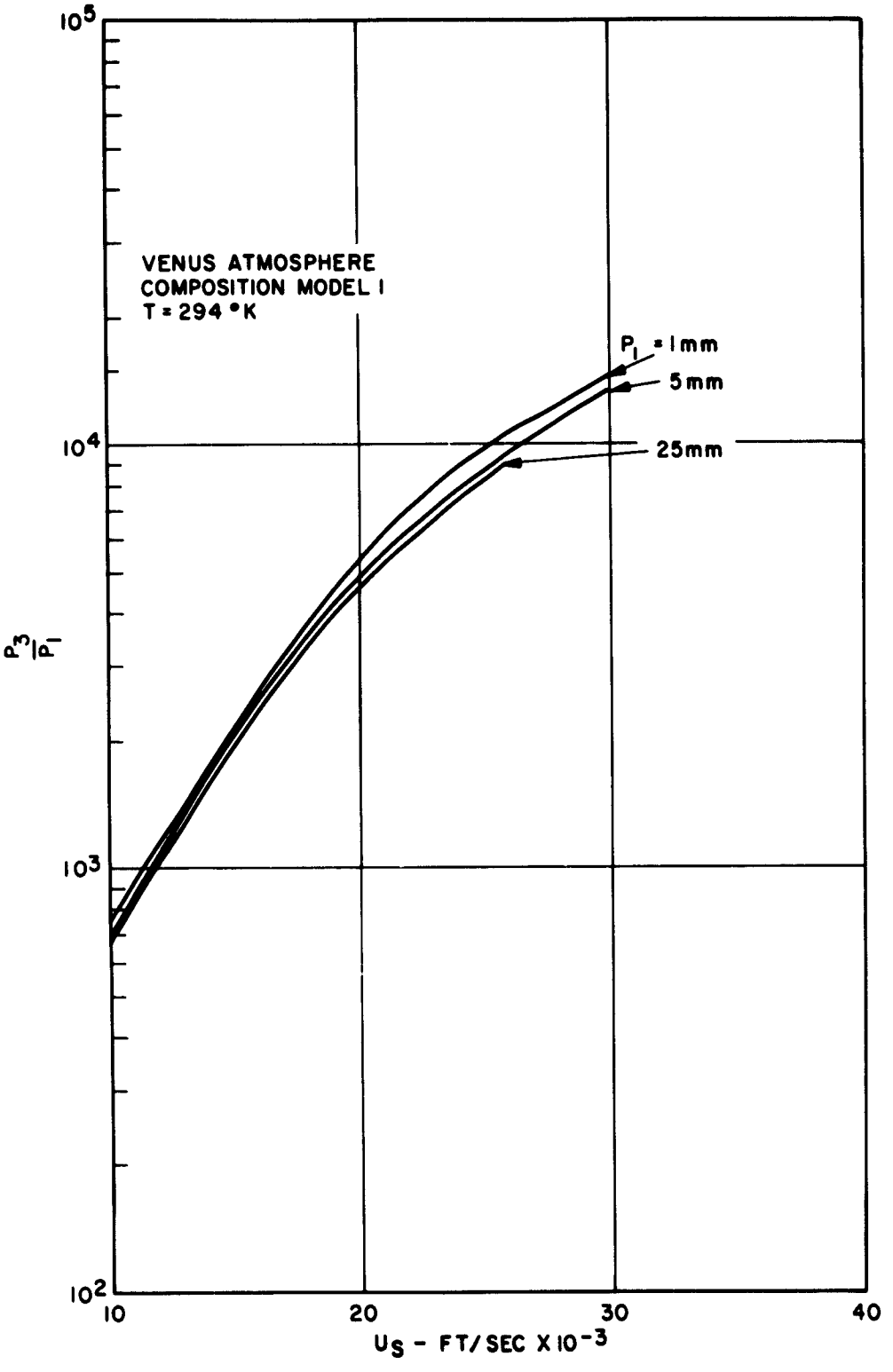

Figure 3.14 Pressure Behind Normal Shock

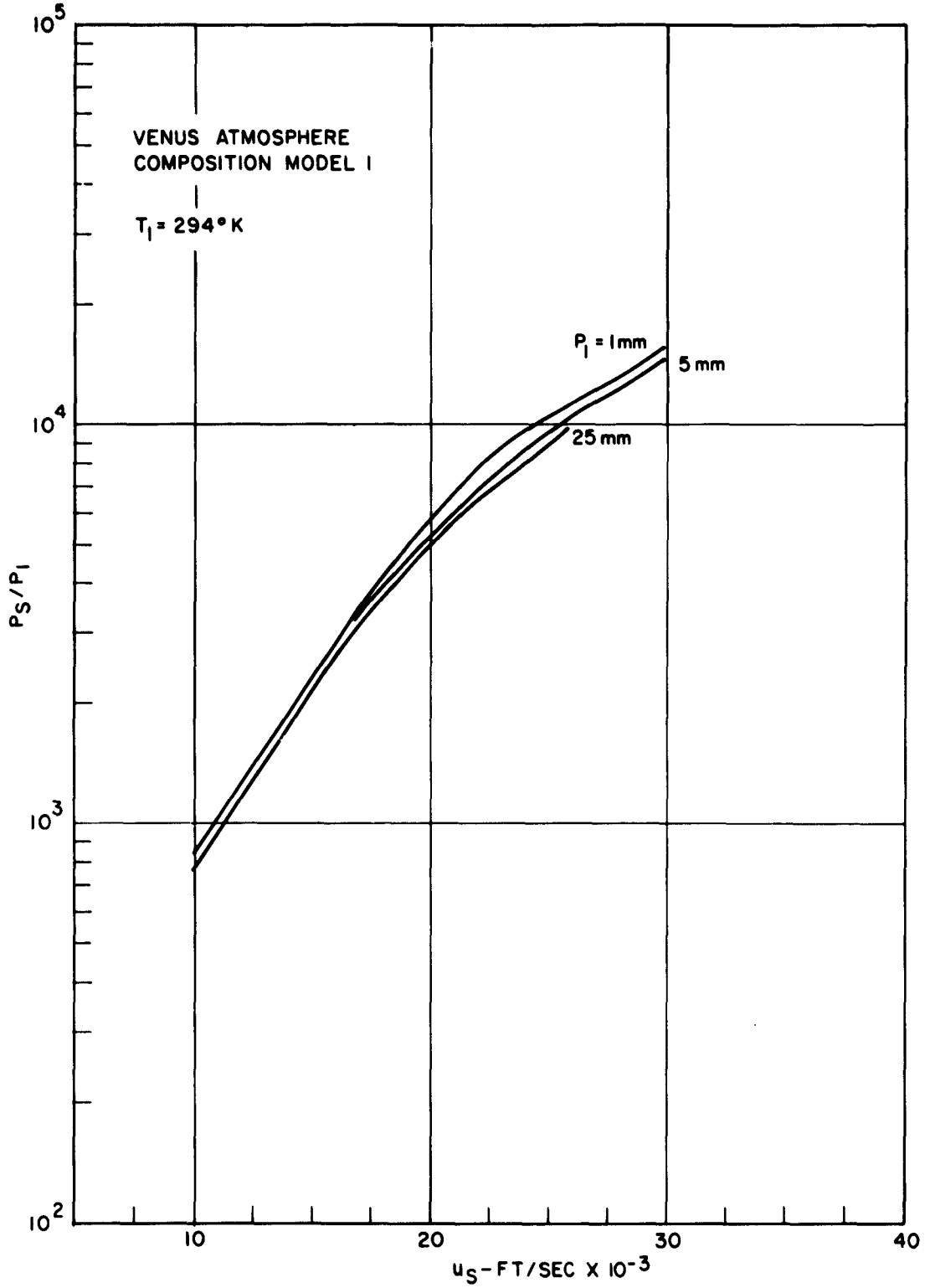

Figure 3.15 Stagnation Pressure

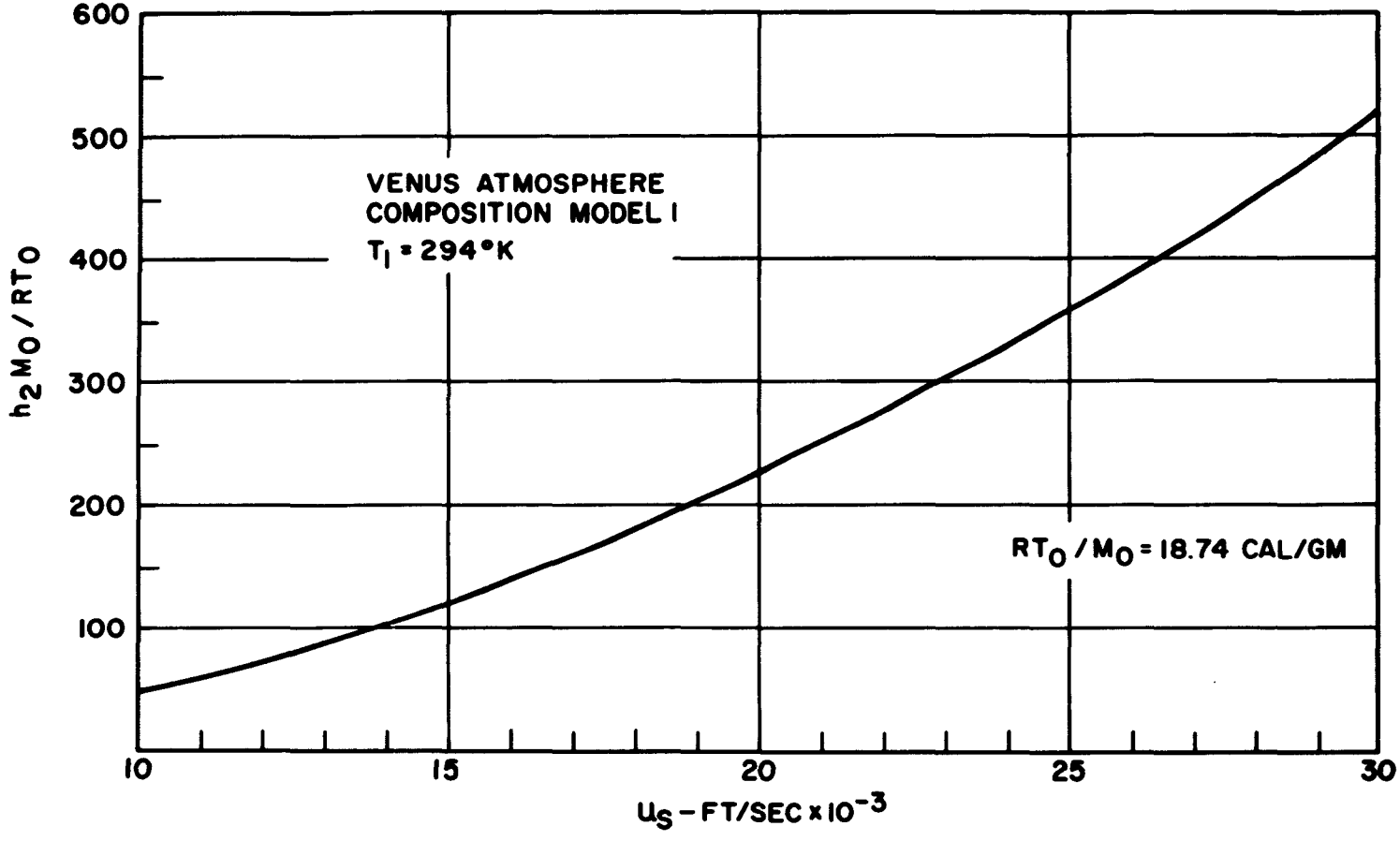

Figure 3.16 Enthalpy Behind Incident Shock

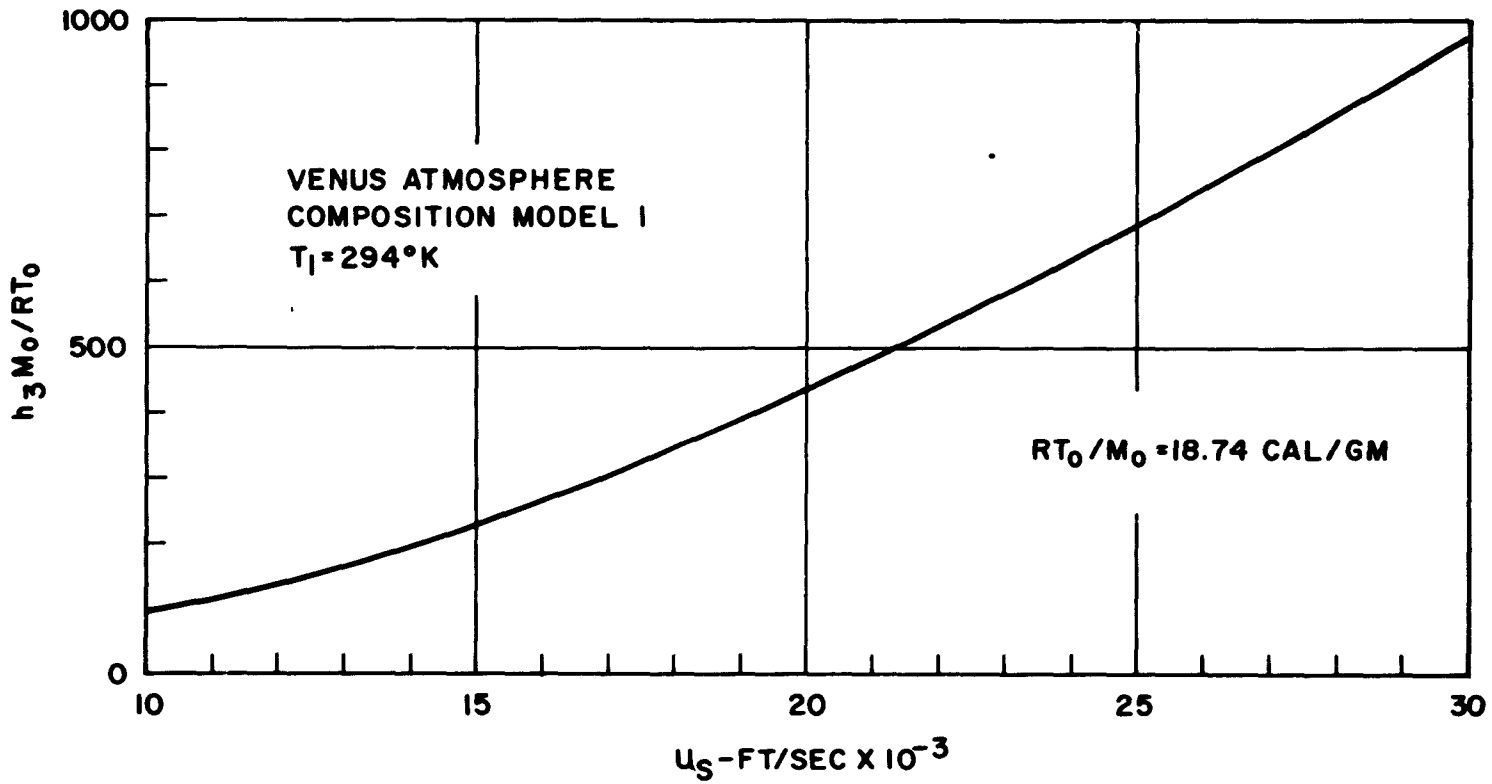

Figure 3.17 Enthalpy Behind Normal Shock

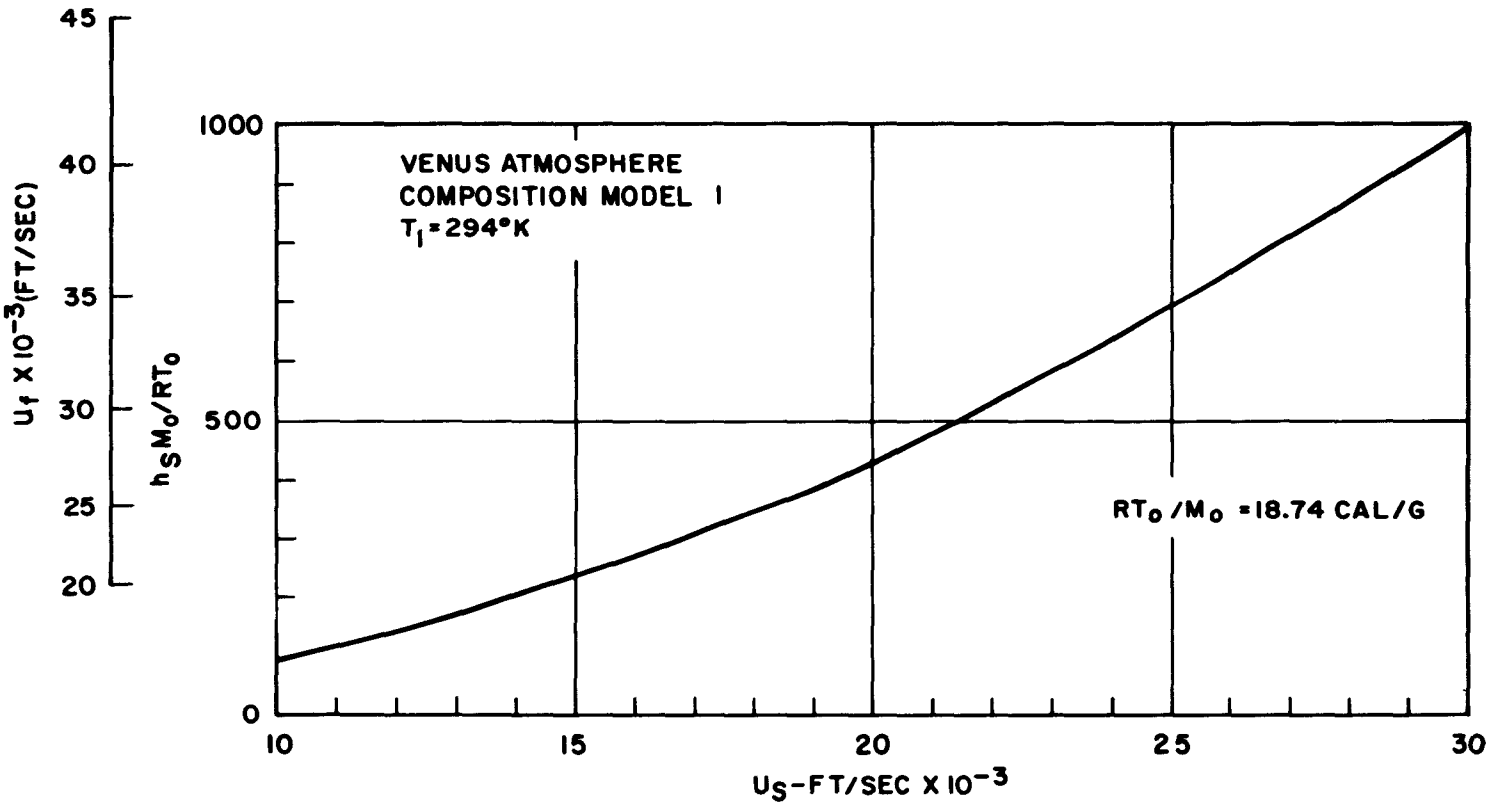

Figure 3.18 Stagnation Enthalpy

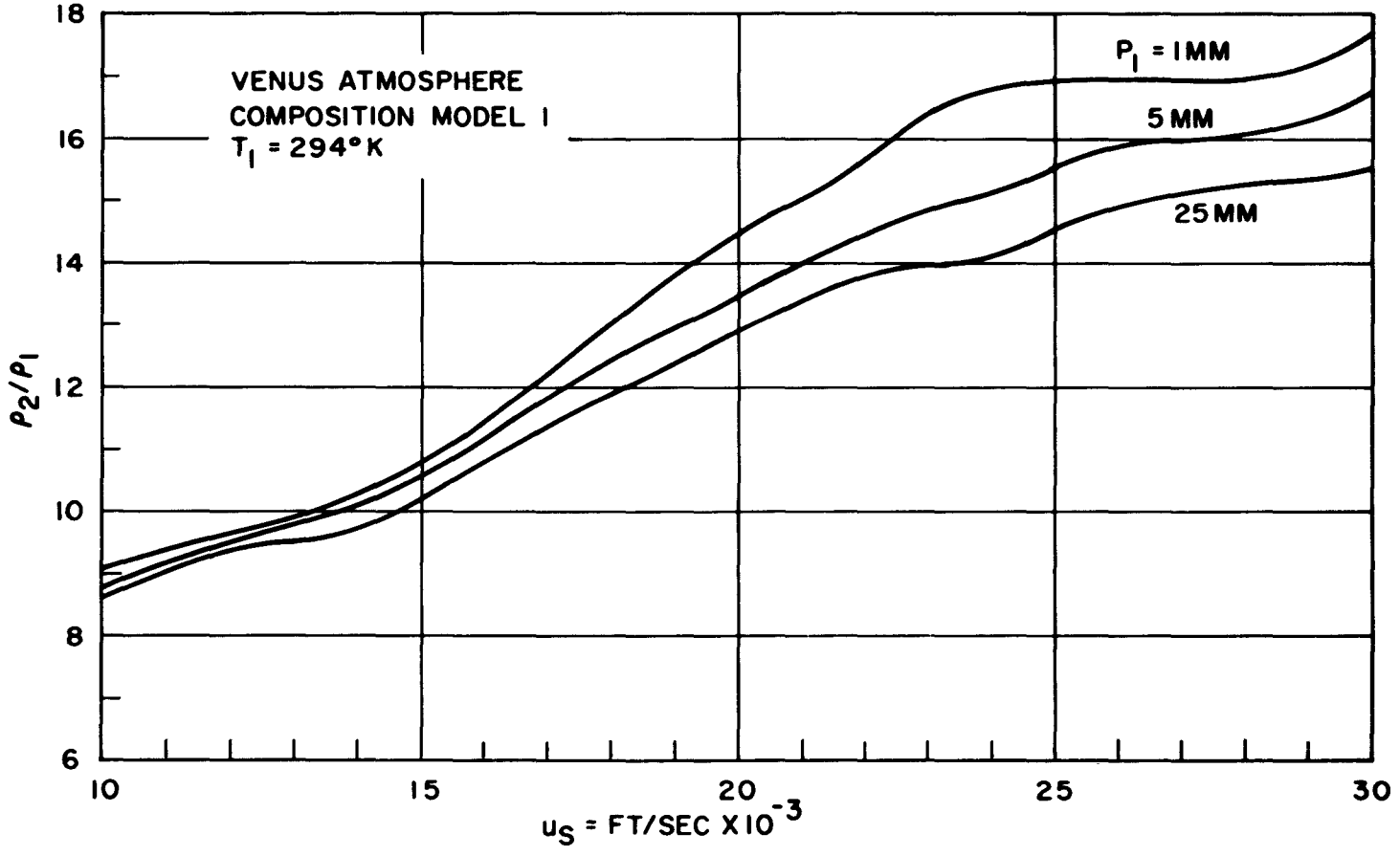

Figure 3.19 Density Behind Incident Shock

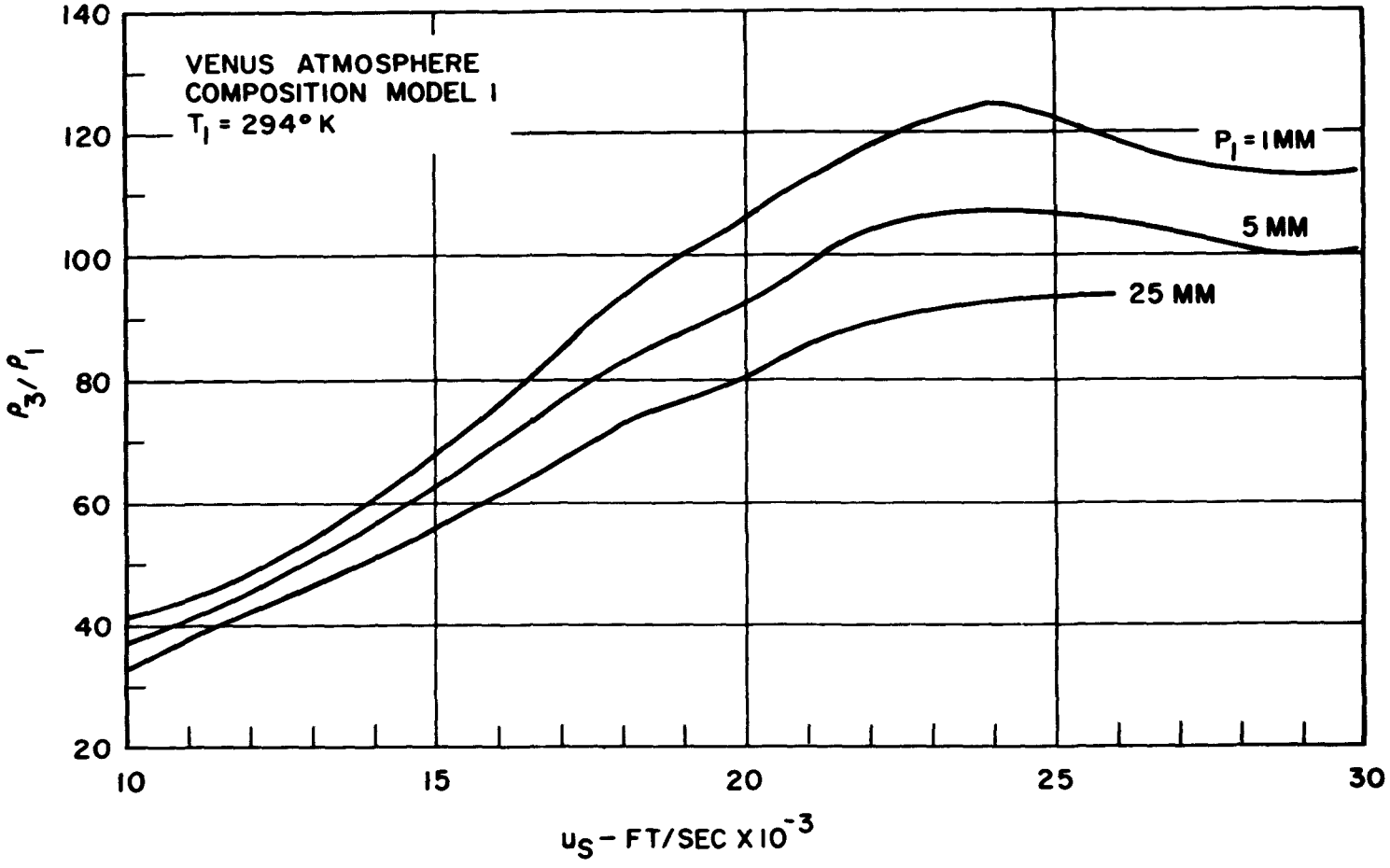

Figure 3.20 Density Behind Normal Shock

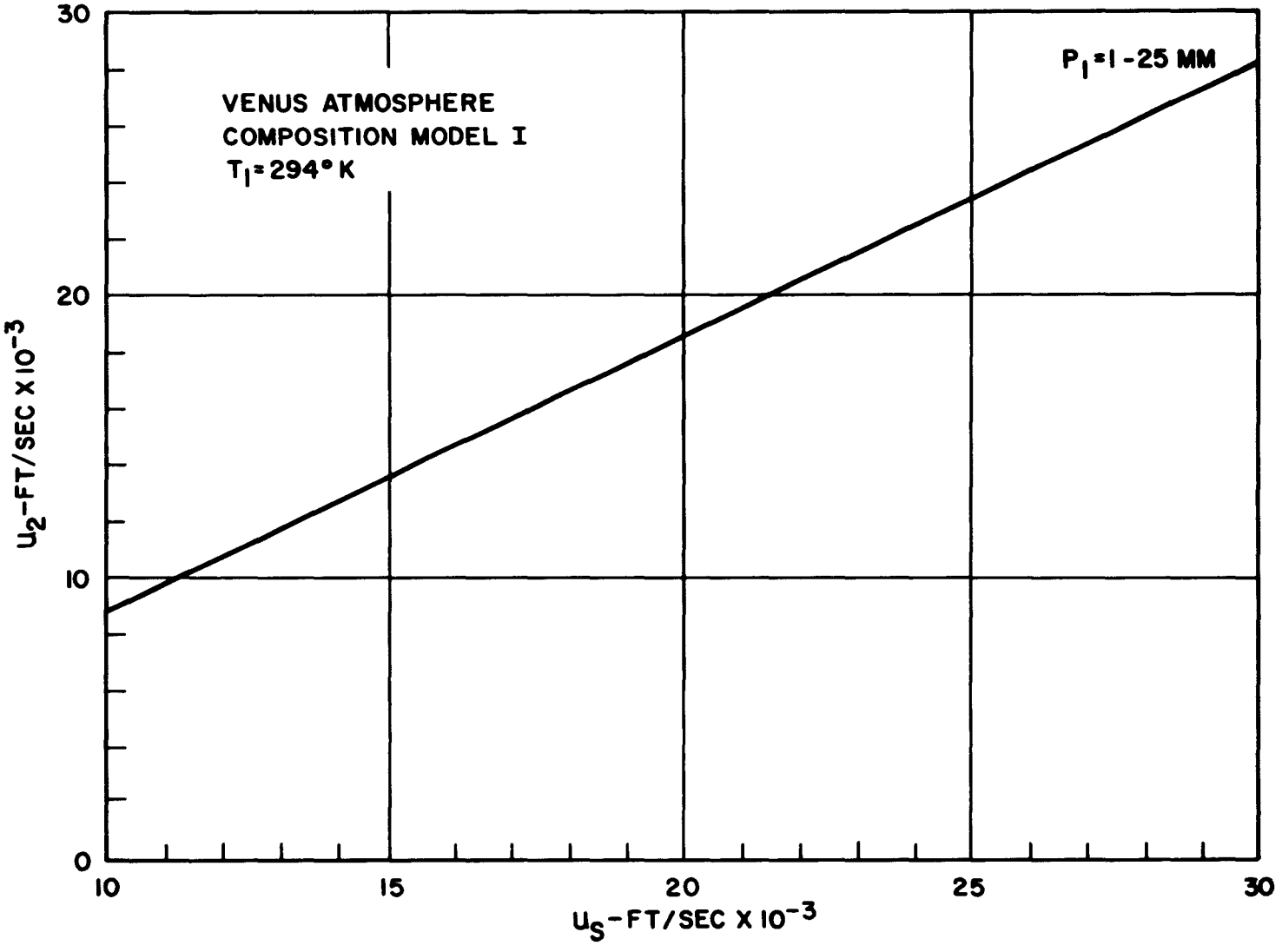

Figure 3.21 Velocity Behind Incident Shock

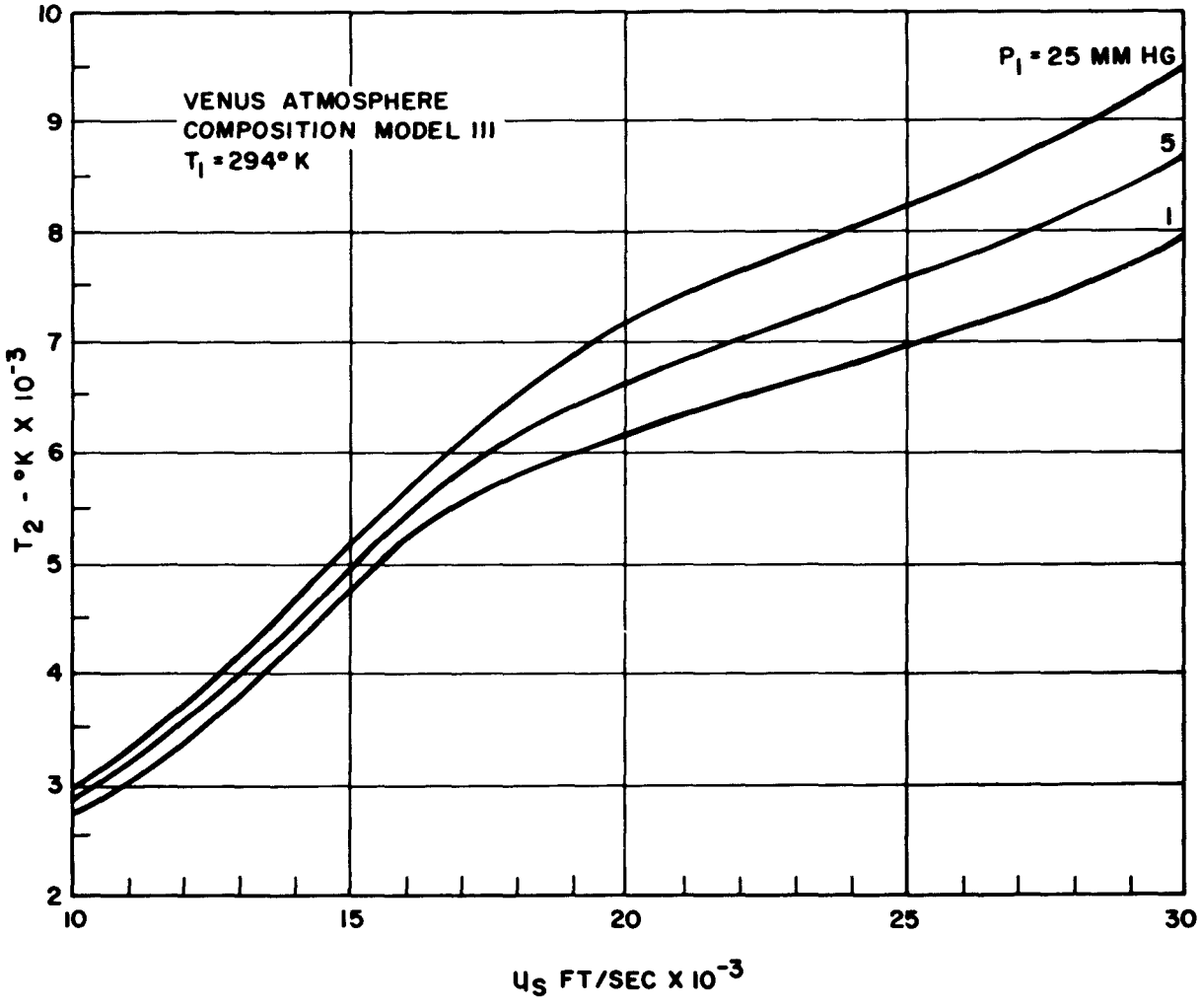

Figure 3.22 Temperature Behind Incident Shock

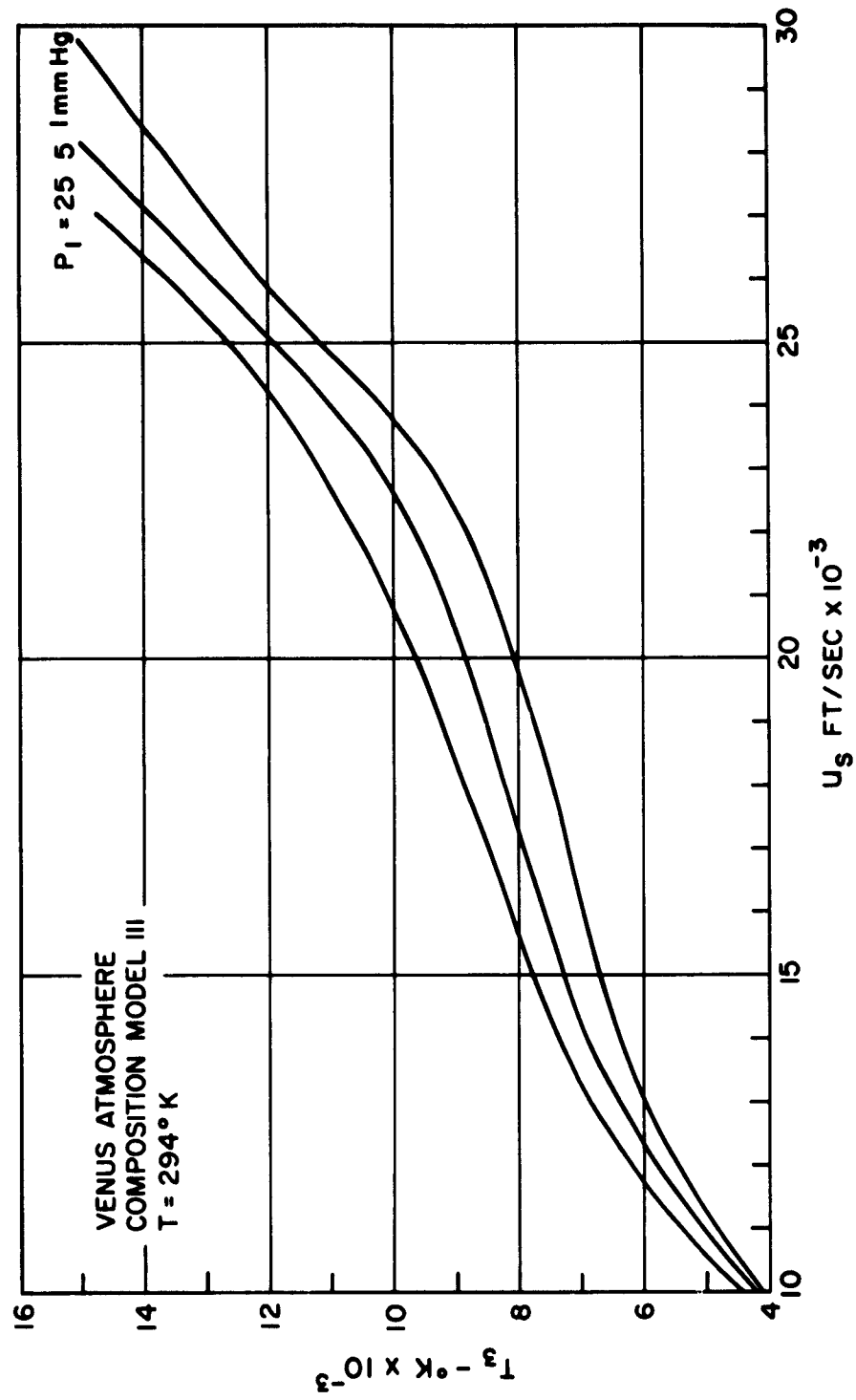

Figure 3.23 Temperature Behind Normal Shock

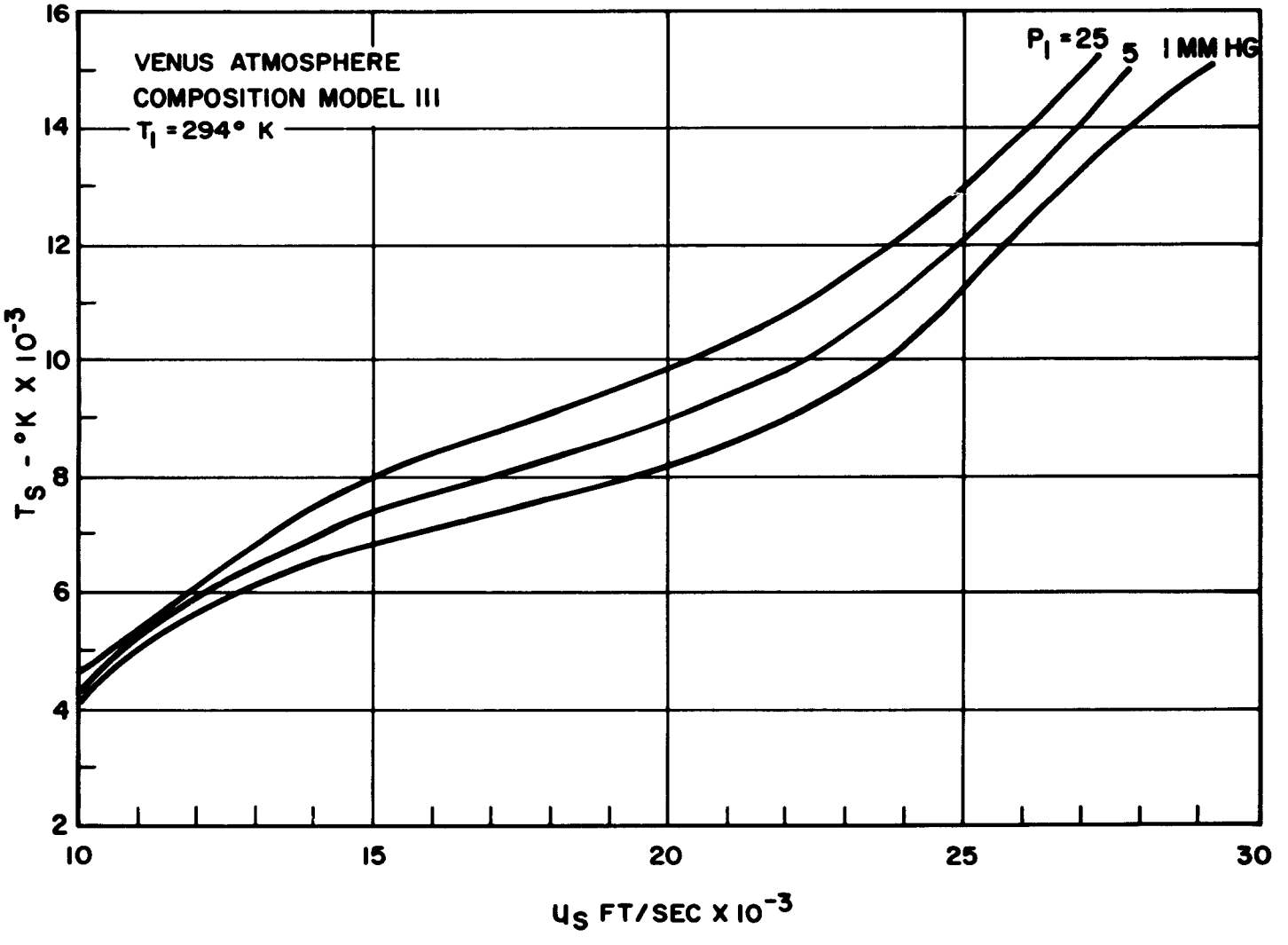

Figure 3.24 Stagnation Temperature

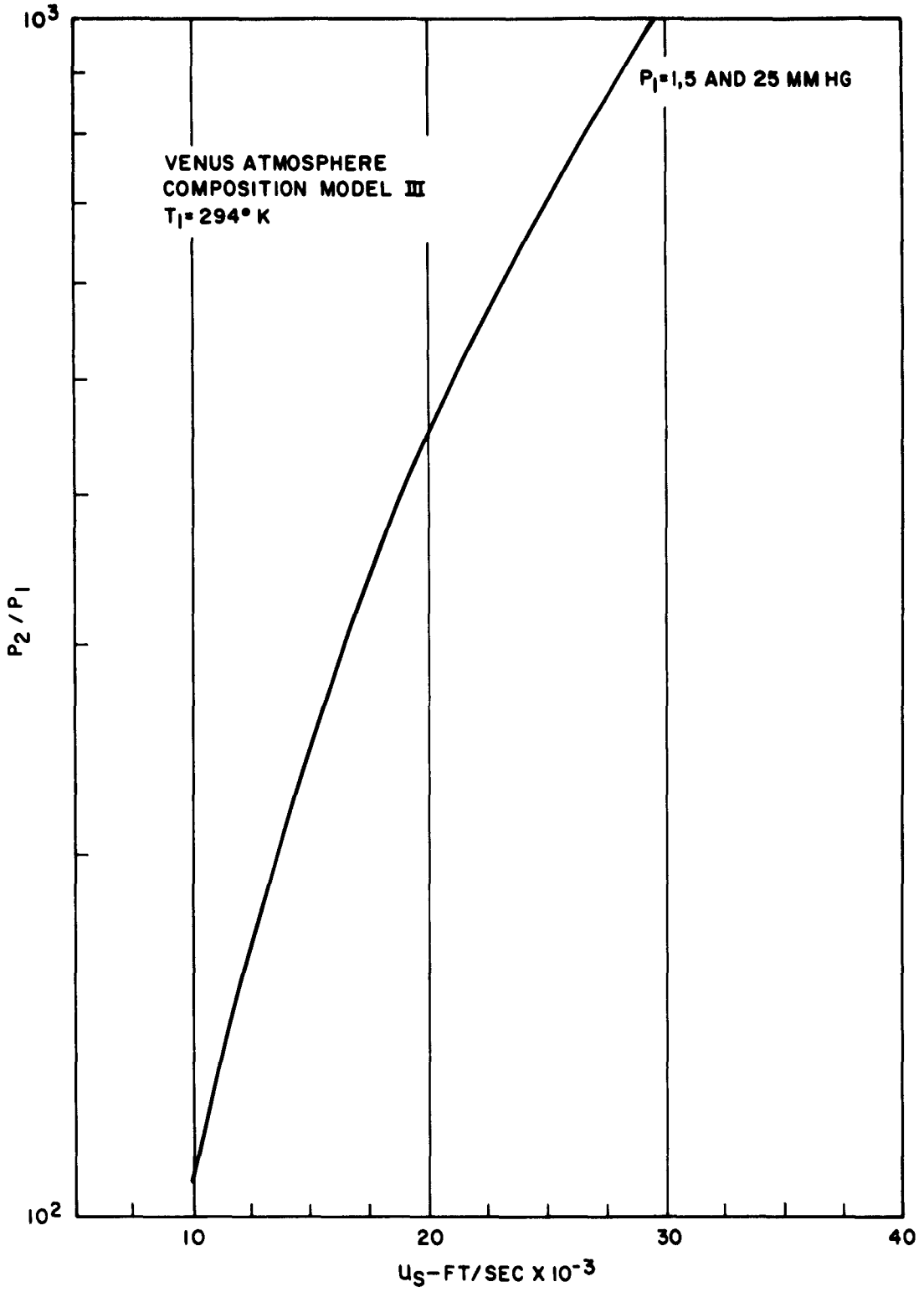

Figure 3.25 Pressure Behind Incident Shock

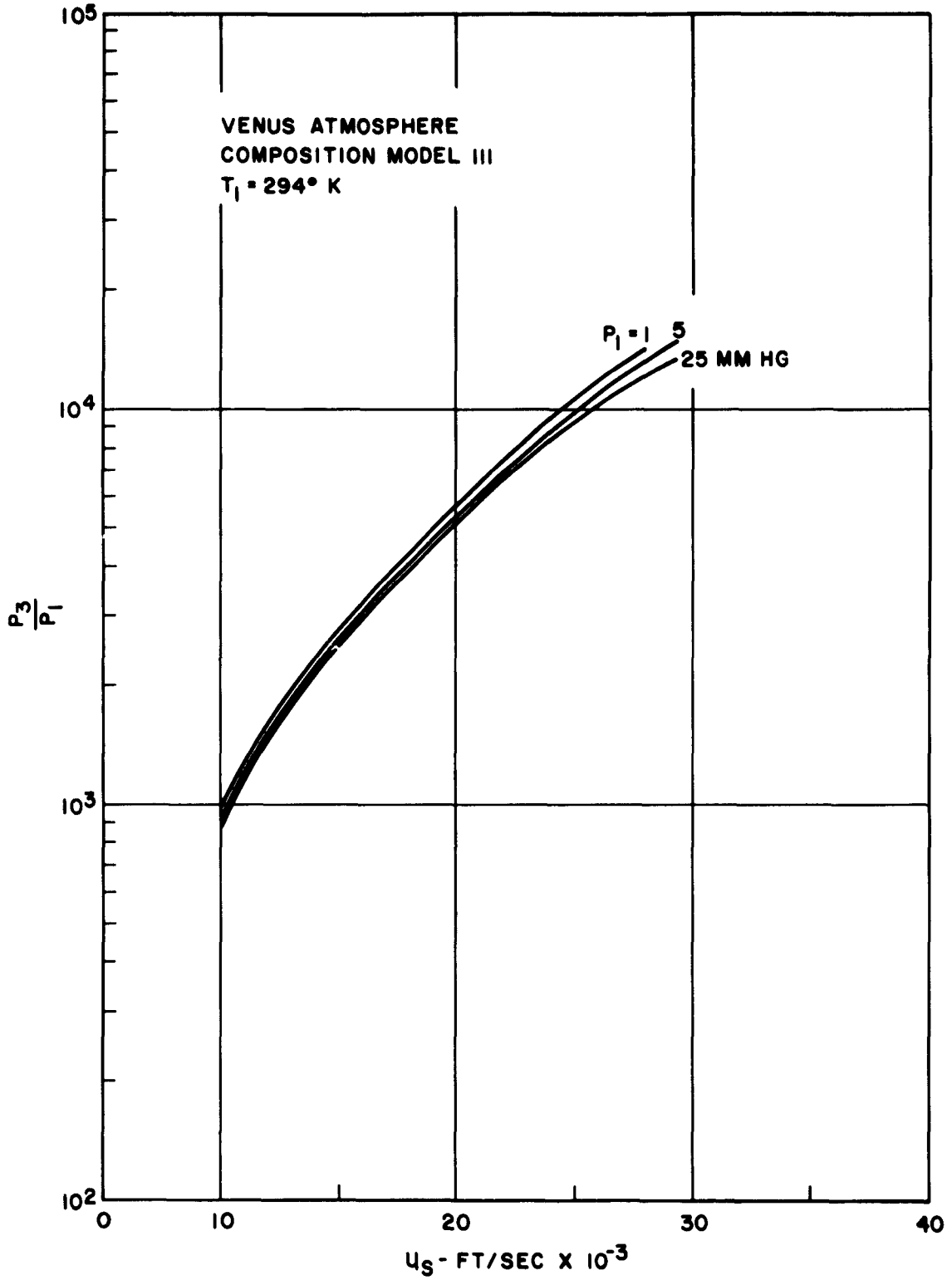

Figure 3.26 Pressure Behind Normal Shock

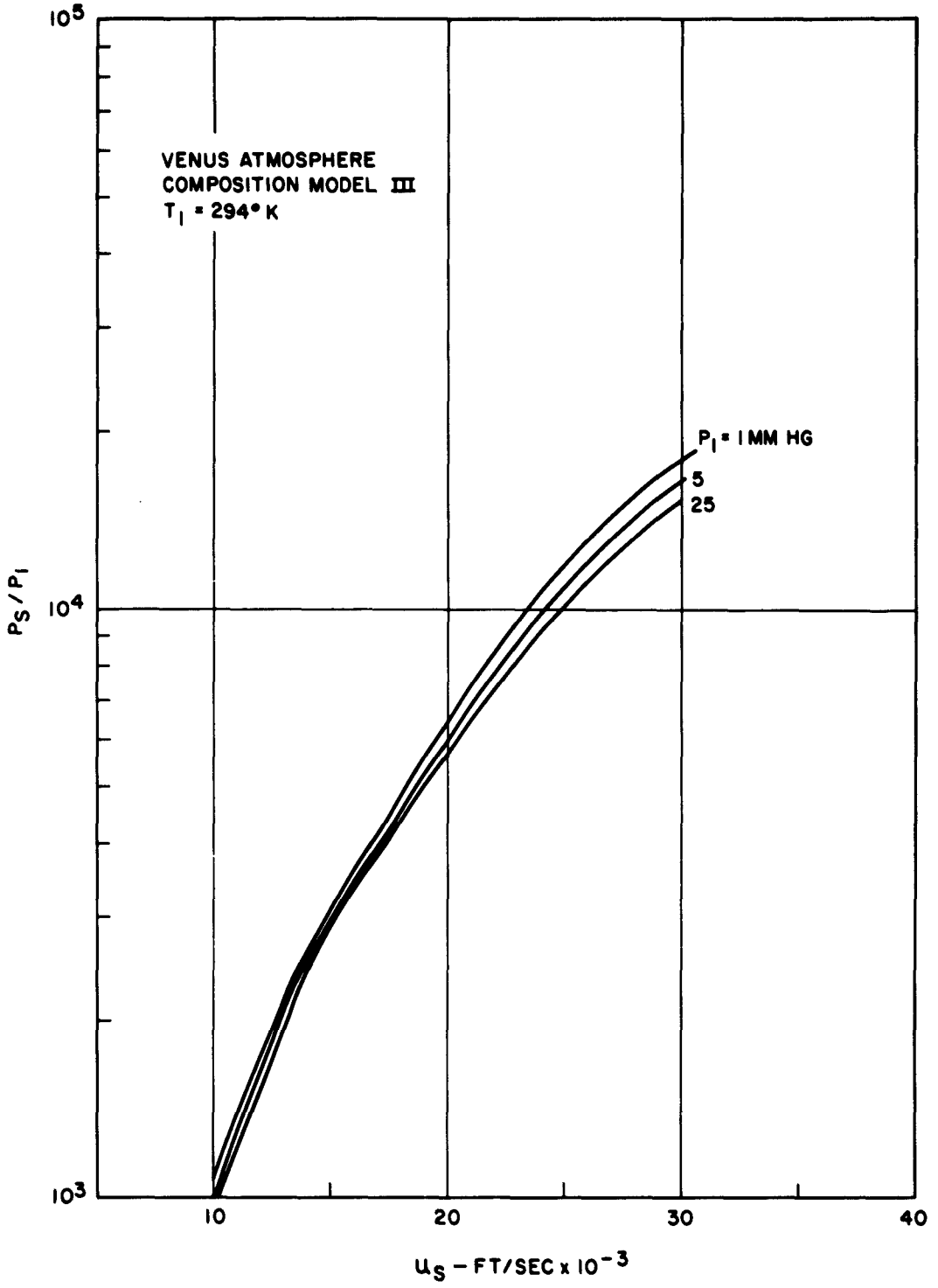

Figure 3.27 Stagnation Pressure

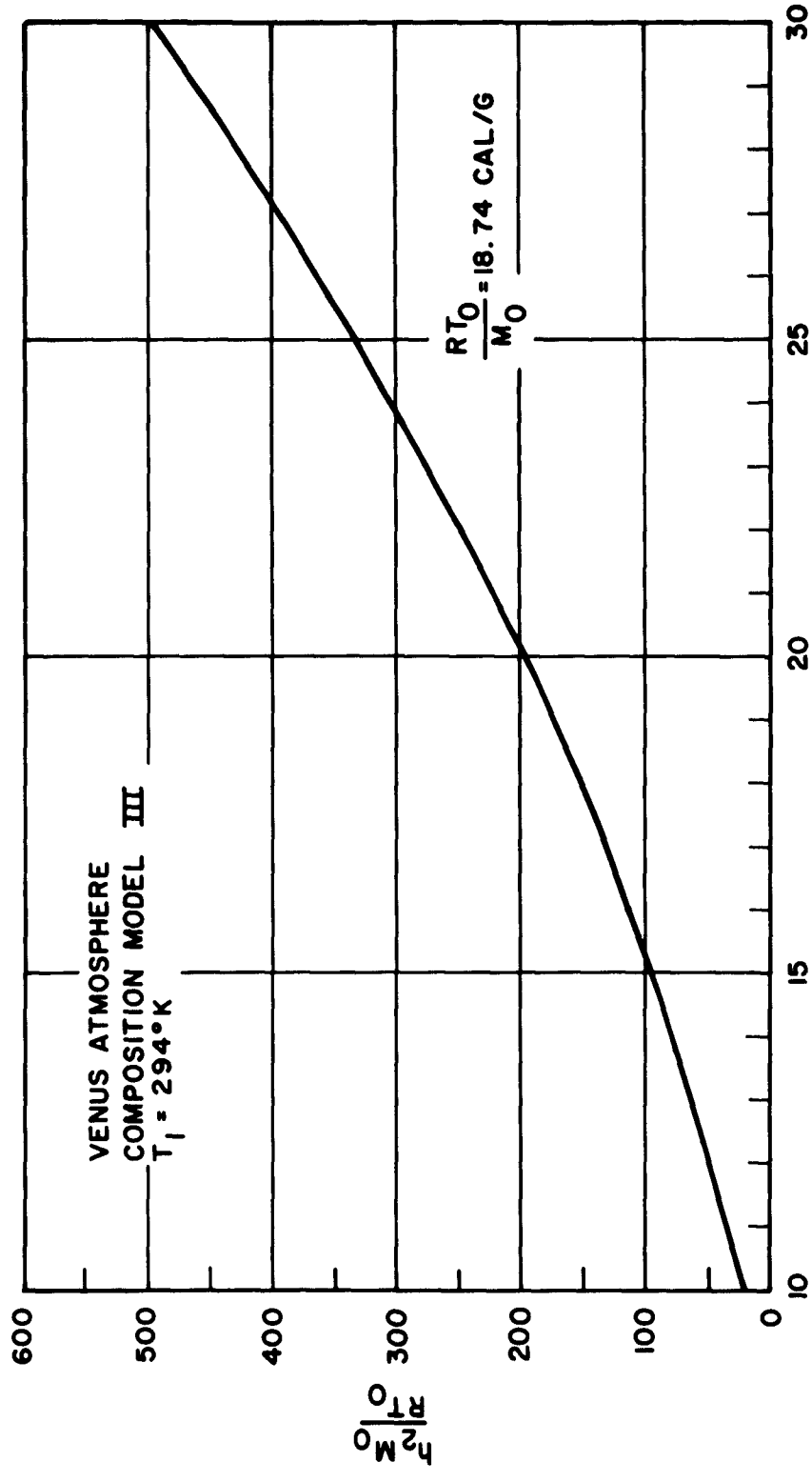

Figure 3.28 Enthalpy Behind Incident Shock

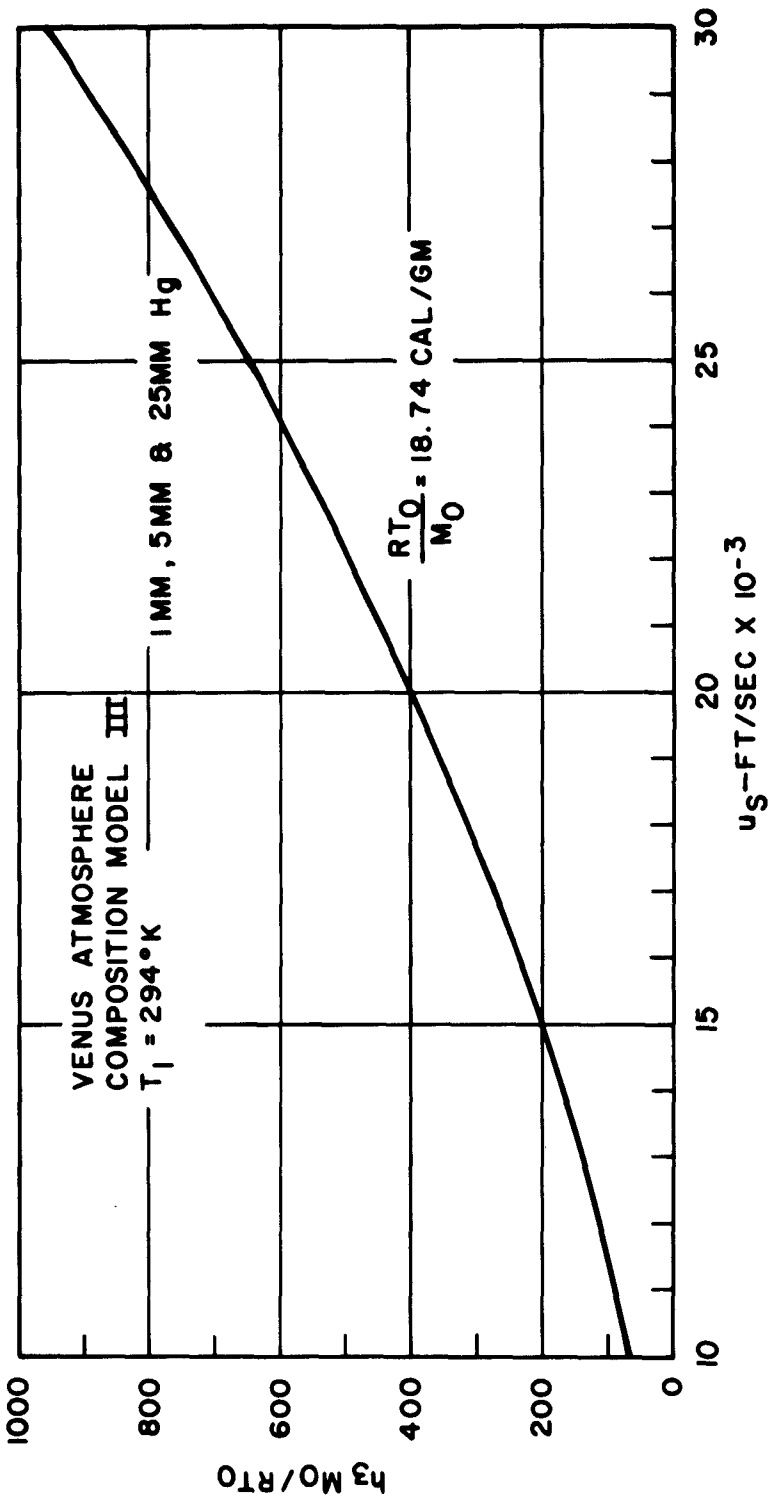

Figure 3.29 Enthalpy Behind Normal Shock

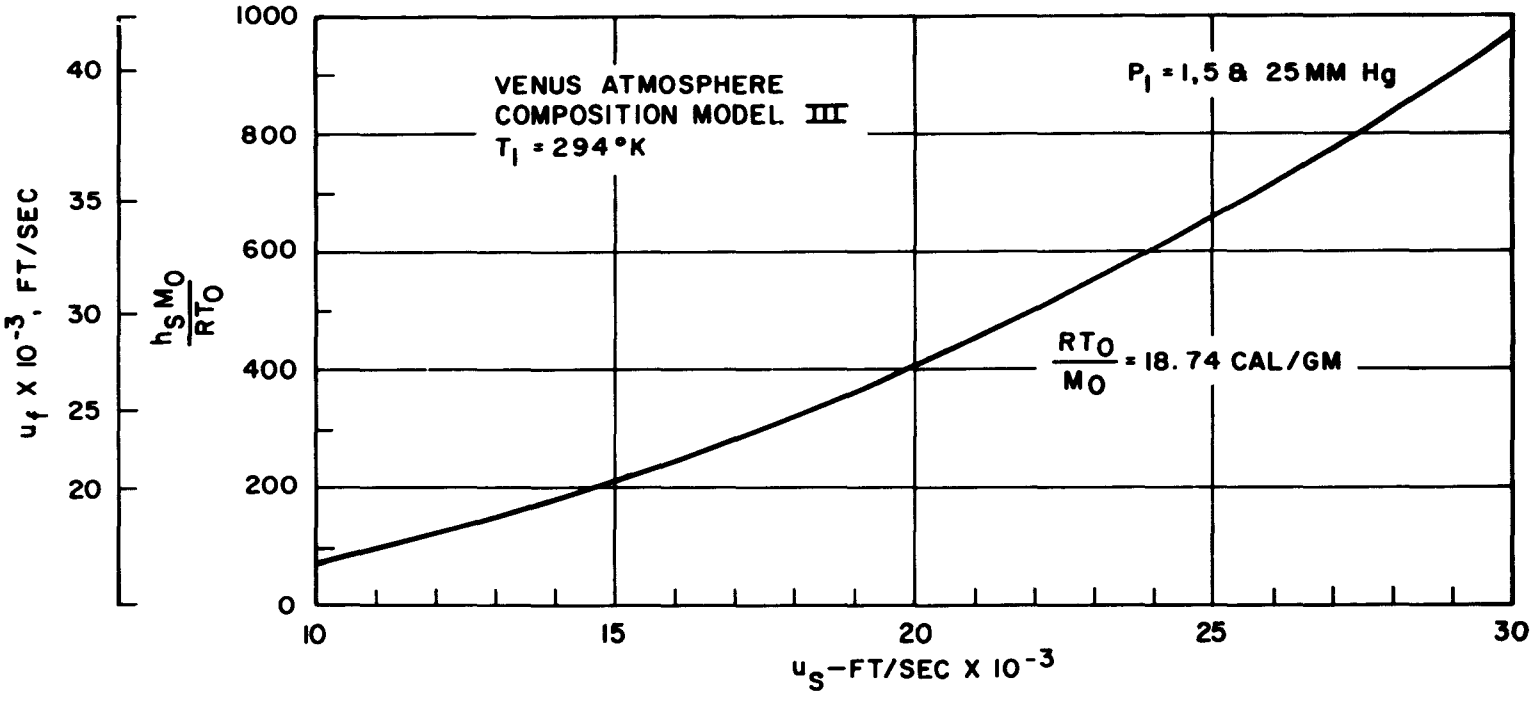

Figure 3.30 Stagnation Enthalpy

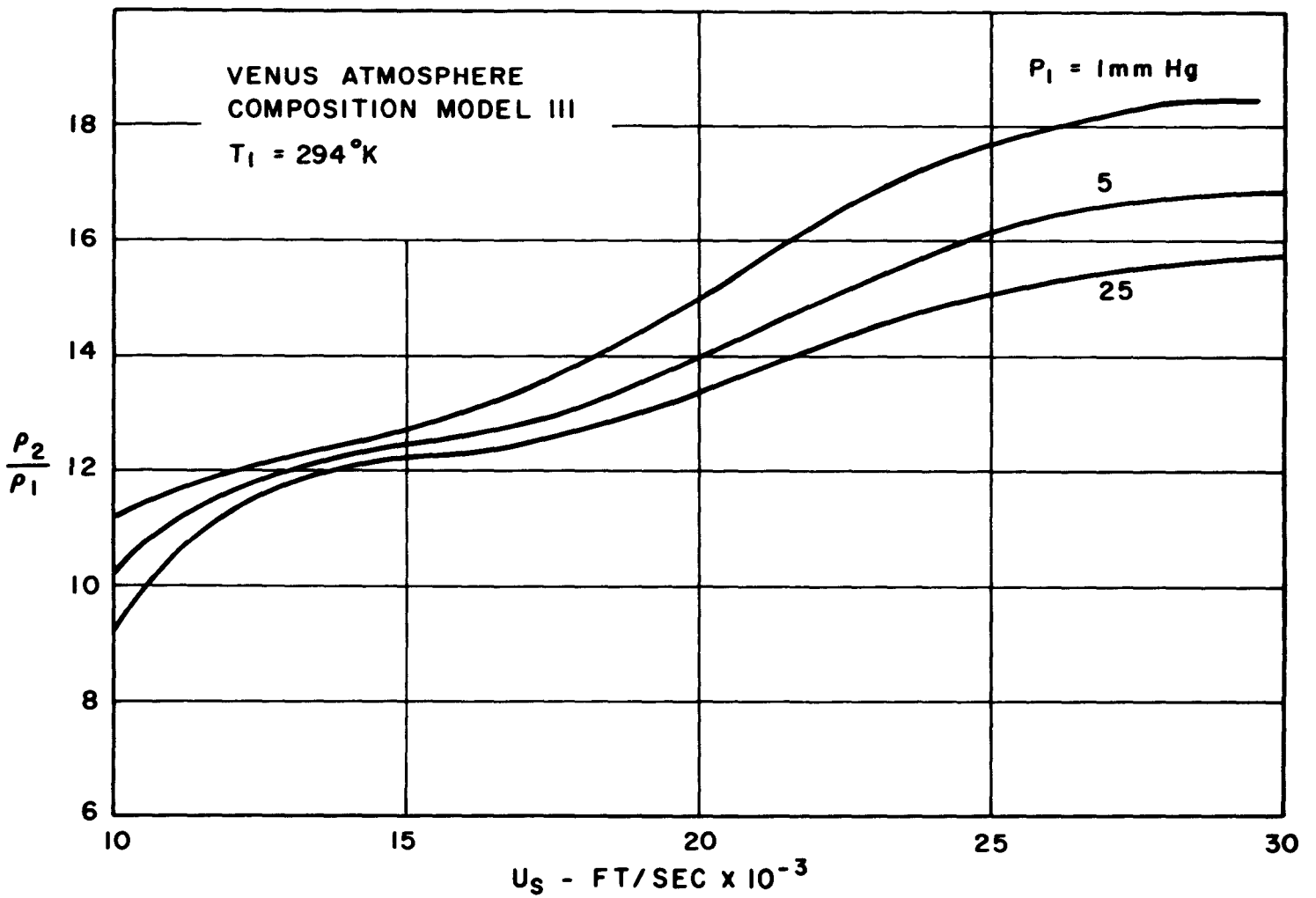

Figure 3.31 Density Behind Incident Shock

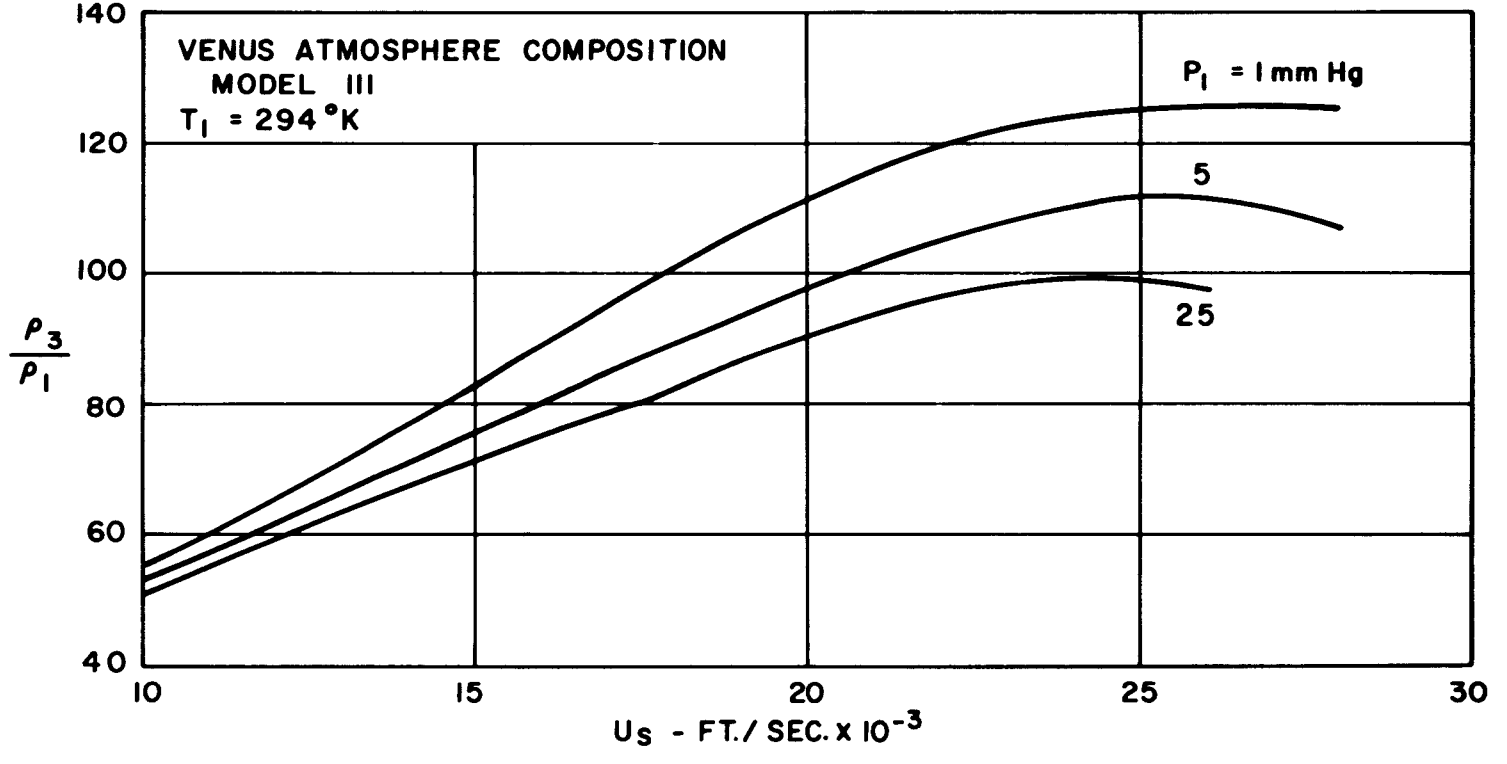

Figure 3.32 Density Behind Normal Shock

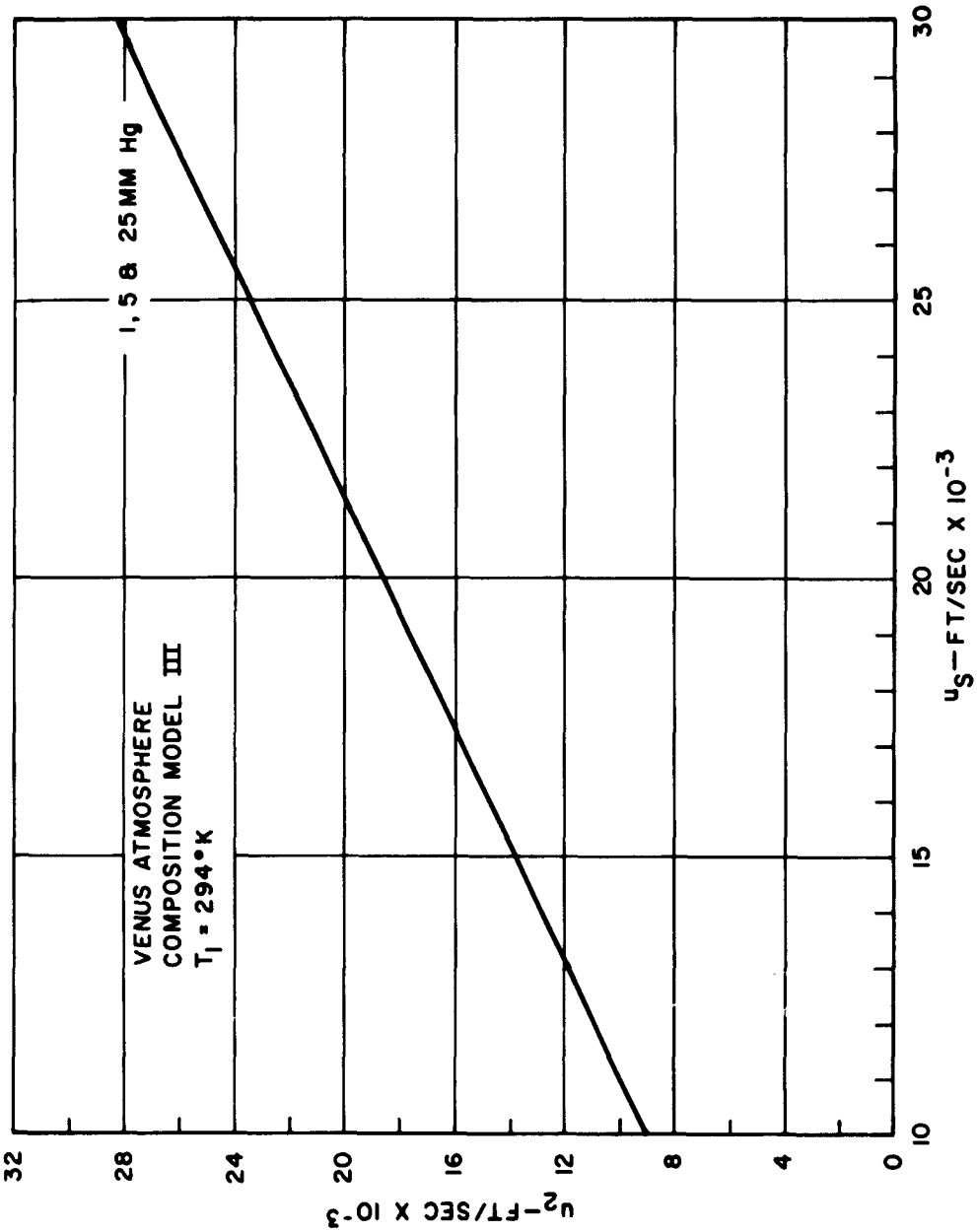

Figure 3.33 Velocity Behind Incident Shock

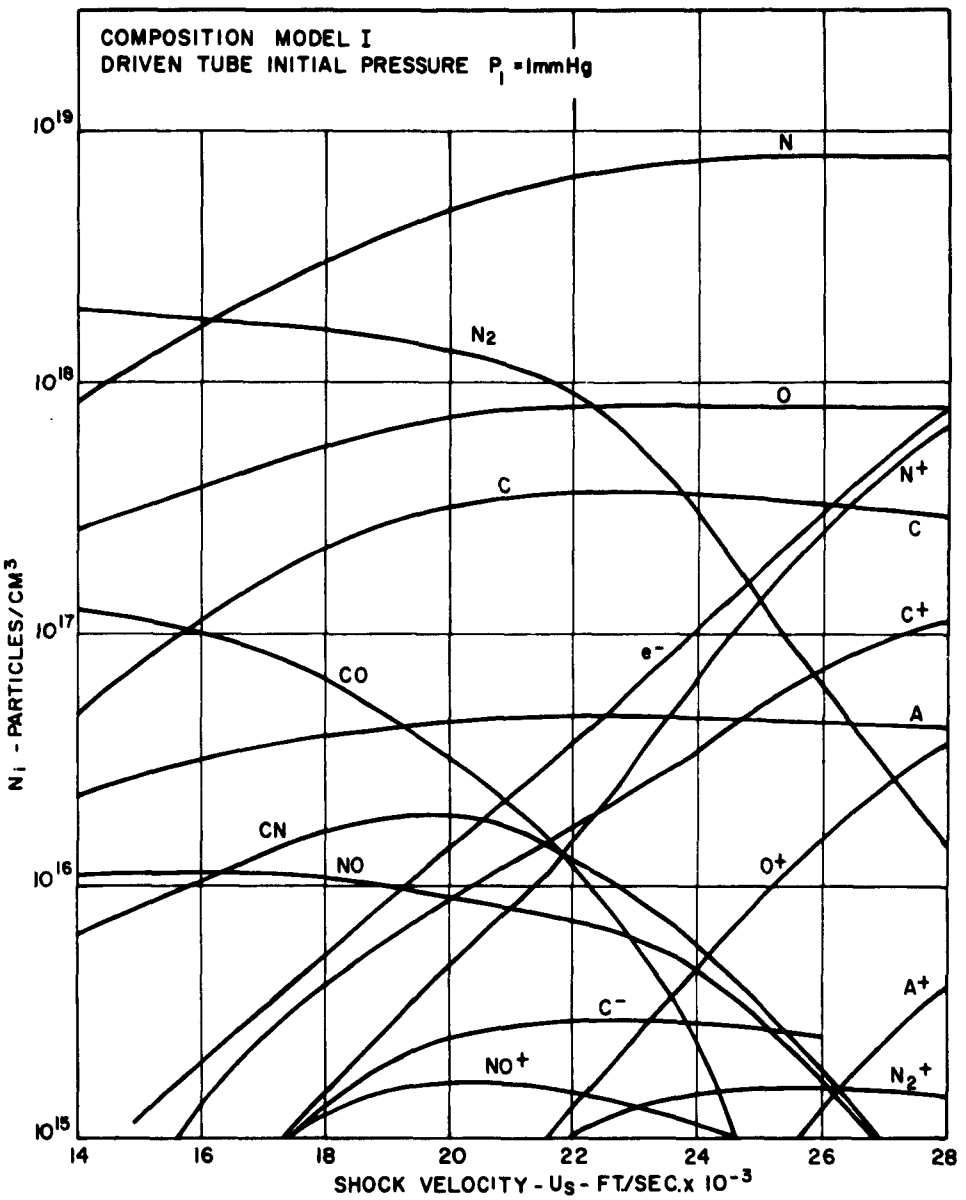

Figure 3.34 Equilibrium Composition of Venus Atmosphere at Stagnation Point of a Hemispherical Model

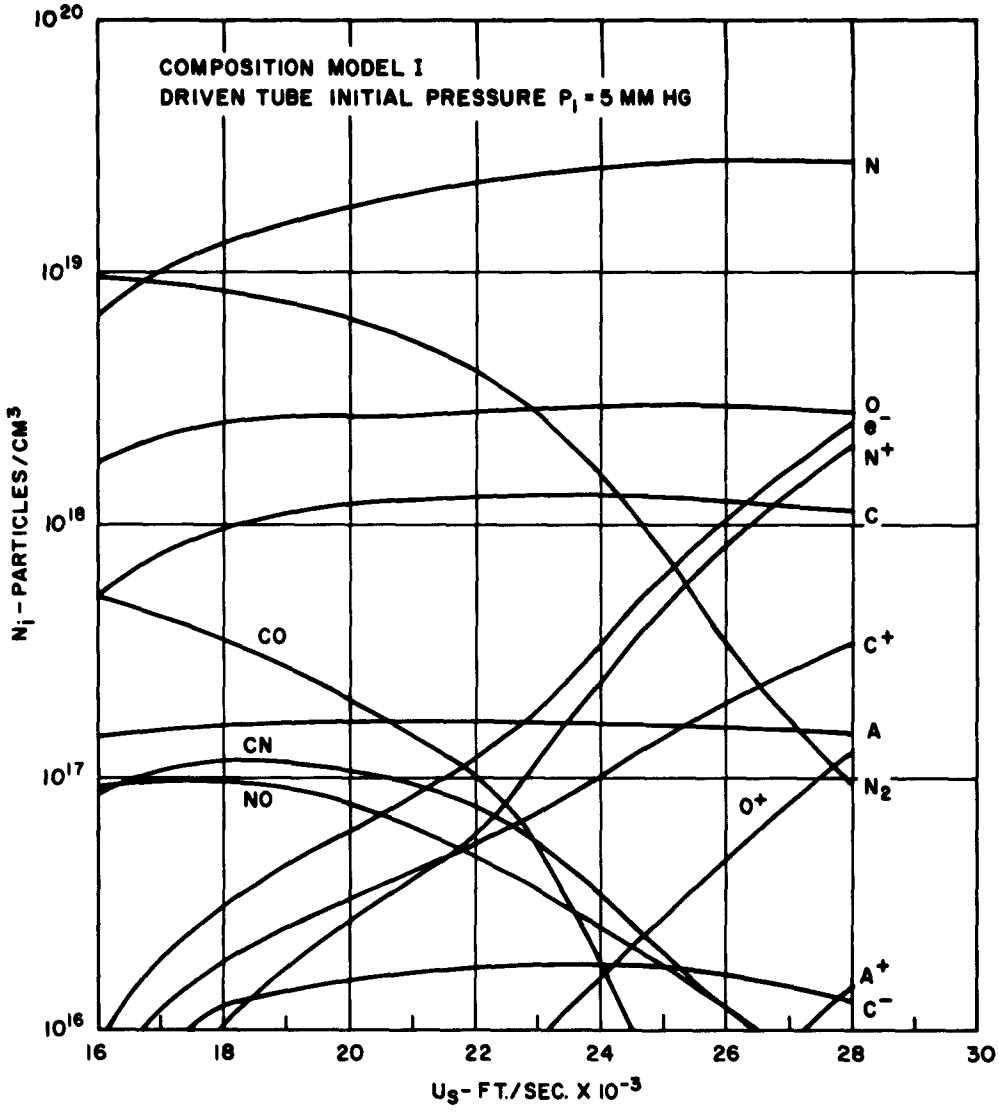

Figure 3.35 Equilibrium Composition of Venus Atmosphere at Stagnation Point of a Hemispherical Model

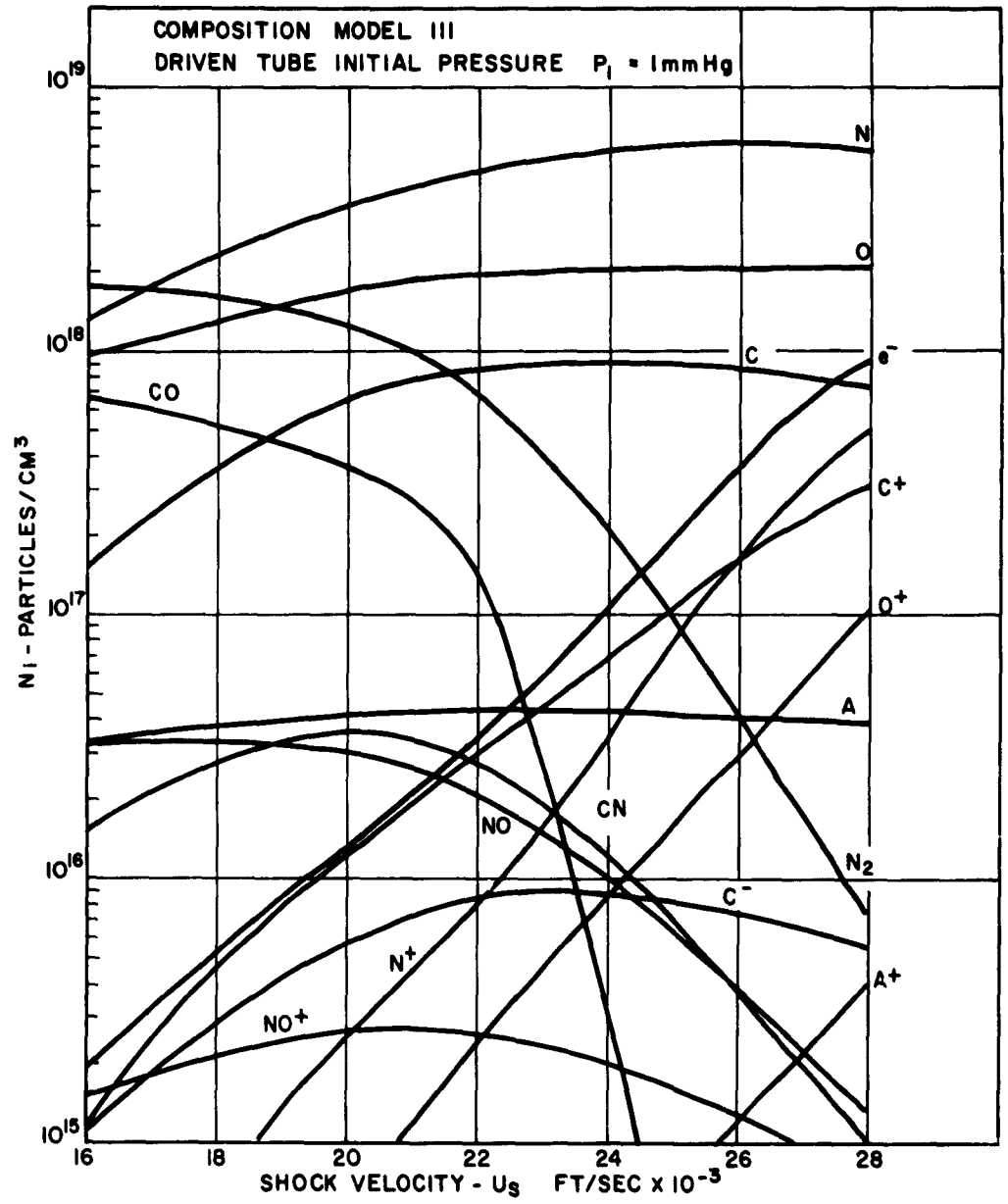

Figure 3.36 Equilibrium Composition of Venus Atmosphere at Stagnation Point of a Hemispherical Model

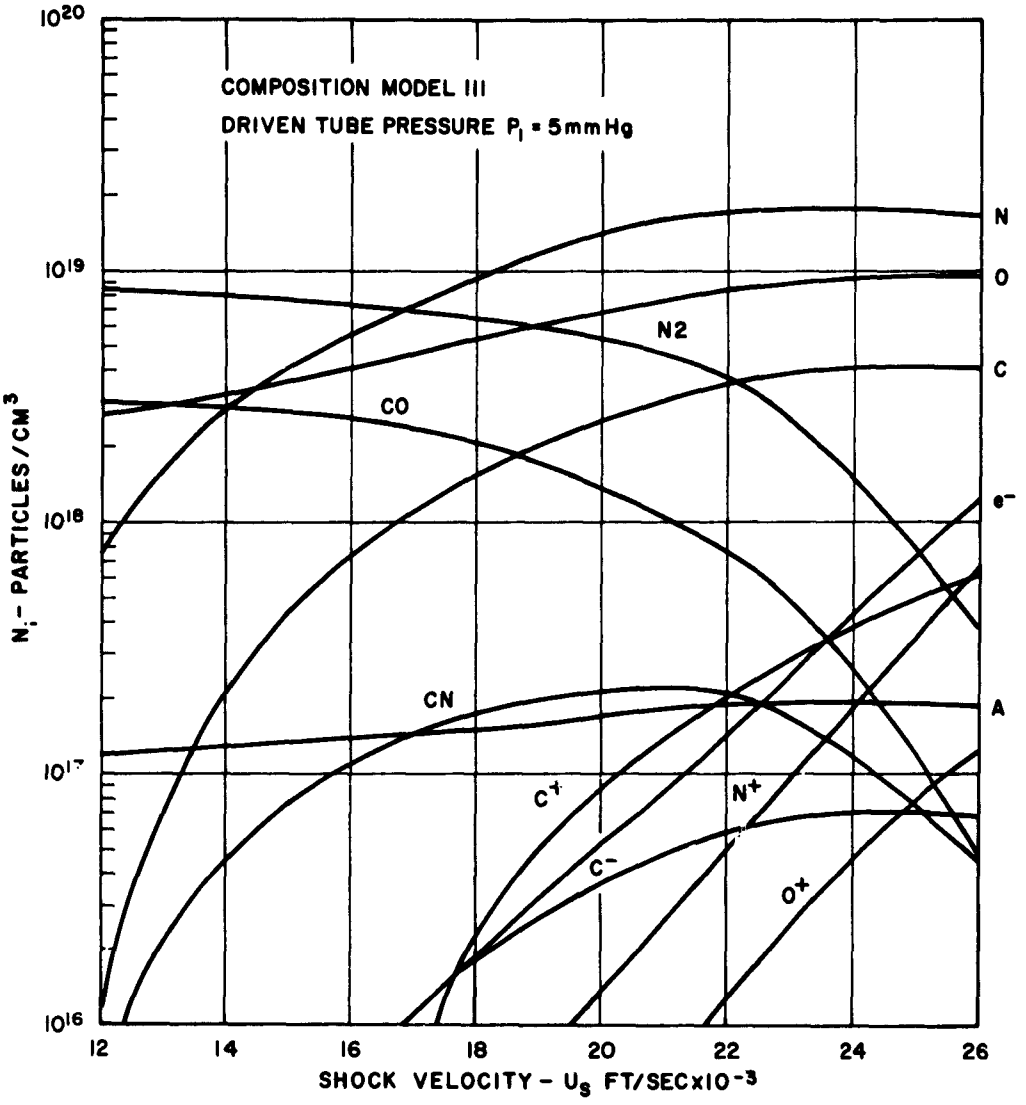

Figure 3.37 Equilibrium Composition of Venus Atmosphere at Stagnation Point of a Hemispherical Model

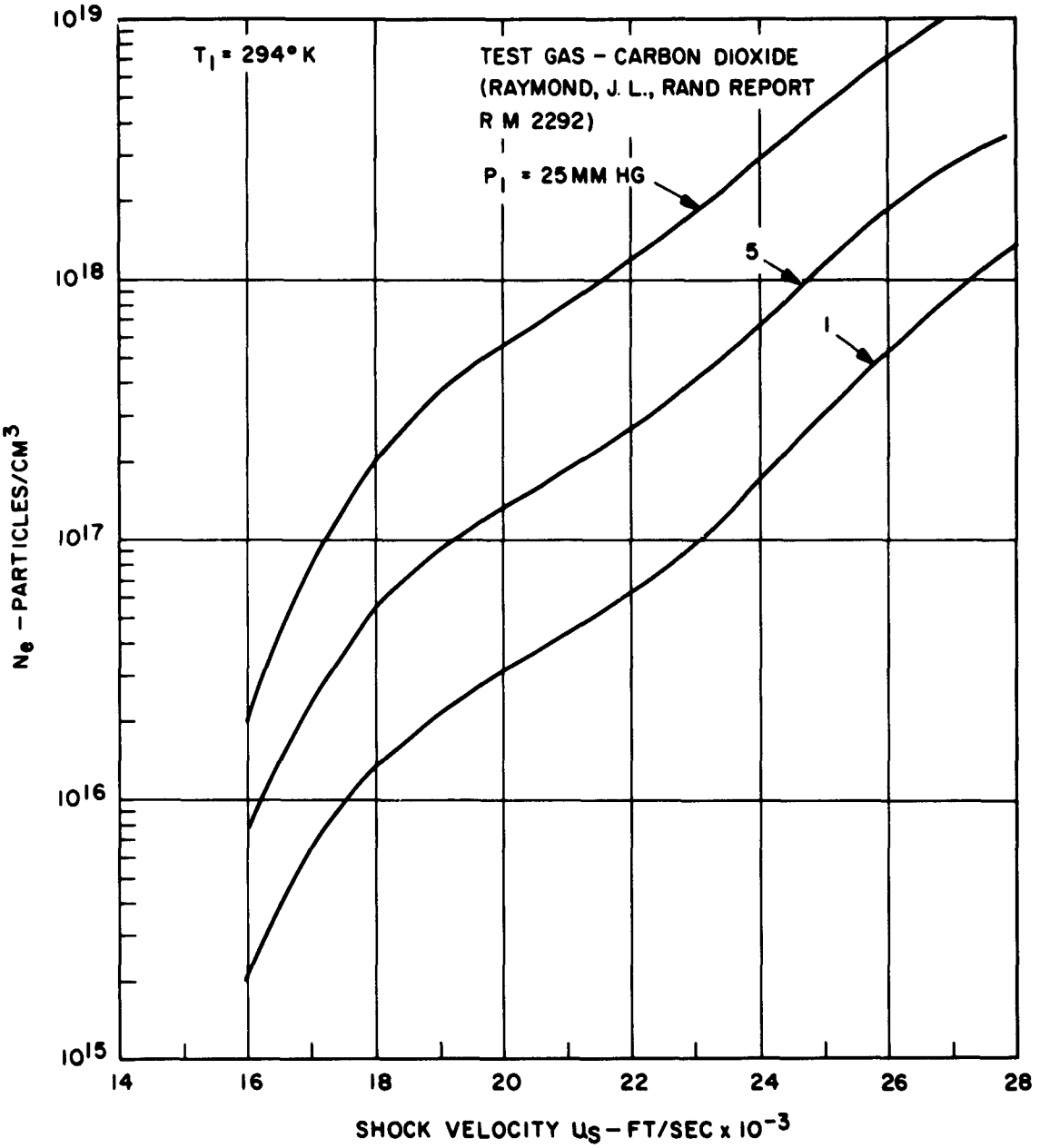

Figure 3.38 Equilibrium Concentration of Electrons at the Stagnation Point of a Hemispherical Model

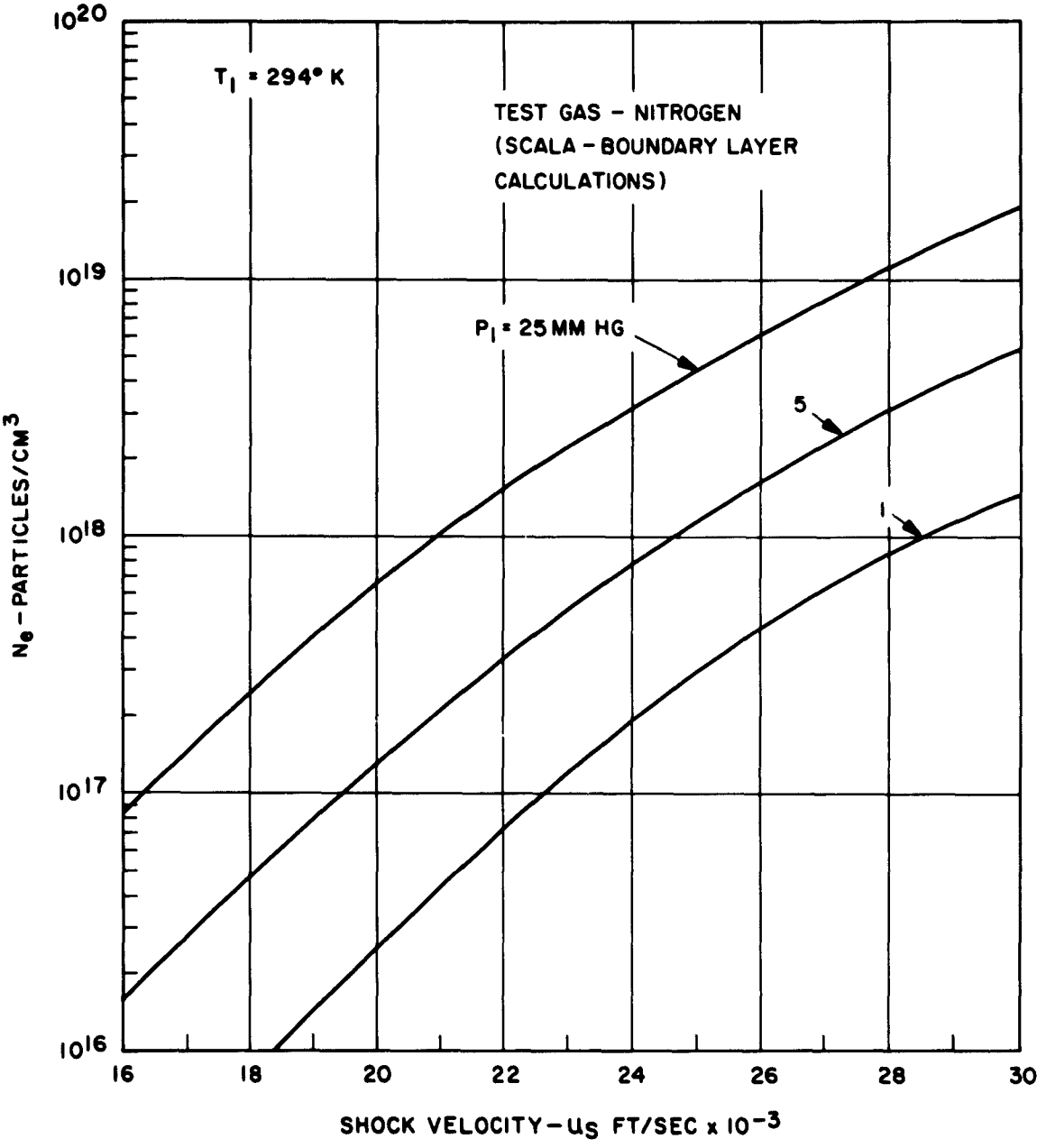

Figure 3.39 Equilibrium Concentration of Electrons at the Stagnation Point of a Hemispherical Model

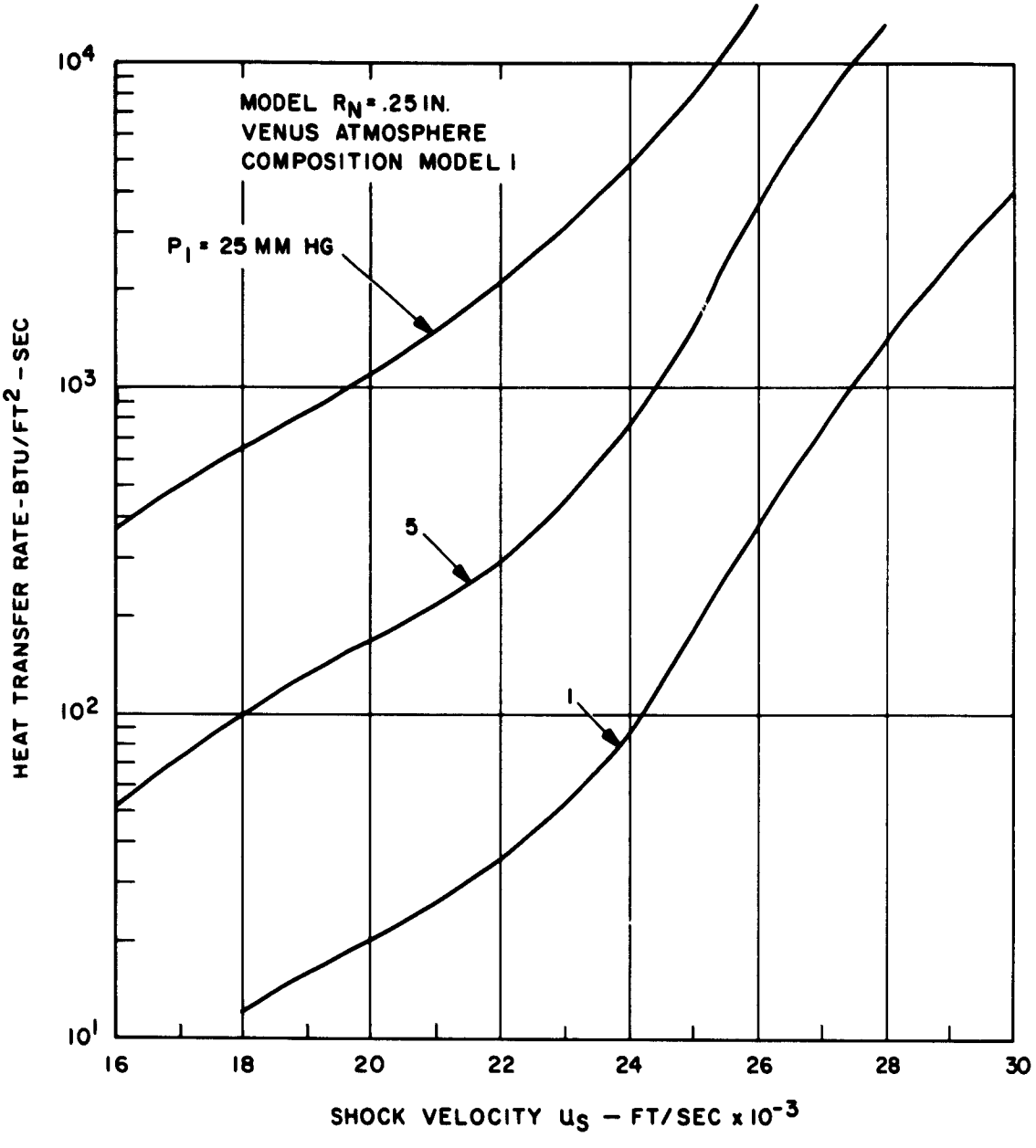

Figure 3.40 Equilibrium Radiative Heat Transfer to the Stagnation Point

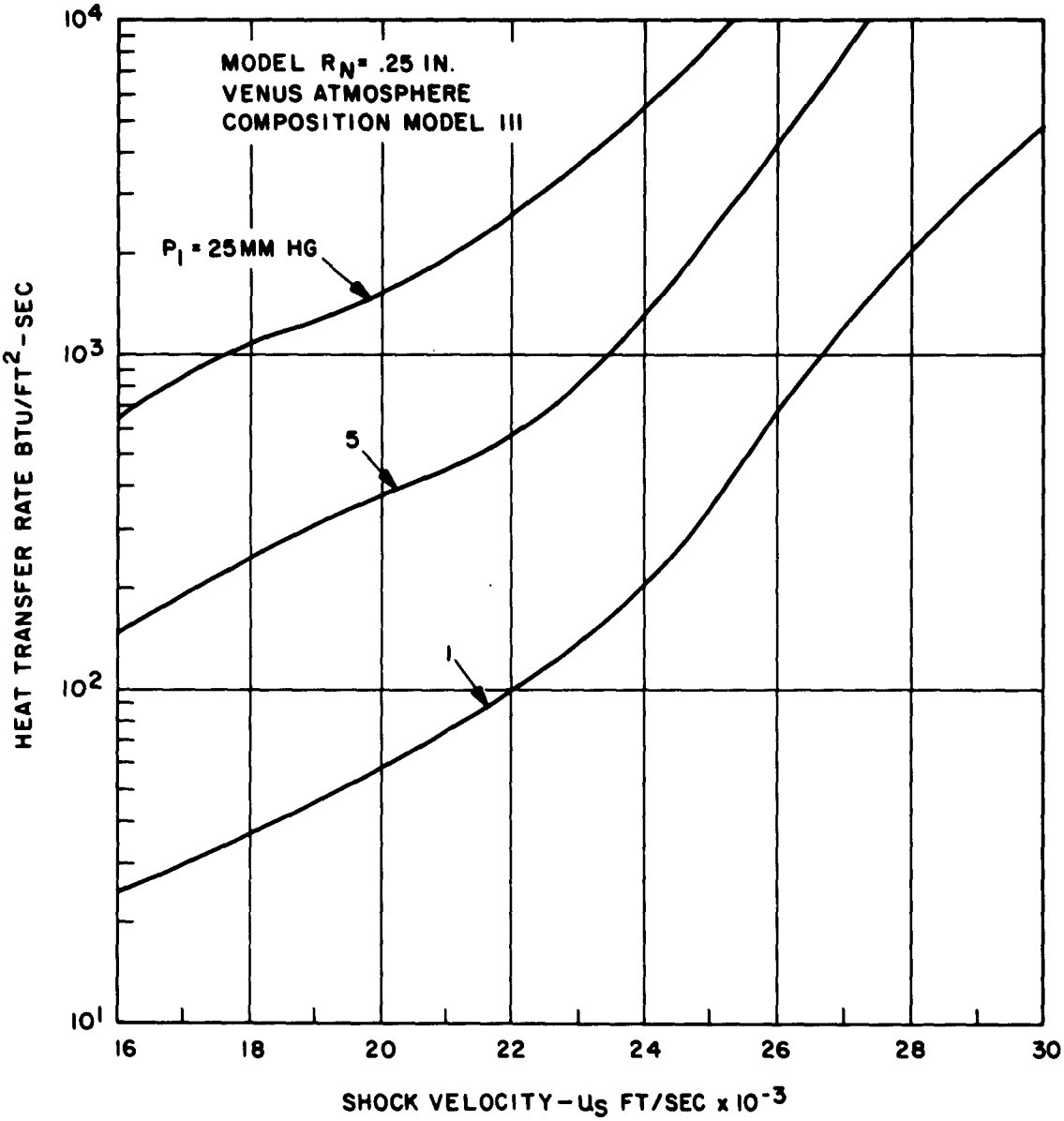

Figure 3.41 Equilibrium Radiative Heat Transfer to the Stagnation Point

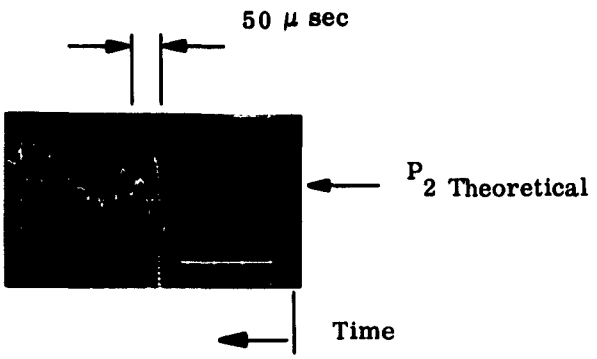

u_s = 20300 Ft/sec

P_1 = 5 mm Hg

P_2 = 45 psi

Figure 3.42 Oscillogram of Pressure Behind Incident Shock (Signal Unfiltered)

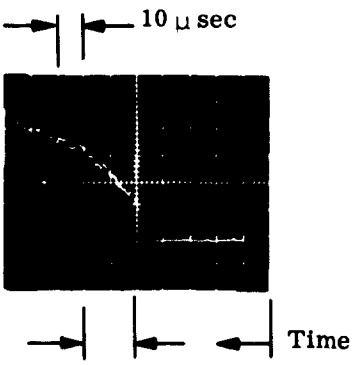

Test Time

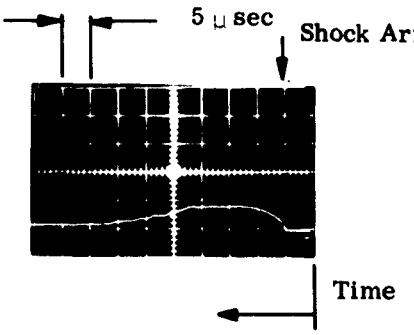

u_s = 20300 ft/sec

P_1 = 5 mm Hg

$\dot{q}$ = 38200 BTU/ft^2-sec

Figure 3.43 Typical Oscillograms from Heat Transfer Gage and Corresponding Pyrometer Signal of Incident Shock Wave

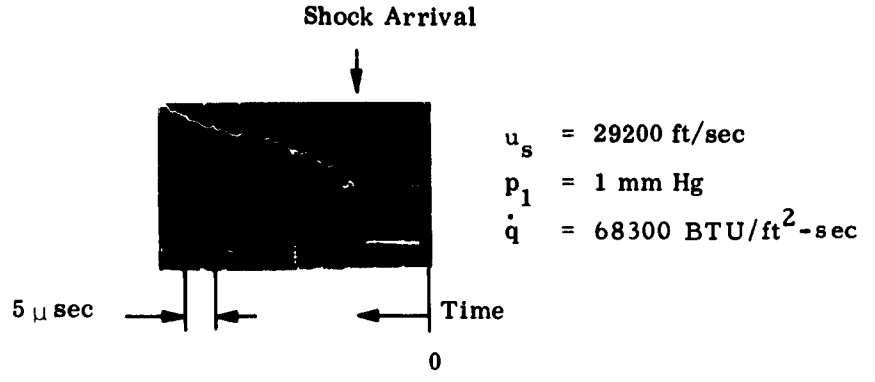

Figure 3.44a Typical Oscillogram from Hytemco Calorimeter Heat Transfer Gage

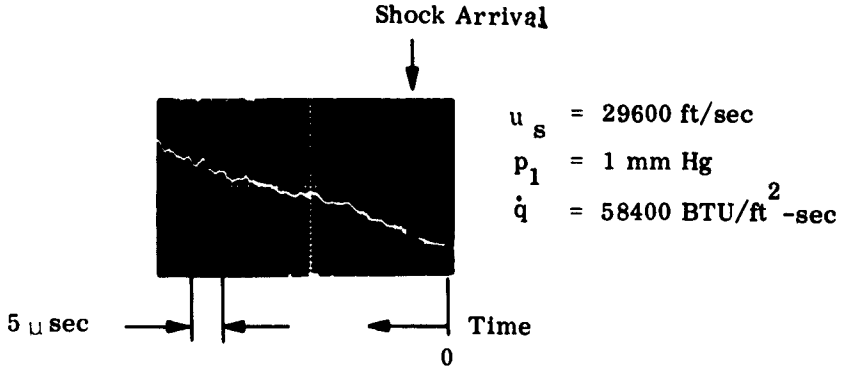

Figure 3.44b Typical Oscillogram from Platinum Calorimeter Heat Transfer Gage

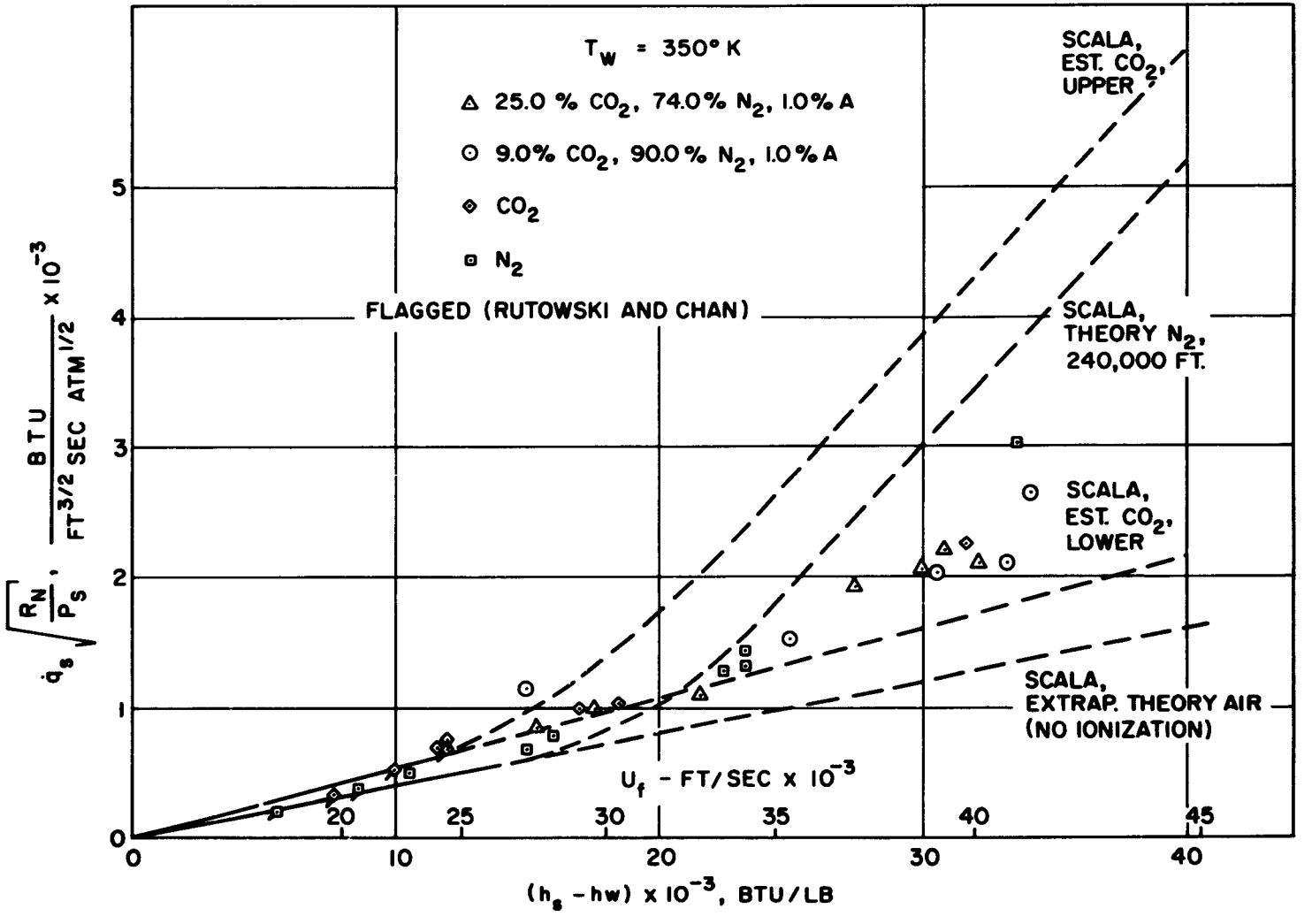

Figure 3.45 Stagnation Heat Transfer

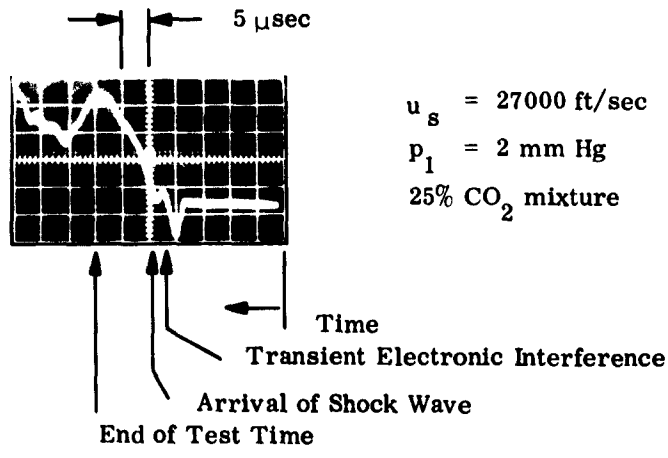

Figure 3.46 Total Radiation Thin Film Cavity Gage Response

III-4 LARGE, HIGH ENTHALPY SHOCK TUBE DEVELOPMENT*

Using as the basis the 2" dia. arc-heated shock tube, a larger facility capable of producing shock velocities up to 40,000 ft/sec was designed. The general arrangement is shown in Fig. 4.1. The driver was made larger by increasing its length to 4 1/2 ft. and its diameter to 3 1/2 in. The energy stored in capacitors used to heat the helium was also increased to 320K joules by adding several more capacitor banks. Most of the basic design features of the prototype unit were retained. The arc is initiated by a tungsten wire suspended coaxially inside a Lexan insulator between the main electrode and the spider at the diaphragm end of the driver. This assures uniform wall losses along the driver. To keep the energy dissipation time short (about 50 microseconds) a parallel-series arrangement of the capacitor circuit is employed. The driver tube is 30 ft. long and 6 in. inside diameter. It is made of steel permitting the mounting of pressure gages along the tube to evaluate flow properties and to sense the arrival of driver expansion wave. Other instrumentation such as the cavity gage which requires contact with the test gas can also be used. The tube is relatively easy to clean and is capable of withstanding the high pressure experienced at high P_1 values.

Considerable improvement of the range of test conditions is achieved

*Principal Investigators: J. S. Gruszczynski, C. J. Harris, D. A. Rogers and W. R. Warren.

by the larger tube in comparison to the 2 in. prototype facility. This is mainly reflected by the test time available at a given initial driven tube pressure P_1 and shock velocity. Figures 4.2 and 4.3 illustrate this point. The range of test conditions behind incident shock wave as shown in Fig. 4.2 is limited by the maximum energy input into the driver corresponding to the final pressure in the driver of 2000 atmospheres and 8000°K temperature on one side, and by the test time which precludes the operation below 100 microns on the other side. A typical low W/C_DA, low θ_l trajectory is superimposed upon the shock tube performance together with the altitude scale of a model of Venusian atmosphere.

Fig. 4.3 shows the performance of the shock tube related to the simulation of stagnation point conditions. Here we see that the flight velocities of 40,000 ft/sec can easily be simulated for stagnation pressures up to 100 atm.

Testing has not commenced in this facility as yet. All the hardware has been procured and is now installed. Fig. 4.4 shows the partially completed capacitors room with the driver in place. The driven tube is shown in Fig. 4.5. The test section which will be mounted on the end of the driver tube is not shown.

The full facility has begun initial operation and is being checked out.

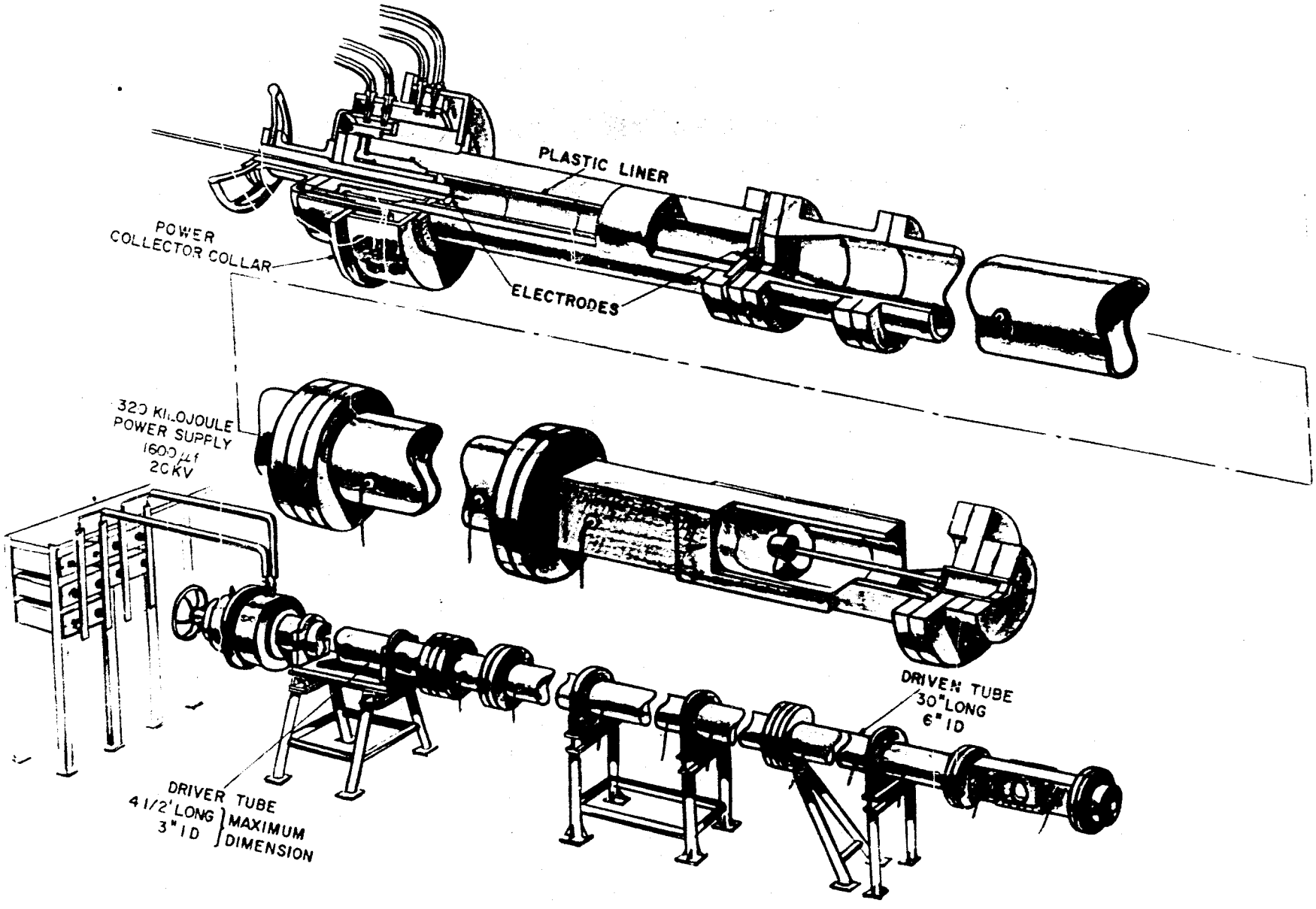

Figure 4.1 Hypervelocity Shock Tube ARC Heated Helium Driver

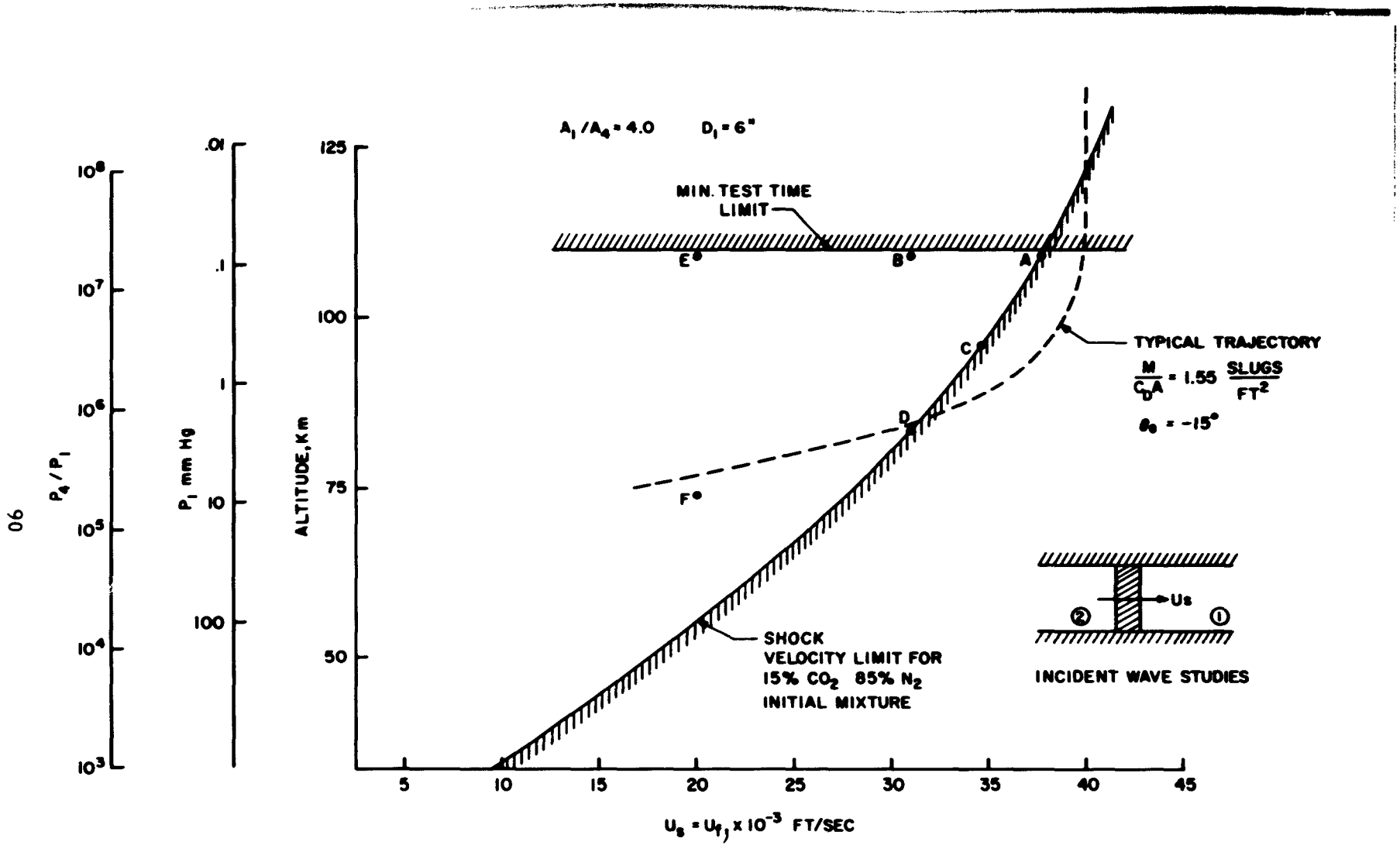

Figure 4.2 Performance Curve for Hypervelocity Shock Tube

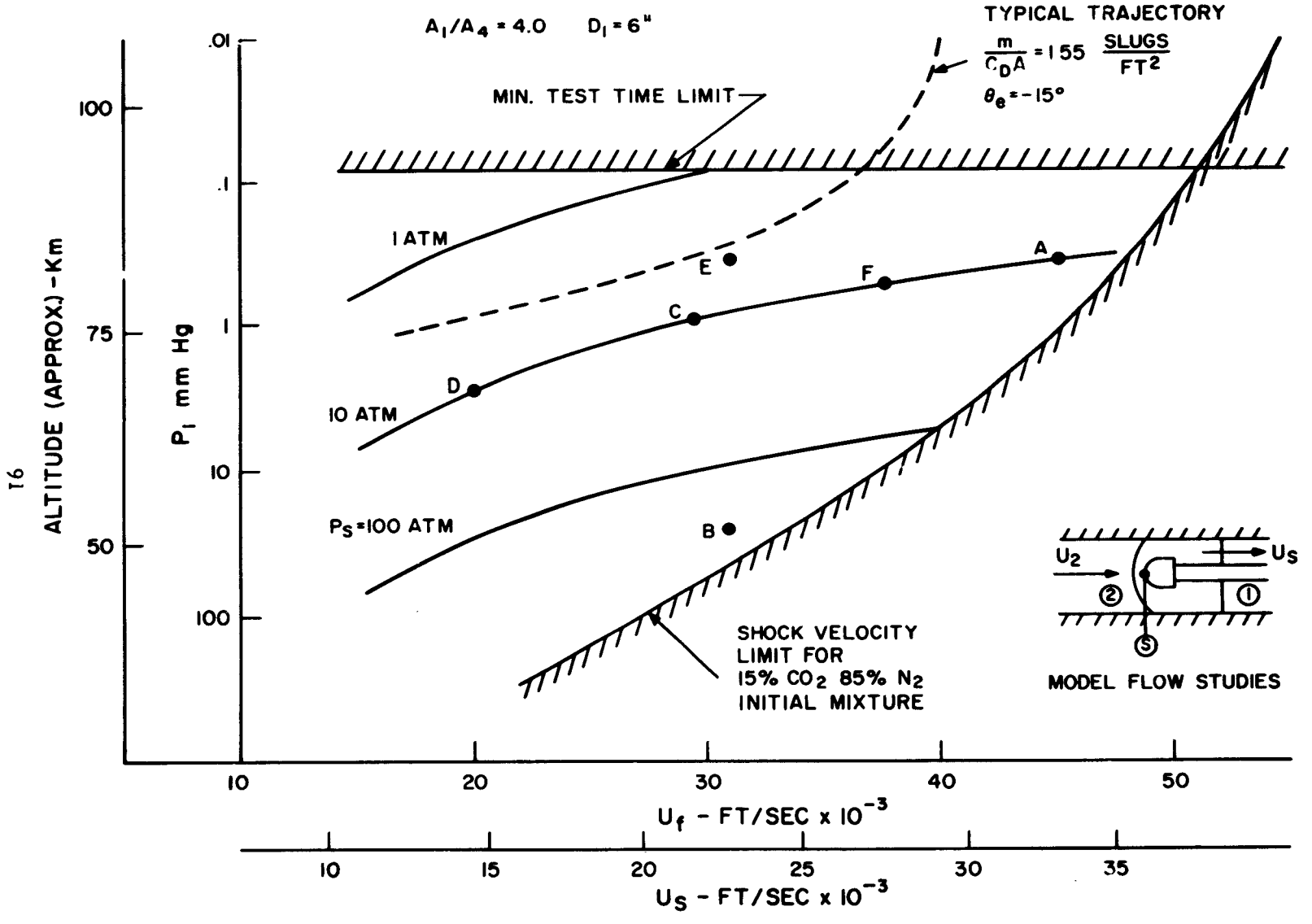

Figure 4.3 Performance Curve for Hypervelocity Shock Tube

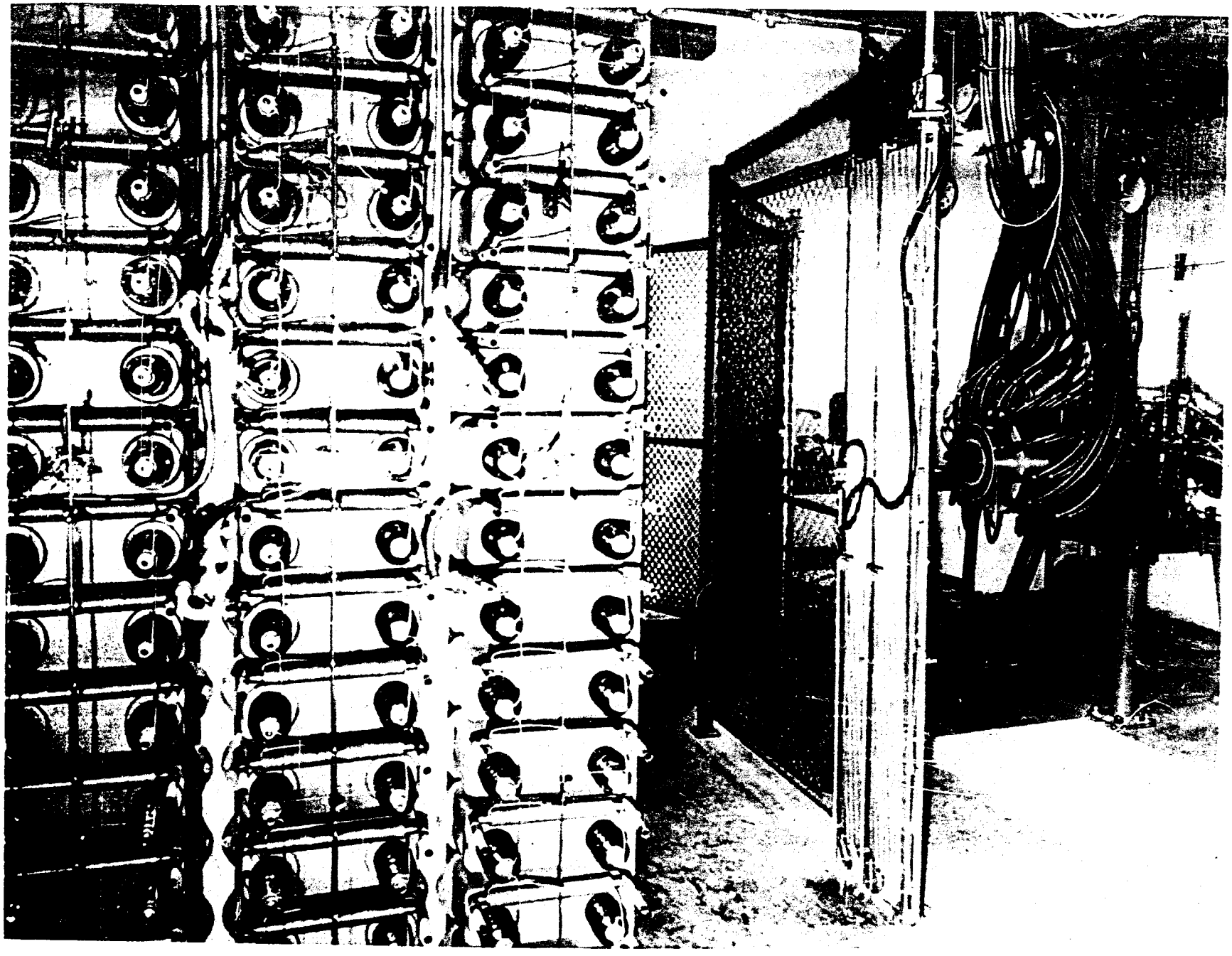

Figure 4.4 Driver Room Hypervelocity Shock Tube

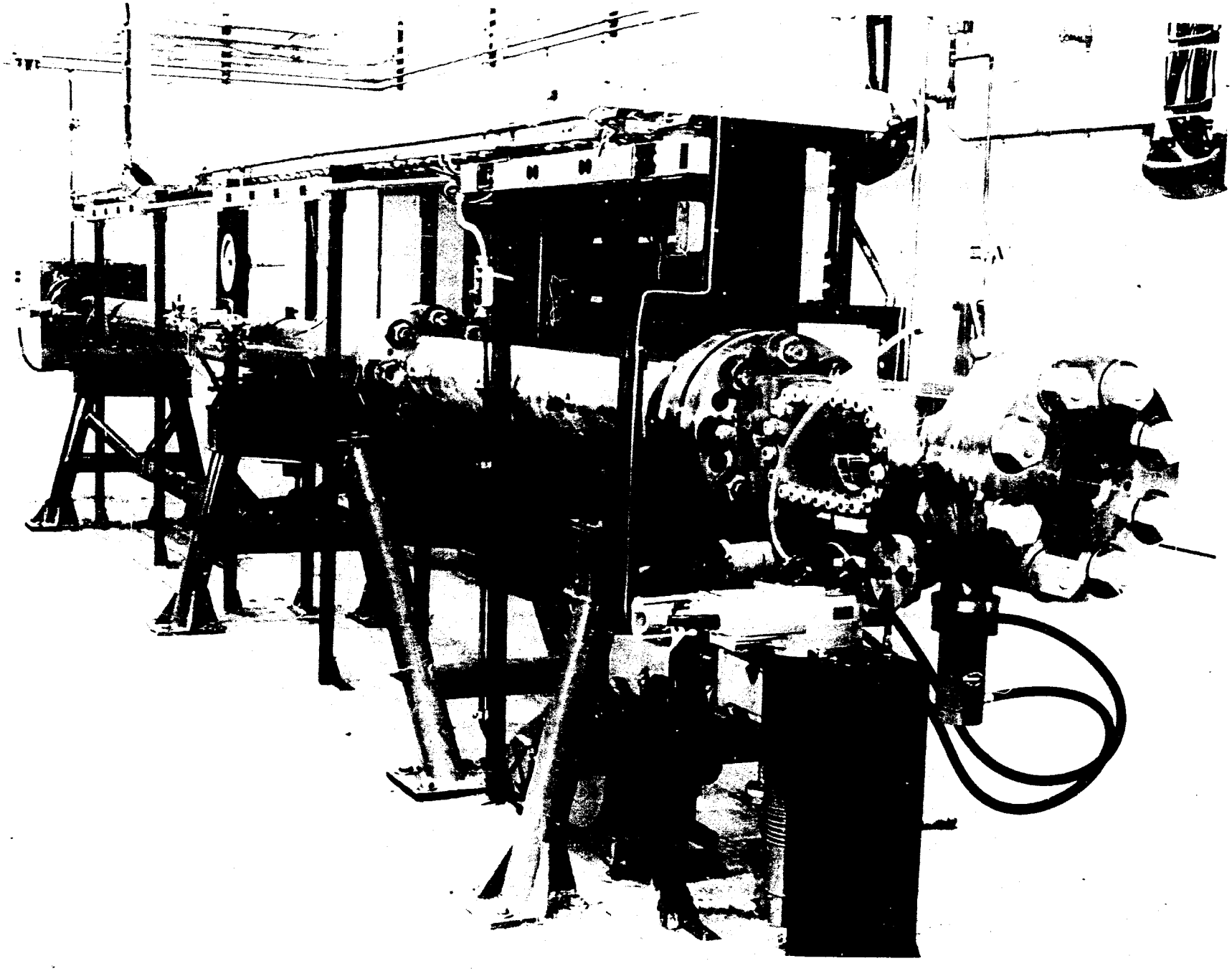

Figure 4.5 Driven Tube Hypervelocity Shock Tube

III-5 HEAT PROTECTION STUDIES *

5.1 Introduction

The thermal protection by ablation of vehicles entering simulated planetary atmospheres was the subject of the present study. The capability for such a study was provided by the Space Sciences Laboratory's tandem Gerdien arc -- a high purity, high enthalpy design. The tandem Gerdien design incorporating the latest "state of the arc" features was adapted to free jet testing. Well known ablation materials typical of three classes of ablators were tested in the arc-heated gas mixtures representative of Martian and Venusian atmospheres. The performance of each material in each gas mixture is evaluated and compared with similar performance in air. The results illustrate the severity of the entry problem for Mars and Venus relative to Earth re-entry for high heating rate or primarily steady state ablation situations. The effects of non-steady ablation and gas radiation on material performance were not studied.

5.2 Arc Test Facility

The tandem Gerdien arc design was adapted to free jet testing of ablation materials. The arc heater provides contaminant-free high enthalpy flow due to its constrictor plate design and the flow velocity distribution in the arc (Figure 5.1). Argon sheathed electrodes were incorporated in order to substantially reduce the electrode consumption rate. Since the inlet gas is divided into four portions, two flowing through the arc, plenum chamber and nozzle (test gas) and two flowing past the electrodes to a dump valve,

*Principal Investigators: N. S. Diaconis, R. A. Sheridan and W. R. Warren

no electrode materials or argon is entrained in the test gas.

The tandem Gerdien arc was developed by McGinn at the Space Sciences Laboratory. It incorporated the principles and experience gained in the seven years of arc technology at the Laboratory. The arc unit included the latest feature of arc development -- argon swirl electrodes. The graphite electrodes are shrouded in argon contained by a water-cooled copper housing. The argon prevents combustion of the electrodes, and the argon and carbon are dumped to prevent contamination of the test gas.

Other modifications of the arc unit were needed to adapt it to free jet testing. The model actuation mechanism is shown in Figure 5.2. A slot was made in the plenum wall for full viewing of the models; the back pots were modified to accommodate the argon swirls, and other changes were made to facilitate the operation of the arc. Power, water, gas and hydraulic lines were installed along with sufficient instrumentation to monitor the operational parameters of the arc.

An advantage gained when the arc became operational was the utilization of the new power source. The rectified power supply provides a more constant source than the old supply and at higher power levels. Improved operation of the arc was clearly noted.

After the initial trial runs with the newly built free jet arc (Fig. 5.3) the purity of the flow was checked spectrographically. The amount of inlet flow past the argon sheathed electrodes and the amount exhausted were varied until the test gas species showed a high degree of purity (contamina-

tion approximately 0.1% by mass).

Some difficulties were encountered in the initial operation of the arc unit. Water leaks and arc covers to the arc parts necessitated several delays while repairs were made. The arc was debugged and brought under control and the performance was measured to a satisfactory degree. The arc current and voltage, the plenum pressure, the purity of the flow, the stagnation temperature and stagnation enthalpy were determined for the arc.

The stagnation enthalpy of the gas mixtures was determined with a water cooled total calorimeter (Figure 5.4). The calorimeter collects the gas, cools it and then exhausts it through a flow meter. The arc conditions are maintained constant until the calorimeter comes to equilibrium. The enthalpy is determined from the water temperature rise and the weight flow of gas.

Model heat transfer rates are determined through transient backwall temperature measurements in a cylindrical slug located at the stagnation point of a plastic model.

5.3 Test Program

The objective of the program was to determine experimentally the behavior of typical thermal protection materials that might be used for Mars and Venus entry vehicles. An approach that would allow compensation for any mis-estimate of the percentages of the nitrogen-carbon dioxide mixture for the planets was used. The percentage of CO_2 (in a CO_2-N_2 mixture) was varied from 0 to 25%. The three mixtures tested then allow re-

sults to be approximated for any mixture by interpolation. Test results in the simulated atmospheres were also compared with air data.

Nominally, the gas mixtures selected for the program were air, nitrogen, and the "best" estimate and the extreme estimate for the Venus atmosphere. The actual N_2-CO_2 mixtures desired and those obtained from the vendor were as follows:

Mixtures Specified	Mixtures Supplied
90% N_2, 9% CO_2, 1% A	88.6% N_2, 10% CO_2, 1.4% A
74% N_2, 25% CO_2, 1% A	74.1% N_2, 24.7% CO_2, 1.2% A

These were considered to be satisfactory mixtures for the purposes of the program.

The materials selected for study are representative of three somewhat general classes of ablators:

Phenolic Nylon -- pyrolizes and chars

ATJ Graphite -- combusts at the surface

Teflon -- sublimes

To permit comparison of the model tests in the different gas mixtures it is necessary to fix certain test parameters. The stagnation pressure was kept essentially constant and the stagnation enthalpy relatively constant for each series of test gases. In this way the results are comparable among themselves and are representative of stagnation region ablation material performance at a specific flight velocity and flight altitude.

The majority of the tests were performed in the stagnation enthalpy

range of 12,000 to 14,000 BTU/lb. A few tests were made in a 10,000 BTU/lb enthalpy range. The maximum simulated flight velocity and altitude values were approximately 26,500 ft/sec and 83 KM (for a simulated Venusian atmosphere).

5.4 Test Results and Discussion

The stagnation enthalpy values determined with the total calorimeter are shown in Table 5.1. The tests were repeated at least twice for each gas mixture and the results indicated that the arc flow conditions are highly repeatable ($\pm 2\%$). Table 5.1 shows the operating pressure in the plenum, the enthalpy increase of the test gas due to arc heating, the stagnation enthalpy and the wall enthalpies at wall temperatures of $1500^{\circ}R$ and $5400^{\circ}R$ for each gas mixture. Also shown are the heat transfer rates for each gas at the two wall temperature conditions of interest. The calculated equilibrium thermochemical properties given in References 24 and 25 were used to determine the necessary properties used below in the data presentation (h_{∞}, h_w).

Model stagnation point heat transfer rate data (non-ablating) was obtained for each gas. The results indicated that many additional runs would have to be made to obtain reliable mean heat transfer rates for each gas. The reasons for this are that at the high test heat transfer rates (of the order of 2500 BTU/ft^2-sec), first, the plastic calorimeter holder ablates quickly near the copper insert, and second, the surface temperature of the copper quickly approaches its melting level. Thus, during the time for

which the calorimeter responds accurately it is difficult to measure the temperature slope data (with present equipment). The result is an appreciable scatter in the reduced heat transfer rates ($\pm$ 10 to 15%).

There was insufficient time to conduct the number of tests required for each gas in this program; therefore, a semi-empirical method was used. The mean heat transfer rate in air was determined from several experiments at the high h_s levels (Table 5.1). Theoretical relationships for air, nitrogen, and CO_2 (Refs. 21 and 22) were then used to establish heat transfer ratios between each test gas and air at the appropriate stagnation enthalpy level. Thus, the heating rate for each gas was calculated according to

$$q_{o_t} = \dot{q}_{air_{meas}} \frac{(h_s - h_w)_t}{(h_s - h_w)_{air}} \cdot \frac{(\dot{q}\sqrt{R_o/p_s})_t}{(\dot{q}\sqrt{R_o/p_s})_{air}}$$

where

$$R_{o_t} = R_{o_{air}} \text{ and } p_{s_t} \approx p_{s_{air}}$$

Since the enthalpies and theoretical heating rates for each gas differ from the air values only by the order of 20% and 10%, respectively, this procedure should be satisfactory. A further justification is found in the good facility operation repeatability. As a check on the measured heating rate levels, calculations for air at the test conditions were made for stagnation point velocity gradients corresponding to incompressible potential flow and the modified Newtonian prediction. The potential value agrees (within 3%) with the mean measured value as would be expected for the subsonic free jet test condition used.

The different ablators were tested for durations up to 6 seconds. Longer test times would be meaningless because of the large amount of material loss and shape change of the models. However, at the heating rates of interest, steady state ablation conditions are established for most materials in a small fraction of this time. Figure 5.5 shows typical models tested for four seconds duration. The shape changes are to be noted, especially for the teflon. The phenolic nylon has a strong thick char layer so that the shape change is not as pronounced as with teflon. However, the shape change of the virgin phenolic nylon is quite large because of the side heating and char growth. ATJ graphite* data is not shown, although the material was tested in each gas. The mass loss in air at a measured surface temperature of 5400°R was significantly higher than expected. The theory for graphite and its experimental verification are presented in References 23 and 24. The increased mass loss occurs after the test flow is terminated, that is, the surface continues to combust in the room air as the model cools. Due to the heat capacity of graphite the duration of temperature decay is several times the test duration. This problem was not found for the other materials tested since with them little total heat is absorbed during test, and what is, stays near the surface resulting in a short cool down period. Thus, the graphite data are not included since the results could be misleading. Even with the apparent (and erroneous) increase in mass loss, the material ablation rate was still much less than for PN at the same test conditions. It must be remembered, however, that graphite

blocks much less heat than does, for example, PN, resulting in its high internal temperatures. Therefore, mass loss becomes a relatively less important design consideration for graphite.

It is noted that this problem for graphite can be eliminated in future studies by providing an inert gas bath for the test models during the cooling period.

The models before test (Figure 5.5) are hemisphere-cylinders 1/2 inch in diameter. A 3/16 inch diameter by 1 inch long slug of the same material is inserted at the stagnation point of the model. All test measurements are made for this slug. This technique allows the obtaining of stagnation region data as opposed to data integrated over the complete model surface. The right fit eliminates effects due to the model-slug joint.

Weight and length measurements are taken from the slug before and after test. Typical test specimens are shown in Figure 5.6. Note the char cap positioned above the phenolic nylon specimen. This becomes detached from the slug when it is removed from the model after test. The weight loss and char thickness for the series of runs for phenolic nylon and teflon are given in Table II. The ratios of the initial model radius (R_o = 1/4") to the average radius after test (R_t) are also shown.

Spectrograms were taken of each model in each test gas to attempt to justify the use of a two-color pyrometer to determine the surface temperature history of the test specimens. The spectrograms showed that neither color nor brightness temperatures could be determined with the pyrometer

for the majority of the tests. That is, the gas radiation continuum was too intense and extensive to provide "windows" of sufficient frequency interval to see the model surface satisfactorily with the pyrometer. To obtain some information on the surface temperatures, a few additional spectrographic measurements were made. The temperatures determined from analysis of the spectrograms were as follows:

High Enthalpy Test Conditions

Test Gas	Material	Surface Temperature
10% CO_2, 88.6% N_2, 1.4% A	ATJ graphite	$3900^{\circ}K \pm 100^{\circ}K$
Air	ATJ graphite	$2900^{\circ}K \pm 100^{\circ}K$
Air	Phenolic nylon	$3000^{\circ}K \pm 100^{\circ}K$

The surface temperatures assumed for all the tests were $3000^{\circ}K$ for phenolic nylon and $1500^{\circ}R$ for teflon (based on previous experimental and theoretical experience with teflon (Refs. 25 and 26). It is interesting to note that the surface temperatures of graphite are significantly higher in the 10% CO_2 mixture than in air. This is expected since the ablation mechanism for graphite is primarily combustion. (Note that sublimation should start at about $3700^{\circ}K$ for graphite at one atmosphere.) It is not anticipated that PN or teflon will exhibit this type of change since their ablation mechanisms are not dominated by combustion. However, this point should be checked in future studies.

Figure 5.7 shows the weight loss vs. time for teflon and phenolic nylon in each test gas mixture at the two nominal enthalpy levels. The data

do not show a linear correlation since the model heating rate is decreasing with time (nose radius changing). The data was reduced on the basis of instantaneous values. The mass loss is computed from the slope of the weight loss-time curve and a heat transfer rate, appropriate to the model nose radius at the same time of test, is calculated according to

$$\frac{\dot{q}_t}{\dot{q}_{o_t}} = \frac{R_o}{R_t}$$

The heat of ablation is defined as

$$Q^* = \frac{\dot{q}_t}{\dot{M}}$$

where $\dot{q}_t$ and $\dot{M}$ are determined as above with $\dot{q}_t$ corrected for back radiation from the model surface.

The heats of ablation for teflon and phenolic nylon in each test gas are shown in Figures 5.8 and 5.9 as a function of $(h_s - h_w)$. The range of data is shown by a bar in some cases where variation in values were obtained for the different times of test at which the data was evaluated.

The heats of ablation for teflon in air show reasonable agreement with the theory of Scala (Ref. 25). Good agreement was obtained at low enthalpy levels by Diaconis, et al (Ref. 26).

The heat of ablation values for phenolic nylon exhibit a reasonable trend with respect to the approximate theoretical curve shown. It is pointed out that the heat of ablation for a charring material depends upon the distribution of the various parts of the total heat input. Thus, the heat of ablation

can vary depending upon the char thickness and its variation with time, the virgin material boundary wall temperature, the rate of oxidation, the molecular weight of the transpired gases and other factors that are difficult to include accurately in a theoretical description. The theory shown is for an "idealized" charring ablator and is not meant to represent an accurate theory for the test case.

5.5 Conclusions

The stagnation point steady state ablation performance of two general types of ablators were evaluated in a high purity-high enthalpy free jet arc facility in air and nitrogen-carbon dioxide gas mixtures. The mixtures are assumed to represent possible Mars and Venus atmospheres. The ratio of radiative to convective heat transfer was small and therefore the results do not reflect material performance in a highly radiating environment.

The heat of ablation results suggest that ablation is more severe in air and the 25% CO_2 mixture than in N_2 and the 9% CO_2 mixture; however, the maximum spread between data points is only about 10% for phenolic nylon and 20% for teflon. Thus, it is concluded that the steady state ablation performance does not differ grossly between air and the simulated planetary atmospheres at least for the materials and test conditions investigated.

The test results for graphite were found to be in error because of the large mass losses experienced during cooldown after the test flow was terminated. However, the mass losses were still less than those found for

phenolic nylon. Also, the surface temperatures for graphite measured during the test flow were significantly higher than those for phenolic nylon.

TABLE 5.1
ARC TEST CONDITIONS

High Enthalpy Test Conditions	Air	N_2	10% CO_2	25% CO_2
P_s (psig)	3.0	2.8	2.9	3.1
h/RT_o	364	415	400	384
h_o/RT_o	3.9	3.9	-11.5	-35.5
h_s/RT_o	368	419	388	348
h_w/RT_o ($T_w = 1500^oR$)	11.4	11.4	-4.2	-28.3
$\frac{h_s - h_w}{RT_o}$ ($T_w = 1500^oR$)	357	408	393	377
$\dot{q}_{o_t}$ ($T_w = 1500^oR$)	2480	2900	2900	2920
h_w/RT_o ($T_w = 5400^oR$)	52	45.6	40.3	26.8
$\frac{h_s - h_w}{RT_o}$ ($T_w = 5400^oR$)	316	373	348	322
$\dot{q}_{o_t}$ ($T_w = 5400^oR$)	2260	2610	2540	2480
Low Enthalpy Test Conditions				
P_s (psig)		2.3	2.4	2.5
h/RT_o		286	306	306
h_s/RT_o		290	295	270
$\frac{h_s - h_w}{RT_o}$ ($T_w = 1500^oR$)		279	299	299
$\dot{q}_{o_t}$ ($T_w = 1500^oR$)		1940	2120	2240
$\frac{h_s - h_w}{RT_o}$ ($T_w = 5400^oR$)		244	254	244
$\dot{q}_{o_t}$ ($T_w = 5400^oR$)		1740	1840	1840

$R_o = 1/4"$

$RT_o = 33.86$ BTU/LB

$\dot{q}_{rad}$ ($T_w = 5400^oR$) = 440 BTU/LB (Back Radiation from surface)

TABLE 5.2
TEST RESULTS

Material	Gas	h_s/RT_o	Time (sec)	(gms)	t char (in.)	$\frac{R_o}{R_t}$
Phenolic Nylon	Air	368	2.4	.0404	.029	--
			3	.0505	.032	.67
			4	.0522	.027	.56
			5	.0615	.034	.47
			6.1	.0745	.040	.25
	N_2	419	2	.0351	.050	
			3	.0382	--	
			6	.0730	--	
	10% CO_2	388	2	.0303	.052	.80
			4	.0463	.055	.64
			5	.0628	.047	.56
			6	.0652	.066	.47
	25% CO_2	348	2.5	.0434	.071	.76
			4	.0613	.053	.58
			6	.0765	.026	.42
Teflon	Air	368	2.3	.1358		.94
			3.9	.2005		.89
			6.2	.2726		.73
	N_2	419	2	.0865		.97
			3	.1218		.94
			6	.2361		.86
	10% CO_2	388	2	.0836		.97
			4	.2063		.91
			6	.3166		.84
	25% CO_2	348	2.2	.0884		.91
			4.2	.1872		.80
			5.8	.2955		.71
Phenolic Nylon	N_2	290	2.2	.0276	.072	.86
			4	.0458	.050	.67
	10% CO_2	295	2	.0293	.055	.80
			4	.0464	.073	.76
	25% CO_2	270	2	.0284	.044	.84
			4.1	.0494	.052	.80
Teflon	N_2	290	2	.1858		.97
			4	.187		.97
	10% CO_2	295	2.1	.0834		.97
			4.3	.1728		.97
	25% CO_2	270	2	.0873		1.00
			4.1	.1887		1.00

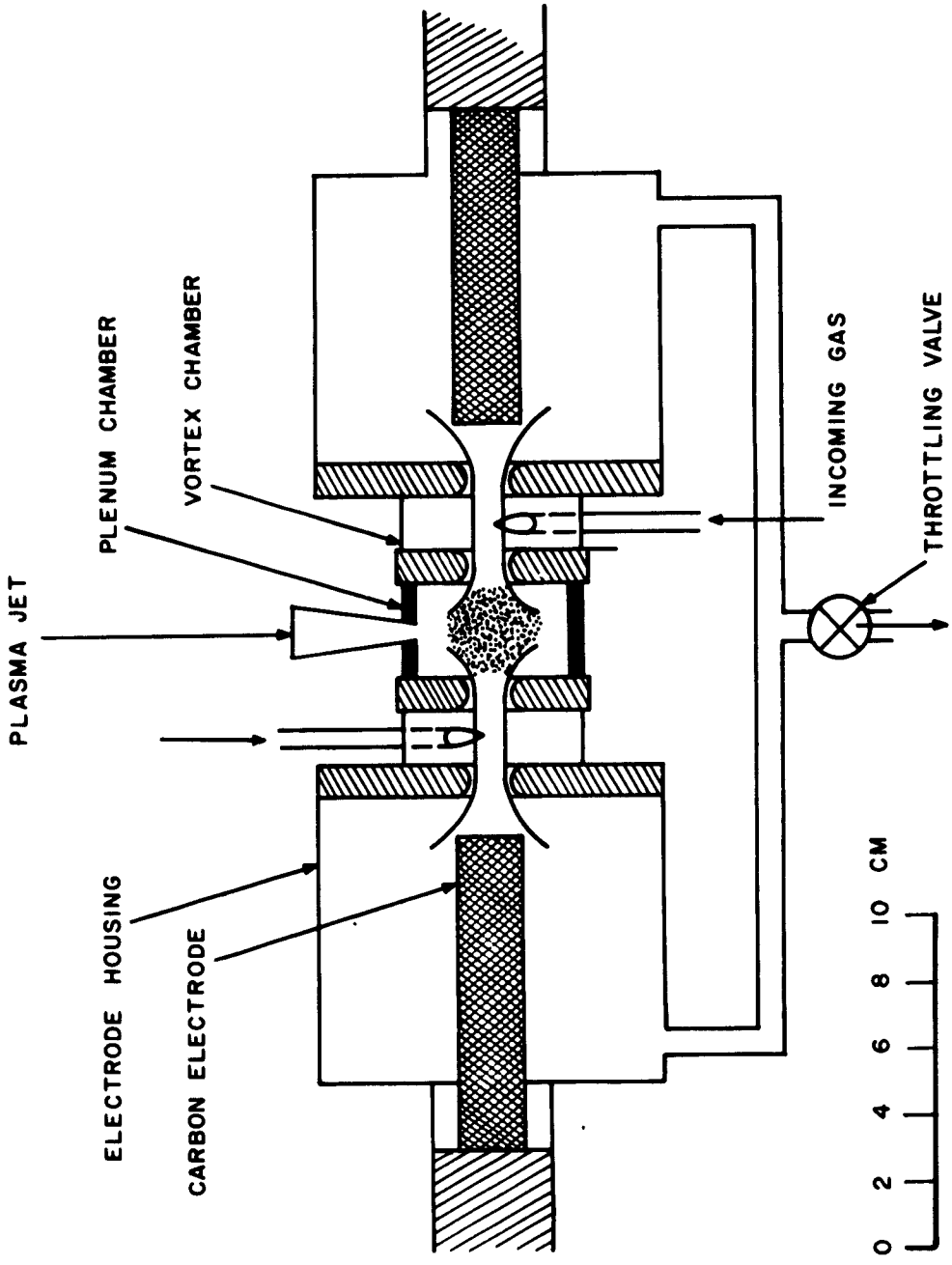

Figure 5.1 Tandem Gerdien Arc Design

a. Model Out

b. Model In

Figure 5.2 Model Testing - Tandem Gerdien Free Jet Arc

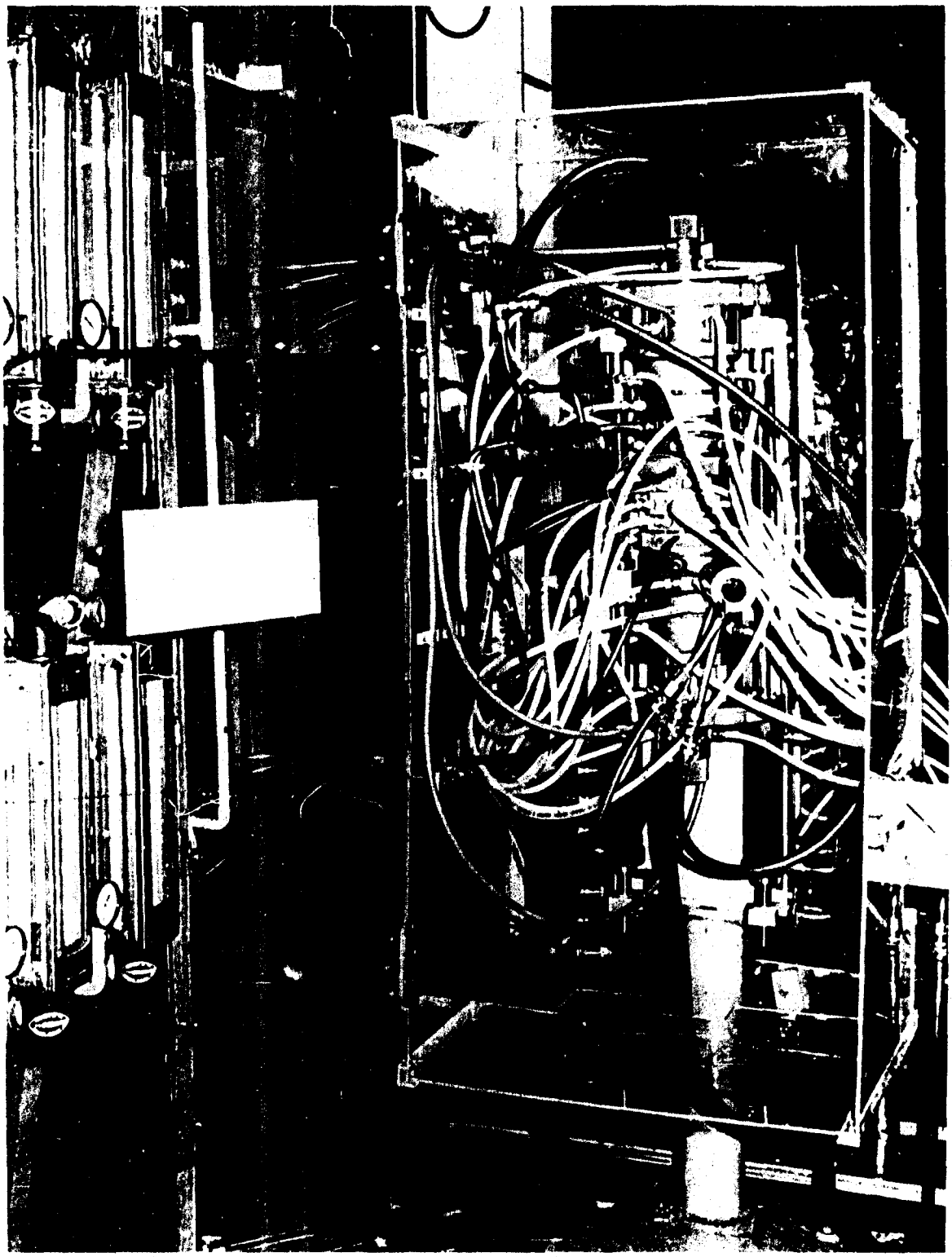

Figure 5.3 Arc Heater - Tandem Gerdien Free Jet

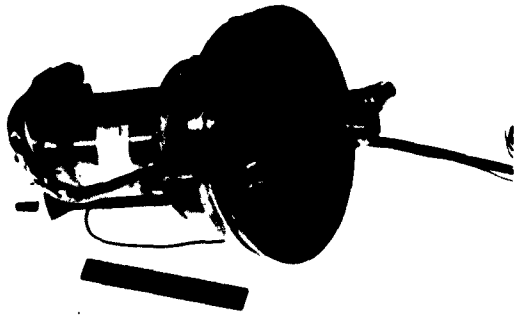

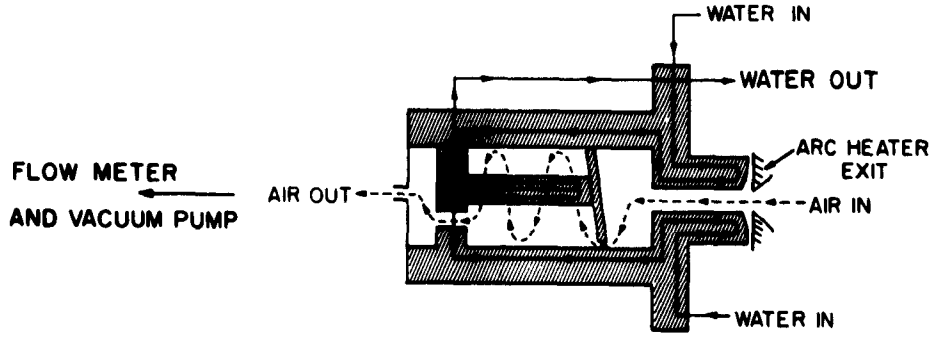

Figure 5.4 Total Enthalpy Calorimeter

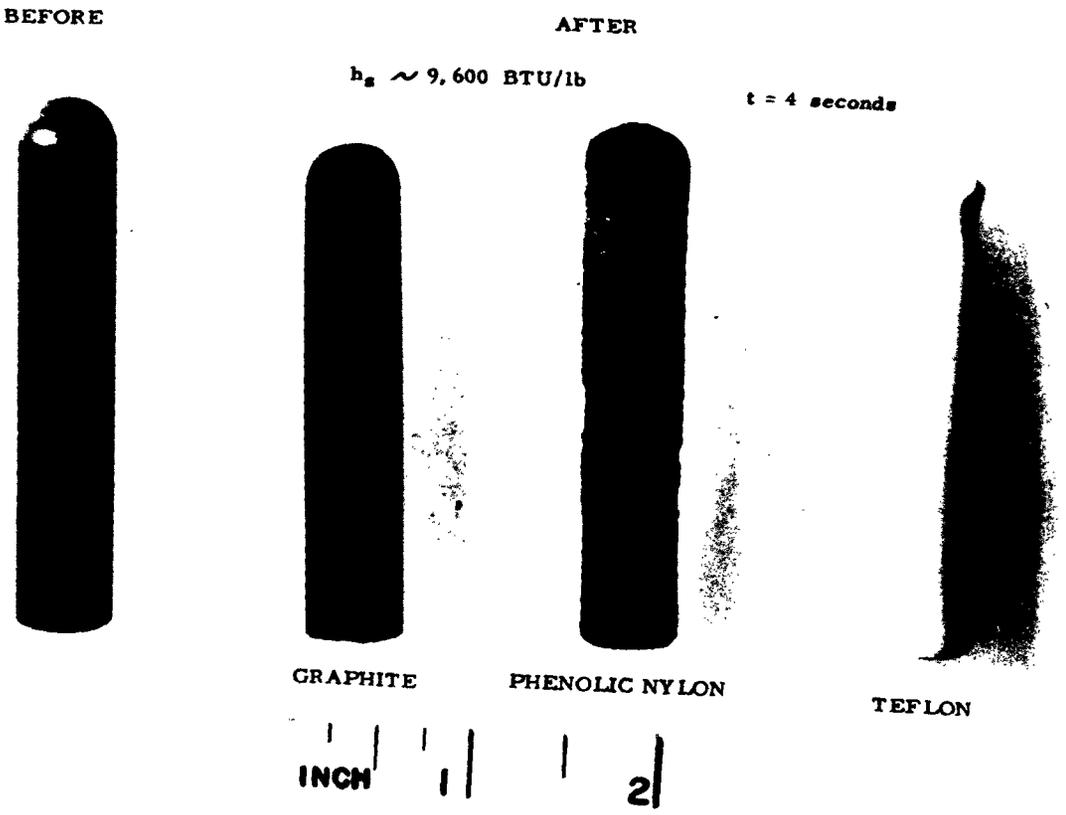

Figure 5.5 Typical Models - Mn

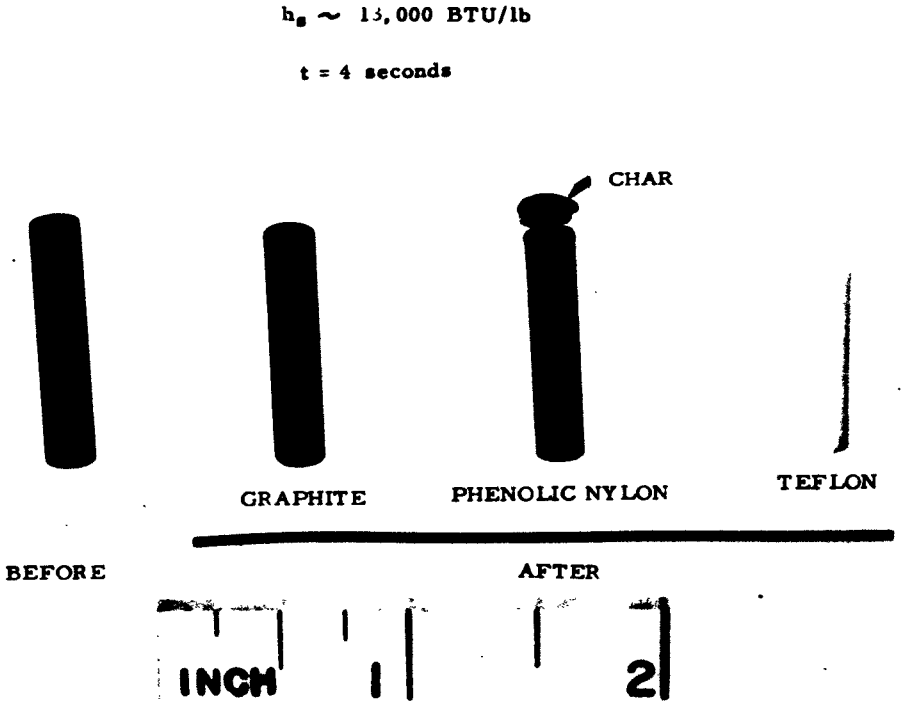

Figure 5.6 Typical Model Specimens

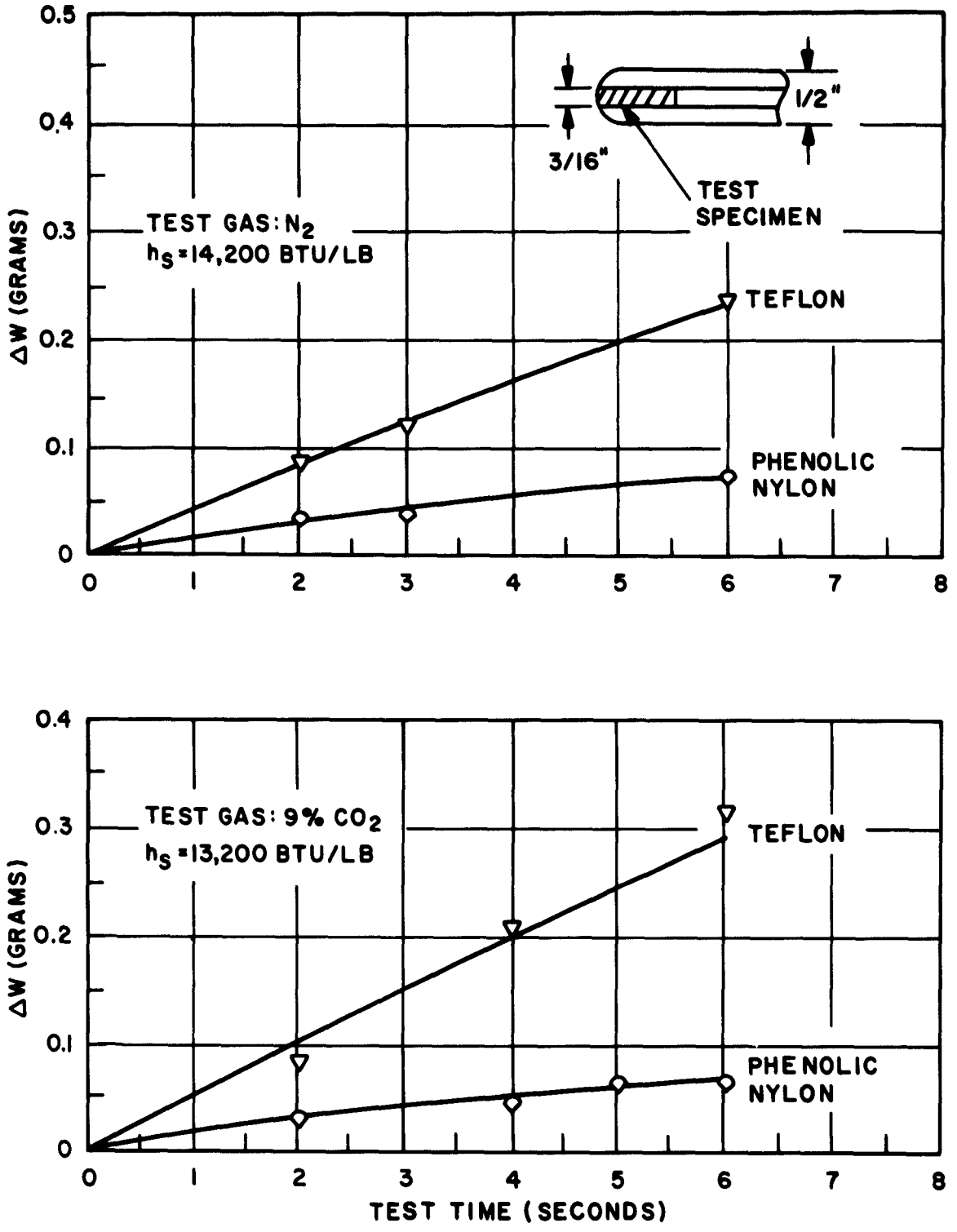

Figure 5.7a Mass Loss of Ablators

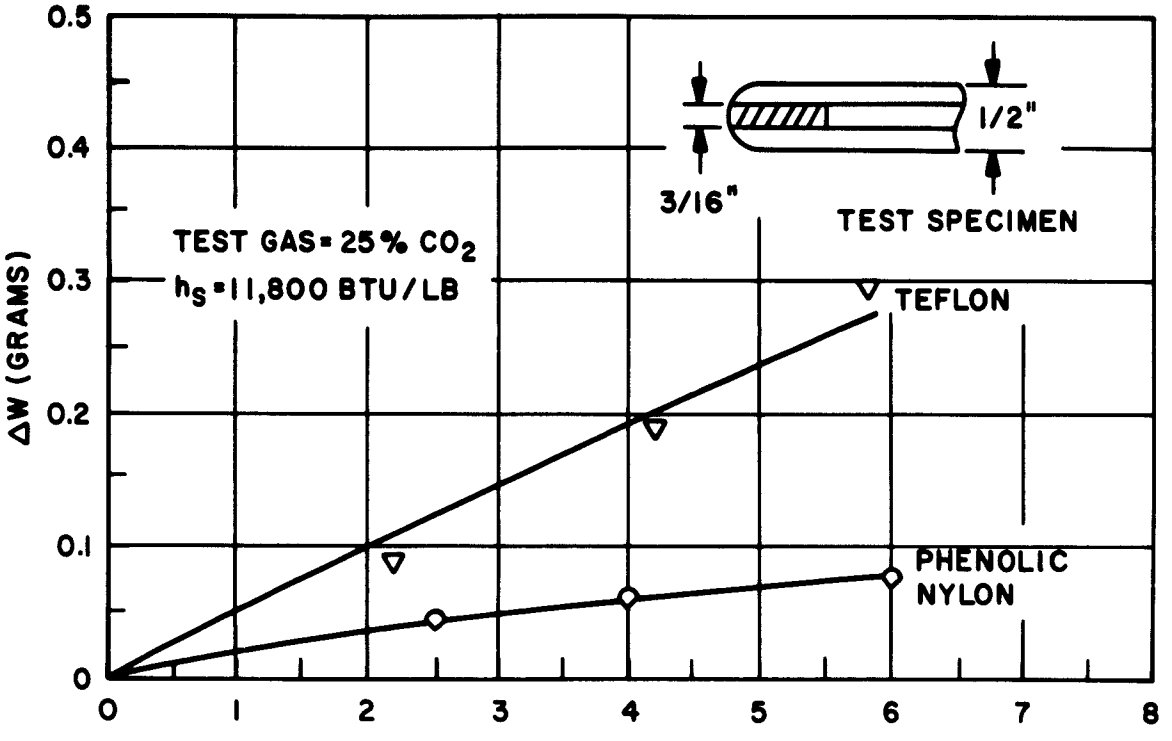

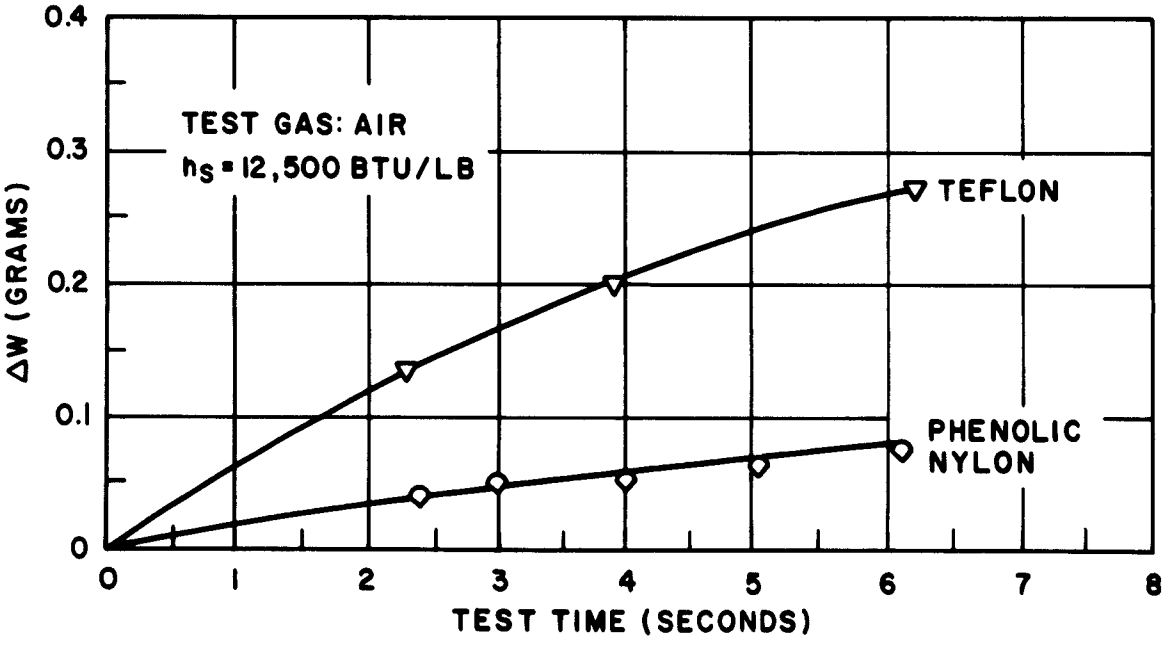

Figure 5.7b Mass Loss of Ablators

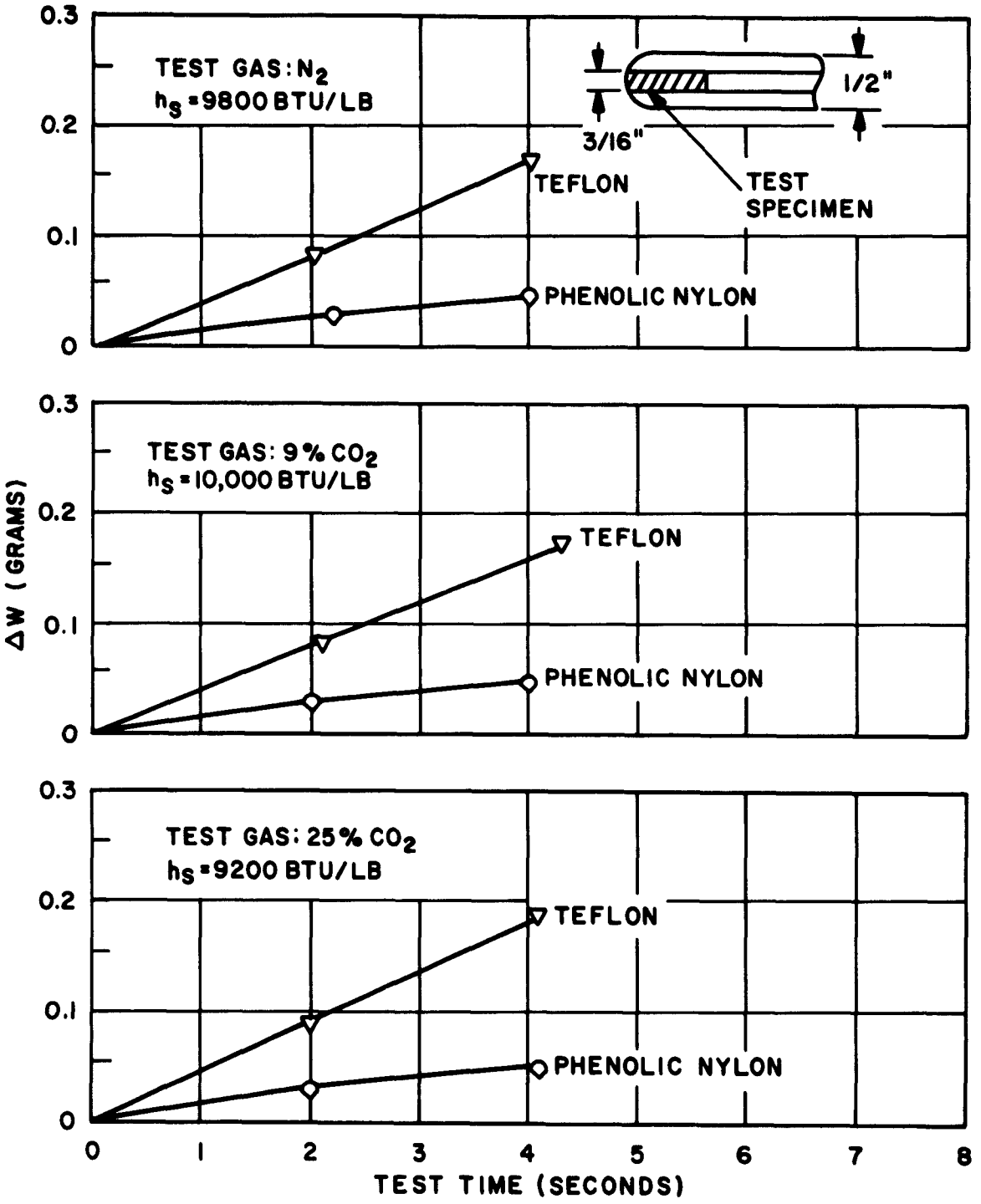

Figure 5.7c Mass Loss of Ablators

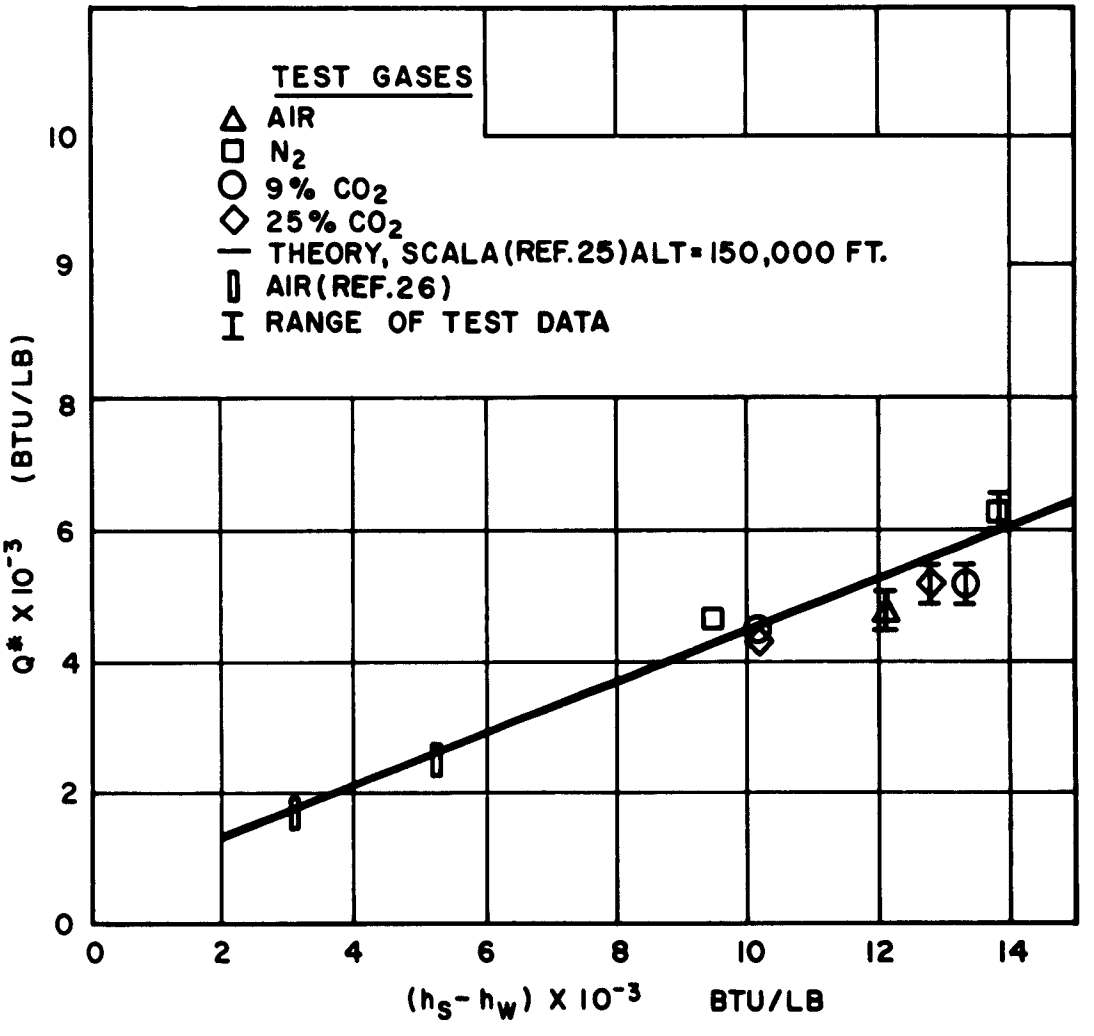

Figure 5.8 Heats of Ablation for Teflon

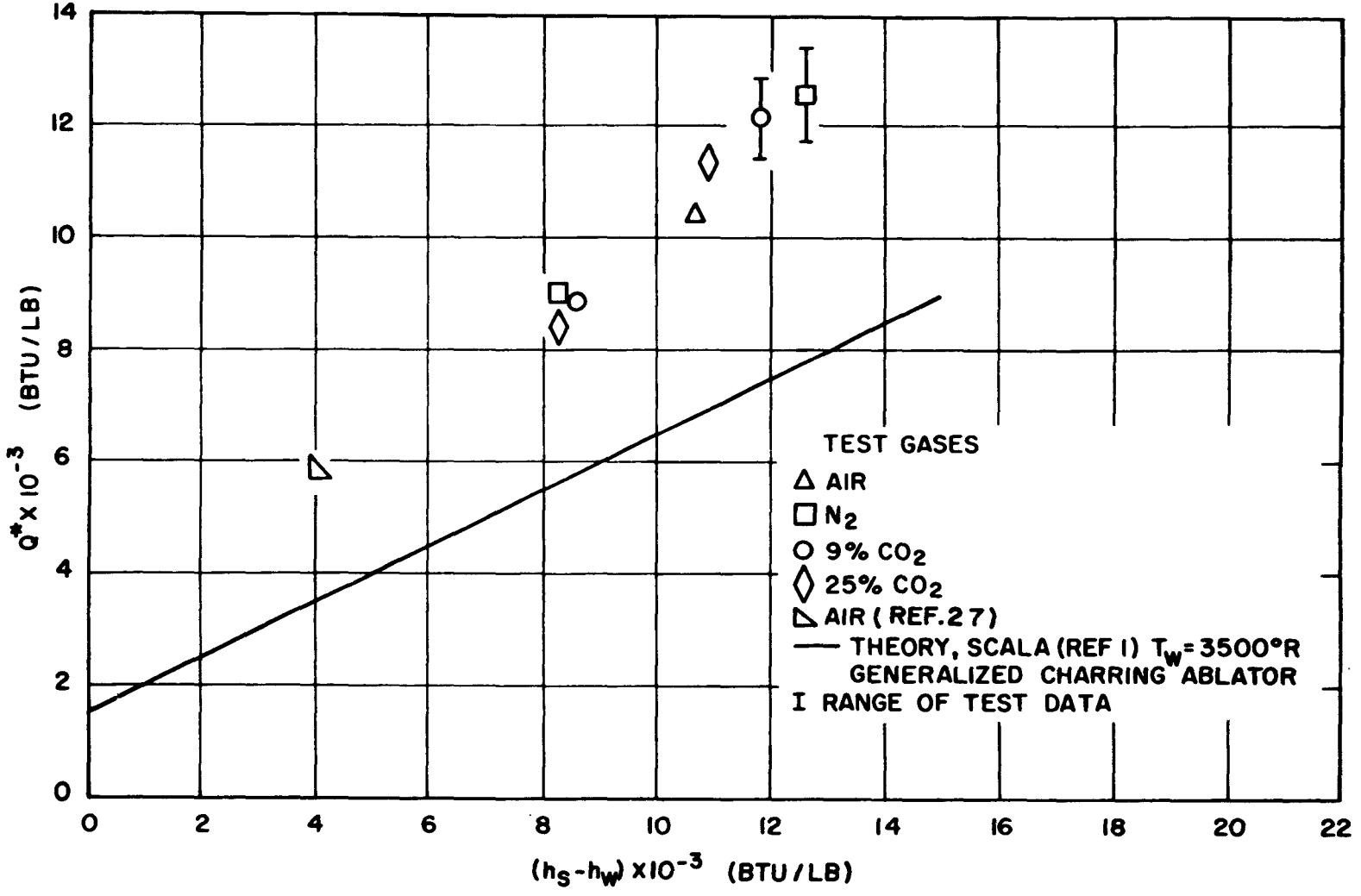

Figure 5.9 Heats of Ablation for Phenolic Nylon

III-6 VENUS IONOSPHERIC ATTENUATION*

6.1 Introduction

The object of this part of the study program was to determine the expected amount of attenuation of a radio-frequency signal passing through the ionosphere of Venus. The attenuation of a signal in the ionosphere depends on the electron concentration and the collision frequency, which in turn depend quite critically on the atmospheric composition. The composition data used for the three models are those given in Section I of this report. The attenuation has been calculated for transmission frequencies of 100 mc and 500 mc.

Initial considerations of the atmospheric models provided by JPL indicated that losses in the ionosphere would be sufficiently small that mathematically convenient assumptions might yield results of acceptable accuracy for the present study. The results appear to justify these assumptions. The two basic assumptions are that the propagation can be treated in a piecewise-linear manner and that reflection at the boundaries can be neglected. The resulting expression is:

$$P = P_o \, e^{-\sum_i \alpha(z_i) \, (\Delta z)_i} \qquad (6\text{-}1)$$

where P_o is the power incident on the ionosphere and $\alpha(z)$ is the attenuation coefficient, given by (Ref. 28):

$$\alpha(z) = (f_p/f)^2 \, \nu(z) \, (1 - f_p^2/f^2)^{-1} \, c^{-1} \qquad (6\text{-}2)$$

where,

$$f_p = e \sqrt{N_e/\pi m} \qquad (6\text{-}3)$$

*Principal Investigators: S. Visvanathan and W. C. King

is the critical frequency

N_e is the electron concentration, given by JPL as 10^6/cc.

f is the signal frequency

c is the velocity of light

$\nu(z)$ is the collision frequency of the electrons

6.2 Collision Frequencies for the Three Atmospheric Models

The collision frequency is given by (Ref. 29):

$$\nu(z) = N(z)\,\sigma_{eff}\,V \qquad (6\text{-}4)$$

where,

N (z) is the density of the electrically neutral particles at altitude z

σ_{eff} is the effective cross-section of the electrons

T is the temperature of the electrons

V is the mean velocity of the electrons, given by

$$V = \left(\frac{8KT}{\pi M}\right)^{1/2} \qquad (6\text{-}5)$$

The effective collision cross section for the Venus model atmospheres is subject to considerable uncertainties. As observed from experimental work reported in Massey & Burhop (Ref. 29), and also in Brown (Ref. 30), experimental data in the energy ranges of interest (considerably less than one electron volt) is sufficiently scarce as to be unreliable. Extrapolation of experimental data permits a reasonable choice within a range of about an order of magnitude.

For the purposes of this study, the effective cross sections for the three model atmospheres are taken as follows:

Best Model: $\sigma_{eff} = 7.64 \times 10^{-16}\ cm^2$

Extreme I: $\sigma_{eff} = 7.2 \times 10^{-16}\ cm^2$

Extreme II: $\sigma_{eff} = 8.73 \times 10^{-16}\ cm^2$

The collision frequencies were computed from Equation (6-4), using these values of the cross section and the corresponding values for the neutral density N and the thermal velocity. The results of these calculations are given in Table 6.1.

Table 6.1

Best Atmosphere

Height in km	Collision Frequency no/sec
110	7.52×10^{5}
122	1.31×10^{5}
133	3.62×10^{4}
144	1.19×10^{4}
178	8.12×10^{2}
235	8.16×10^{1}
292	0.11

Extreme I

Height in km	Collision Frequency no/sec
110	9.58×10^{5}
122	2.94×10^{5}
133	3.67×10^{4}
144	6.44×10^{3}
178	7.70×10^{2}
235	2.73×10^{2}

Extreme II

Height in km	Collision Frequency no/sec
100	1.69×10^{5}
150	0.6
200	2.28×10^{-4}
250	6×10^{-10}
300	3×10^{-14}

6.3 Attenuation in the Venusian Ionosphere

The critical frequency for the Venusian ionosphere, taking the electron concentration as 10^6/cc is

$$f_p = 8.984 \text{ mc} \qquad (6\text{-}6)$$

The attenuation $\alpha(z)$ has been computed for the three models using equation (6-2) and the above data. The results are presented in Table 6.2 below for the signal frequencies f = 100 mc and 500 mc.

Table 6.2

Best Atmosphere

Height in km	Attenuation in cm^{-1} (f = 100 mc)	Attenuation in cm^{-1} (f = 500 mc)
110	1.023×10^{-7}	3.76×10^{-9}
122	1.78×10^{-8}	6.56×10^{-10}
133	4.92×10^{-9}	1.81×10^{-10}
144	1.62×10^{-9}	5.94×10^{-11}
178	1.10×10^{-10}	4.06×10^{-12}
235	1.11×10^{-11}	4.08×10^{-13}
292	1.50×10^{-14}	5.50×10^{-16}

Extreme I

Height in km	Attenuation in cm^{-1} (f = 100 mc)	Attenuation in cm^{-1} (f = 50 mc)
110	1.30×10^{-7}	4.79×10^{-9}
122	4.00×10^{-8}	1.47×10^{-9}
133	1.40×10^{-8}	5.14×10^{-10}
144	4.50×10^{-9}	1.84×10^{-10}
178	8.76×10^{-10}	3.22×10^{-11}
235	1.05×10^{-10}	3.85×10^{-12}
292	3.71×10^{-11}	1.37×10^{-12}

	Extreme II	
Height in km	Attenuation in cm^{-1} (f = 100 mc)	Attenuation in cm^{-1} (f = 500 mc)
100	2.30×10^{-8}	8.45×10^{-10}
150	8.16×10^{-14}	3.08×10^{-15}
200	3.82×10^{-17}	1.15×10^{-18}

The total attenuation was obtained by summing the contributions from the altitude-increments:

$$\alpha_{TOTAL} = \sum_i \alpha(z_i)\ (\Delta z)_i$$

The calculated attenuations in decibels are given in Table 6.3 for the three atmospheric models.

Table 6.3

Model	Path Length	Total Attenuation at 100 mc	Total Attenuation at 500 mc
Best	182 km	0.80 db	0.02 db
Extreme I	182 km	0.52 db	0.017 db
Extreme II	100 km	1.35 db	0.05 db

These attenuations, of course, are for a vertical propagation path through the ionosphere. The attenuation vs. path length and altitude is shown in Figures 6.1 and 6.2.

Table 6.3 shows that there is no problem in communicating through the ionosphere of Venus. The Extreme II model yields the pessimistic estimate, and Extreme I yields the optimistic estimate. It should be pointed out, however, that it is not known exactly where the ionosphere of Venus begins; it has been estimated that it starts around 100 km. For a true evaluation of the attenuation, one should know the variation of the electron con-

centration with altitude, particularly around 100 km, where the collision frequency gets higher; this aspect needs to be investigated more carefully when better knowledge of the composition of the Venusian atmosphere becomes available.

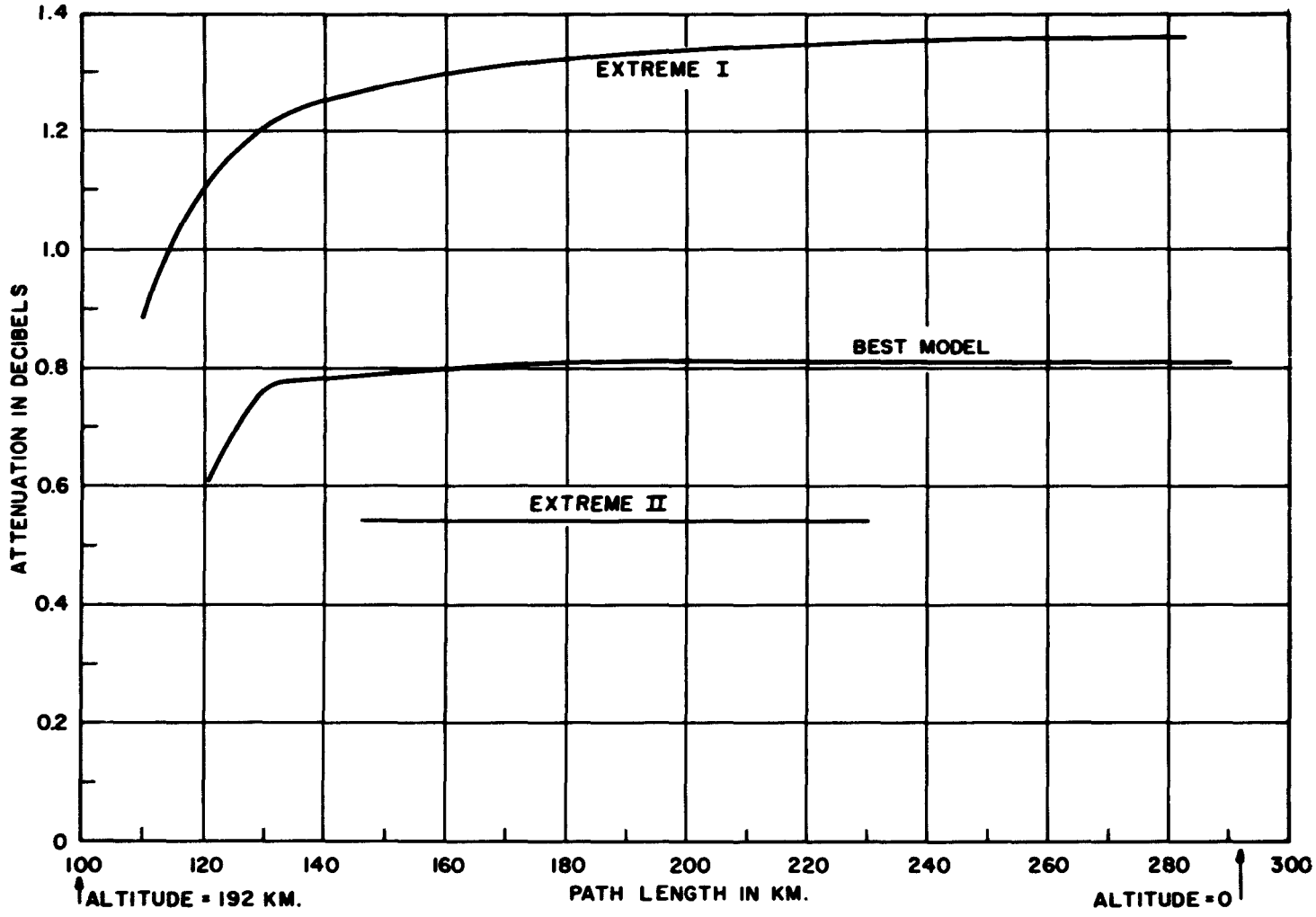

Figure 6.1. Venus Ionospheric Attenuation vs. Path Length at f = 100 mc.

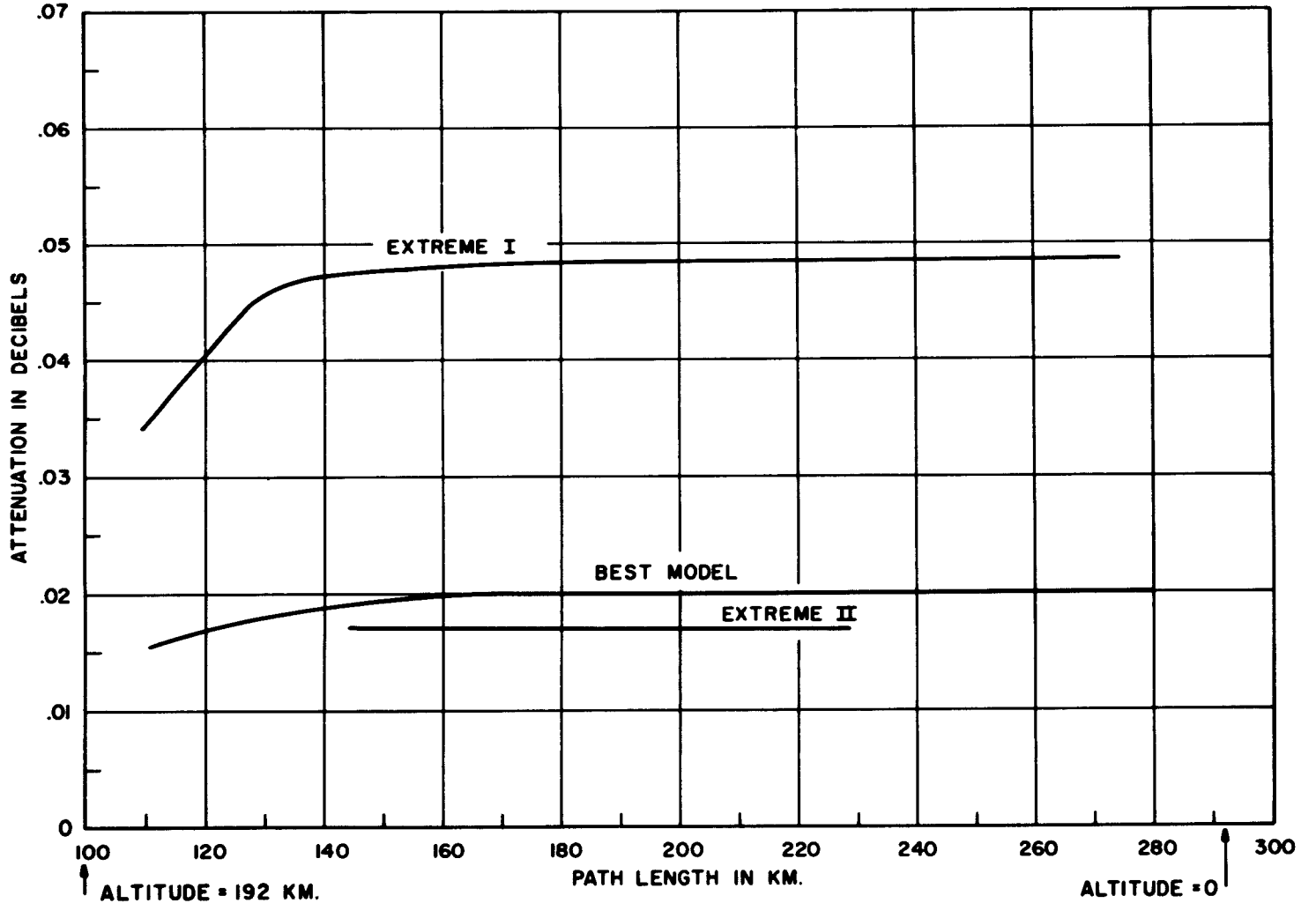

Figure 6.2. Venus Ionospheric Attenuation vs. Path Length at f = 500 mc.

IV. RECOMMENDED FOLLOW-ON RESEARCH AND DEVELOPMENT PROGRAM

Though not all of the planetary entry problems could be solved in a single short program, this program has accomplished the following: First, it has achieved the majority of the objectives established for the program (see section II). Second, it has indicated additional real and potential problem areas. Third, it has established techniques and procedures for future investigation of these problems. The following recommended programs do not include all of the recognized problem areas, but rather represent those that should be pursued as the recommended follow-on studies of this program.

IV-1 EQUILIBRIUM THERMOCHEMISTRY

The Rand method program should undergo extensive check-out and verification with the results compared to those of the Brinkly method program. Subsequent to the verification, equilibrium thermochemistry tables should be prepared for the mixtures where greater accuracy is desired than is available from the Brinkly method. Upon establishment of the Mars and Venus atmospheres, tables and Mollier type charts should be prepared for these atmospheres. Charts of this nature will be utilized as major references similar to the AVCO chart for air which is prevalently used by the industry today.

IV-2 DISSOCIATION RATE STUDIES

With the completion of the study of the dissociation of nitrogen behind combustion generated shock waves, an investigation should be continued

to determine the influence on these results that would be caused by the presence of small quantities of CO_2. This would provide information pertinent to the atmosphere of Mars. Additional investigations should be undertaken of the CO system, then of the CO_2 system and then, at a later date, an extensive investigation should be made of the combined carbon dioxide-nitrogen system.

At the contemplated entry velocities of 40,000 feet per second into the atmosphere of Venus there should be enough thermal energy available to partially dissociate CO, which is one of the decomposition products of CO_2. Since we have recently completed a shock tube study of the dissociation of nitrogen (Ref. 6) (which is the chief component of the atmospheres of Mars and Venus), it is proposed to study the thermal dissociation of CO behind strong shocks.

While it is generally believed that the ambient Martian atmosphere contains chiefly nitrogen and some carbon dioxide, a recent paper by Opik (Ref. 31) has suggested that the CO_2 on Mars may be decomposed into CO and O by ultraviolet absorption. However, the work of Mahon (Ref. 32) tends to contradict this suggestion, indicating that photolysis of CO_2 leads to the formation of ozone, which would prevent further break up of the CO_2 by solar radiation. In any event, CO will be present in the flow surrounding a vehicle and will probably be partially dissociated.

The 2-inch square shock tube which utilizes combustion driving described in section III-2 is well suited to the task of studying the thermal dis-

sociation of CO. In the case of the dissociation of the CO, the carbon atom's first ionization potential lies only slightly above the dissociation energy of the CO. Therefore, there is the interesting possibility that some of the carbon atoms may be ionized. If there is enough energy available to form C^+, then there will be enough to excite the O atoms. The oxygen atom has a line that is particularly well suited for Stark broadening measurements. A method has been formulated which permits the calculation of the Stark broadening. With combustion driving it will be possible to dissociate up to 10% of the CO behind shocks in pure CO and up to 70% in CO-Ar mixtures. On the basis of the recent nitrogen (Ref. 6) study it is likely that the temperature may fall by $2,000^{\circ}K$ in the reaction zone. Such a temperature drop will probably prohibit much C^+ formation. If very little C^+ is formed, then the dissociation process is most likely bimolecular. The program written for the IBM 1620 in the nitrogen experiment can be readily applied to CO.

An additional study that will produce early results with a minimum of expended effort is an investigation of oxygen. The nitrogen results are in disagreement with previous results for nitrogen (Ref. 7) and differ from the results on oxygen (Refs. 33 and 34). It is suggested from this that the previous results (Refs. 33 and 34) inferring that O is some 3-5 times more efficient than O_2 in dissociating O_2 may be in error.

Knowing the relative efficiency of O in dissociating O_2 is of applied interest for space vehicles. It has been shown (Ref. 35) that, of all the rates in the air system, electron production is most sensitive to the rate of disso-

ciation of oxygen. In fact, a change by a factor of 10 in the oxygen dissociation rate leads to a change in the rate of production of electrons by 200. At stagnation temperatures of 6,400°K the O_2 almost completely dissociates; hence, the oxygen molecules are dissociated principally by collisions with oxygen atoms and nitrogen molecules. It is clear that changing the rate of dissociation of O_2 through collisions with O by a factor of 3 may lead to a change in the over-all rate of production of electrons. In vehicles flying at high altitudes a change by an order of magnitude in the rate of production of electrons could move the point of equilibrium electron concentration a sizeable distance relative to the vehicle. Such a result could have a profound influence on the choice of antenna location, radio frequency and power requirements.

It is not proposed here to do a complete study of oxygen dissociation, but rather to make a careful check to see if the reported rates (Refs. 33 and 34) will properly fit the experimental density profiles under conditions of good experimental accuracy. Such data should clarify the question of the reported anomalously high efficiency of the O atom. If the previously reported values are not found to be sufficiently accurate to predict the density profile, then a more exhaustive study would be in order.

IV-3 BLUNT-BODY STAGNATION-POINT HEAT TRANSFER - EXPERIMENTAL STUDY

Two problems have not been investigated fully in the present study which will have bearing upon the stagnation region heating problem of a blunt

body entering the atmosphere of Venus (or Mars). First, the radiative heat transfer may be a large contributor to the total heat transfer. Second, the flow behind the bow shock wave and in the shock layer may not be in equilibrium for important ranges of flight conditions. This could add significantly to the radiative heat transfer, if there are radiation overshoots in the non-equilibrium regions, and may appreciably affect the convective or boundary layer heat transfer as well. The influence of small concentrations of water vapor on the non-equilibrium characteristics of simulated Venus atmosphere should be considered as an important part of this program.

Therefore, the following two study are recommended. First, an experimental program should be undertaken to measure the equilibrium and non-equilibrium heat transfer rates from shocked gases over a range of mixtures (including small concentrations of water vapor or hydrogen to simulate water) that simulates the atmospheres of Venus and Mars. The extent of non-equilibrium regions, the properties and concentrations of gases within them, and their dependence upon flight conditions would be determined as part of this program. Emphasis would be placed upon total radiation measurements (with a cavity gage), but time resolved spectroscopic observations would also be made to identify the radiating species and their importance in both the equilibrium and non-equilibrium regimes. These results would be compared with existing theoretical predictions. The effects of body flow field property gradients would also be studied. Second, the present convective heat transfer measurements should be extended to wider ranges of variables. Also, the effects of boundary layer and shock layer non-equilibrium, as identified

by the radiation study, on the convective heating should be determined.

The two recommended studies should be conducted in a high performance shock tube that is capable of producing test flows in simulated atmospheric mixtures over a range of pressure levels and to velocities beyond 40,000 ft/sec. The new GE-MSD 6" hypervelocity shock tube which is driven by arc-heated helium (300 KJ power supply) is such a facility.

IV-4 BLUNT-BODY LAMINAR AND TURBULENT HEAT TRANSFER-EXPERIMENTAL STUDY

The radiative and convective heat transfer to surfaces away from the stagnation region of a body should be investigated for conditions and gas mixtures simulating Venus (and Mars) entry flight. Convective heat transfer distributions should be measured as a function of body shape and size and for a range of simulated altitudes and velocities to greater than 40,000 ft/sec. Model pressure levels should be varied at an appropriately high enthalpy level to cover the range from fully laminar to turbulent body boundary layer. The date should be compared with existing theoretical predictions and plotted against appropriate correlation parameters. Thus, the suitability of currently useful analytical and empirical techniques for the gases in question at the high stagnation enthalpy levels of interest would be assessed. A possibly important result of this work would be the production of new boundary layer transition data which would be compared with results now available for lower flight velocity simulation. Because of the high pressures and large model sizes available with the MSD-SSL 6" shock tube, it should be possible to produce a turbulent boundary layer on the forward portions of a blunt shape

(that is, in the regions of high free stream temperature and ionization levels) so that the effects of pressure gradient or turbulent heating and transition can be studied.

Total radiative heating to surfaces away from the stagnation region of a body should be measured to determine the extent of the radiative heating problem. This would be done on bodies of various shapes and sizes using optically measured shock layer shapes and surface total heat transfer gages (cavity gage). These experiments would be conducted in high enthalpy flows in which the shock layer is dominated by equilibrium radiation. Approximate analytical methods would be developed using previously determined non-equilibrium radiative data for normal shock waves to construct the complete radiative heating distributions for bodies in atmospheric flight over the desired ranges of altitudes and velocities.

The recommended experimental study would be conducted in the GE-MSD 6" hypervelocity shock tube. This facility is driven by arc-heated helium (300 KW power supply). This tube, in addition to being capable of producing flight velocity simulation to greater than 40,000 ft/sec, can also produce and contain high stagnation pressure levels which are required for turbulent boundary layer studies. (The order of 100 atmospheres at greater than 30,000 ft/sec simulated flight velocity is possible with the present tube design and power supply.)

IV-5 AEROTHERMODYNAMIC PERFORMANCE OF HEAT PROTECTION MATERIALS - EXPERIMENTAL STUDY

5.1 Introduction

The heat protection materials study conducted for the present program considered the relative performance of several materials representative of various classes of ablators exposed to high levels of convective heating in the subject simulated environments. Trajectory analyses performed in the recent Venus-Mars Capsule Study, conducted by the Missile and Space Division of the General Electric Co. under contract to the NASA Jet Propulsion Lab, clearly point out, as expected, that the extremely high velocities associated with the Venus-Mars re-entry problem will impose an appreciable radiative heating load upon the stagnation region of the vehicle; this can be a dominating factor in the heat protection design (Ref. 18). This facet of the materials evaluation was not examined in the above study. In addition, consideration of the skirt and aft portions of such a vehicle, where heat transfer is an order of magnitude or more lower than stagnation point values, can also impose thermal protection problems unlike those examined previously. Material performance in this latter case can be classified as non-steady ablation in contrast to the steady state ablation phenomenon exemplified by exposure to high heat transfer environments (Ref. 36). Whereas for steady state ablation the damage of heat penetration of the material proceeds at the same rate as the surface recedes, for so-called non-steady ablation the heat penetrates into the material at a faster rate than the surface recedes.

Physically for steady state ablation there results a damage layer that is thin but moves very rapidly into the material, a situation in which primarily mass loss rather than insulation capability is the critical ablation property. On the contrary, in non-steady ablation the damage layer is rather thick (see Figure IV-5.1) and surface recession is quite slow, making the critical criterion for evaluation of a material the amount of thickness or depth required to maintain a certain level of backwall shield temperature. Both aspects of the heat protection problem, this non-steady ablation phenomenon and the serious radiation heat transfer problem previously mentioned, must be thoroughly examined before an optimum heat protection design is attempted for a Venus or Mars entry capsule. Such a study is described in the ensuing discussion.

Before embarking on any proposed materials evaluation program it is advisable to define the free flight environment of interest. Shown in Figures IV-5.2 and IV-5.5 are typical stagnation point heat transfer profiles determined for the various entry trajectories considered in the Venus-Mars capsule study performed by MSD in the recent study for JPL (Ref. 18). Included are calculations for various model atmospheres and vehicle shapes. A perusal of these data show that over the range of entry parameters considered and indicated on the various figures, peak radiative heating rates might vary from approximately 100 BTU/ft^2-sec to 30,000 BTU/ft^2-sec for a sphere-cone body 1.5 ft. in radius, while the convective values are bracketed between 2,000 and 20,000 BTU/ft^2-sec. Further, the total heating environment

(combined radiative and convective) lies between approximately 30,000 and 70,000 BTU/ft^2 for a 1 1/2 ft. rad. body. The magnitude of these heating rates is extremely large, and the design problem a serious one yet not much work has been performed in ground-based facilities to evaluate materials under such conditions. The lack of extremely high enthalpy $\left(\frac{hs}{RT_o} \sim 700\right)$ material test facilities has precluded the attainment of such values, although short time aerodynamic shock tunnel facilities with such capabilities are presently in operation at MSD and elsewhere (Refs. 37 and 38). As is well known, long time electric arc facilities are required to provide the necessary simulation environments for the evaluation of ablation materials, at least for the establishment of severe convective heating test conditions. Simulation of large radiative heating loads in the laboratory is not as far advanced, due primarily to only the recent requirement for such environments for study purposes. In addition, since the radiative loads attainable are directly proportional to the volume of the radiating species (say test gas), the use of small test models in laboratory test facilities has further complicated the problem of the attainment of large radiative heat transfer values on test specimens.

Recently at the SSL a test technique has been developed whereby it is feasible to conduct studies in controlled radiative and convective heating environments using the tandem-Gerdien arc heater developed at this laboratory (Ref. 39). Unlike most approaches to this problem which are handled by a superposition of a separate radiative source upon a plasma jet flow, this

technique makes use of a single electric arc source for both the radiative and convective heating loads. A salient advantage of this arrangement is that the source of the radiation is high temperature air resulting in a spectral energy distribution similar to that which would be experienced by entering vehicles at high velocity. The technique has been evaluated and correlated at low radiant intensities ($\sim$200 Btu/ft^2 sec) under conditions whereby the gas enthalpy (at one atmosphere pressure) measured at the model specimen location was found to be around 450 RT_o. Subsequent studies have resulted in gas stagnation enthalpy measurements in excess of 800 RT_o with certain test configuration modifications. Currently calibration measurements are being made at environmental pressure levels of five atmospheres which, when coupled with the higher enthalpy test flows, should provide a test radiation intensity in excess of 1000 Btu/ft^2 sec at the specimen surface. Simultaneously with this large radiant source a controllable (depending upon amount of by-passed flow) convective heating load from the flowing high enthalpy gases can also be superimposed on the specimen. In the following section a more detailed description of the test technique is presented.

5.2 The Tandem-Gerdien Radiation Arc

The product of considerable development effort, the Space Sciences Laboratory tandem-Gerdien arc heater produces a high enthalpy air flow with an insignificant trace ($<$ 100 ppm) of carbon contaminant from the electrodes for operating times in excess of 15 minutes. This configuration has been operated with various test facilities (wind tunnel and free jets) in the

Laboratory consistently at air stagnation enthalpy values ($^{h}s/RT_{o}$) in excess of 400; however, to produce high radiant intensity levels for material testing, calculations show that enthalpies in excess of 700 RT_{o} are desired (Ref. 39). Data obtained during the developmental period of the arc heater indicated that the necessary enthalpy requirement could be achieved if the test gas specimen were extracted from the arc column where gas temperatures in excess of 15,000°K had been measured by McGinn (Ref. 40). After considerable study and design evaluation the configuration shown in Figure IV-5.6 was constructed. A photograph of the facility is shown in Figure IV-5.7. The major alteration involved the plenum chamber whose basic shape was changed from a cylindrical section to a tee section; the diameter of all three legs of the tee is equal to that of the restrictor plate orifices. With this arrangement the hot gas that normally mixed in the larger plenum in the presence of the arc column is further energized by the very core of the column before flowing towards the model. Besides the processed gas in the column, calculations show that the gas flowing towards the model contains sufficient energy to contribute appreciably to the radiant intensity at the model surface if sufficiently high enthalpy has been generated by the arc heater ($^{h}s/RT_{o} \sim 700$).

As indicated in Figure IV-5.6, the test configuration is a shroud nozzle so that with a high enthalpy gas generated in the plenum, large convective heat transfer rates would be imposed on a test model in addition to the radiative contributions. (Equivalently high convective values would also be imposed if the test configuration was operated as a free jet).

To minimize the convective heating rates so as not to mask the response of the materials to the gas radiation, a by-pass was incorporated in the modified plenum whereby a large portion of the hot gas would be exhausted overboard just ahead of the model. Using this approach the hot gas flow required for the radiant energy transfer is not disturbed, but the convective heating can be controlled.

5.3 Proposed Study

To characterize the performance of ablation materials in heat transfer environments typical of entry into the planetary atmospheres of Venus and Mars, including the effects of large radiative heating loads and non-steady ablation phenomena where applicable, the following studies are proposed. The work is conveniently subdivided into two distinct studies which are independent of one another.

A. Systems Study

An experimental heat protection systems study would be conducted, taking into account the broad range of trajectory parameters that influence ablation material behavior and exposing test specimens in a controlled manner to the necessary test environments to properly characterize such materials. Included in this study would be an investigation of material degradation in environments which provide appreciable radiative heating loads, large convective rates and others in which non-steady ablation characteristics predominate. Although trajectory calculations indicate even for the more shallow entry conditions that a large percentage of the heat transfer over the rear-

ward portions of the vehicle would be turbulent, the increased heating rates over the laminar values may still be low enough to result in departures from steady state ablation. Certainly when the stagnation point heating as indicated in Figure IV-5.2 is only 100 BTU/ft^2-sec, one could expect heating rates on the skirt, even with turbulent flow that could result in the above-mentioned deviations. It seems desirable, therefore, to pursue this phenomenon.

At least one existing material would be examined, the emphasis of the study being on the prediction of the performance of proven ablation materials (in terrestrial environments) for trajectories typical of a proposed mission. In this respect it is felt that phenolic nylon is well suited to be included in such a study.

Typical entry trajectories would be chosen on the basis of overall systems considerations; that is, a family of entry paths into the planetary atmospheres would be used, covering a range of ballistic parameter, entry angle, entry velocity, etc. For these results the respective stagnation point heating rate histories, both radiative and convective, for a typical vehicle (sphere-cone) would be obtained from the results of the Venus-Mars Capsule Study. From these results for a limited number of cases where it appears desirable, heating rate histories at the aft section of the vehicle (skirt) will also be computed. In view of the uncertainties associated with the correct species determination for the Venus and Mars atmospheres, it is suggested to conduct these studies in the various simulated environments currently being considered by JPL and MSD. These are:

a) 3% CO_2 97% N_2

b) 9% CO_2 91% N_2

c) 25% CO_2 75% N_2

A priori it would be decided which of the calculated trajectories represented extremes in expected material performance, thereby providing the criteria for simulation in the test facilities.

The case(s) chosen as representative of very severe environments both from the radiative and convective viewpoint would be simulated in the tandem-Gerdien radiation arc in which both types of heating environments can be generated. In these tests by varying the operational test parameters -- pressure level (1-5 atm), gas enthalpy ($700 > {}^{h}s/RT_o > 400$), flow by-pass and exposure time, the performance of the ablation materials investigated would be established for both radiative and convective environments. Where possible test, exposure would be extended to total heating as inferred by the chosen heat transfer trajectories (BTU/ft^2). With this information available, the requirements of a full trajectory simulation test will be developed and a study performed in the tandem-Gerdien arc wind tunnel (see Figure IV-5.8). The reference criteria for these tests will be a previously selected typical heat transfer history applicable to the hypothetical vehicle skirt location, although the actual test specimen would be a blunt axisymmetric model evaluated at its stagnation point. The assumptions leading to the choice of simulated trajectory properties could thus be checked and modified conditions investigated if necessary. Model parameters would be material thickness, mass loss, backwall temperature and surface temperature. Analysis of the

results would include comparison with calculated material performance in both the theoretical flight trajectories and the simulated test environments.

The outgrowth of this study with appropriate, well characterized, thermal shield ablation materials should provide the vehicle designer with reliable inputs useful for actual design of a thermal shield for a Venus-Mars entry capsule.

B. Evaluation of Improved Materials

A second facet of this proposed study involves the experimental evaluation of new and improved materials for use as thermal shields on future Venus-Mars entry vehicles. The first study, as indicated, will consider currently available ablation materials which are well characterized and have proven to perform successfully on terrestial re-entry vehicles. For planetary entry, with the anticipated severe environmental conditions, calculations show that the thermal shield can be an appreciable portion of the complete capsule weight (Ref. 18). The use of better performing, lighter total weight ablation materials is, therefore, desirable to improve mission capabilities and assure successful entry. Areas of contemplated material research leading to more efficient thermal shield materials are discussed in section IV-6. Here we wish to present the experimental evaluation approach to the examination of these newer material formulations. Included in what is termed "newer formulations" can be existing materials which look promising but have not received any significant experimental evaluations.

As discussed earlier, ablation material behavior can be characterized

as steady state or non-steady state, depending primarily upon the level of the heating rate and the time duration of the heating pulse. Although both areas are worthy of investigation in any materials program, for general screening of heat protection materials, evaluations in high intensity, high enthalpy environments which produce steady state response will provide a meaningful yardstick. This is not to be considered a downgrading of the need for testing in the non-steady state ablation environments, but rather a choice for the sake of economy between the two test environments in view of the extremely severe stagnation point heating expected for proposed missions. Future studies can further explore subsequently proven newer materials.

This study would also be conducted in the tandem-Gerdien radiation arc under similar conditions as imposed in the previously described systems study. Criteria for the choice of the test conditions would be the same as in that work and similar analyses of test data would be performed.

Choice of materials would be based on the outgrowth of the materials development program discussed in Section IV-6, although this factor need not be very restrictive. Sufficient data are currently available within the Materials Section of the SSL to establish early in this program, during the time of test environment establishment and characterization, the types and formulations of materials with which to initiate testing. Once this initial flow characterization and material testing have been completed it is expected that newly formulated materials emanating from the proposed materials program would be factored into this proposed experimental evaluation. As

mentioned earlier existing, currently uncharacterized materials that look promising can also be included in the program, especially in the early phases.

Listed in Tables 5.1 - 5.5 are the nominal test conditions and the number of runs recommended for these studies.

TABLE 5.1 Nominal Test Conditions Tandem-Gerdien Radiation Arc

h_s/RT_o	$\dot{q}_{RAD}$ BTU/Ft^2/Sec.	$\dot{q}_{CONV}$ BTU/Ft^2/Sec.		
		A	B	C
700	1000	500	1000	3000
		D	E	
550	500	500	1000	
		F	G	
400	200	200	1000	

TABLE 5.2 Nominal Test Conditions Tandem-Gerdien Hypersonic Arc Tunnel

h_s/RT_o	$\dot{q}_{CONV}$ BTU/Ft^2-Sec.
400	50-75

TABLE 5.3 Experimental Program-Run Determination Systems Study - Radiation Arc

1. Measurement of Stagnation Enthalpy

   3 Test Points x 2 Runs/Test x 3 Gases — 18

2. Measurement of Radiant Intensities

   3 Test Points x 5 Runs/Test x 3 Gases — 45

3. Measurement of Combined Radiative and Convective Heat Transfer

   7 Test Points x 3 Runs/Test x 3 Gases — 63

4. Model Testing

   Phenolic - Nylon

   7 Test Points x 6 Testing Times x 3 Gases — 126

   252

TABLE 5.4 Experimental Program - Run Determination Systems Study - Hypersonic Arc Tunnel

1. Measurement of Stagnation Enthalpy	
1 Test Point x 2 Runs/Test x 3 Gases	6
2. Measurement of Convective Heat Transfer	
1 Test Point x 3 Runs/Test x 3 Gases	9
3. Model Testing	
Phenolic-Nylon	
1 Test Point x 2 Test Times x 3 Runs/Time x 3 Gases	18
	33

TABLE 5.5 Experimental Program - Run Determination New Material Study Radiation Arc

2 Test Points (A, C) x 6 Test Times x 3 Gases x 7 mat'l	252

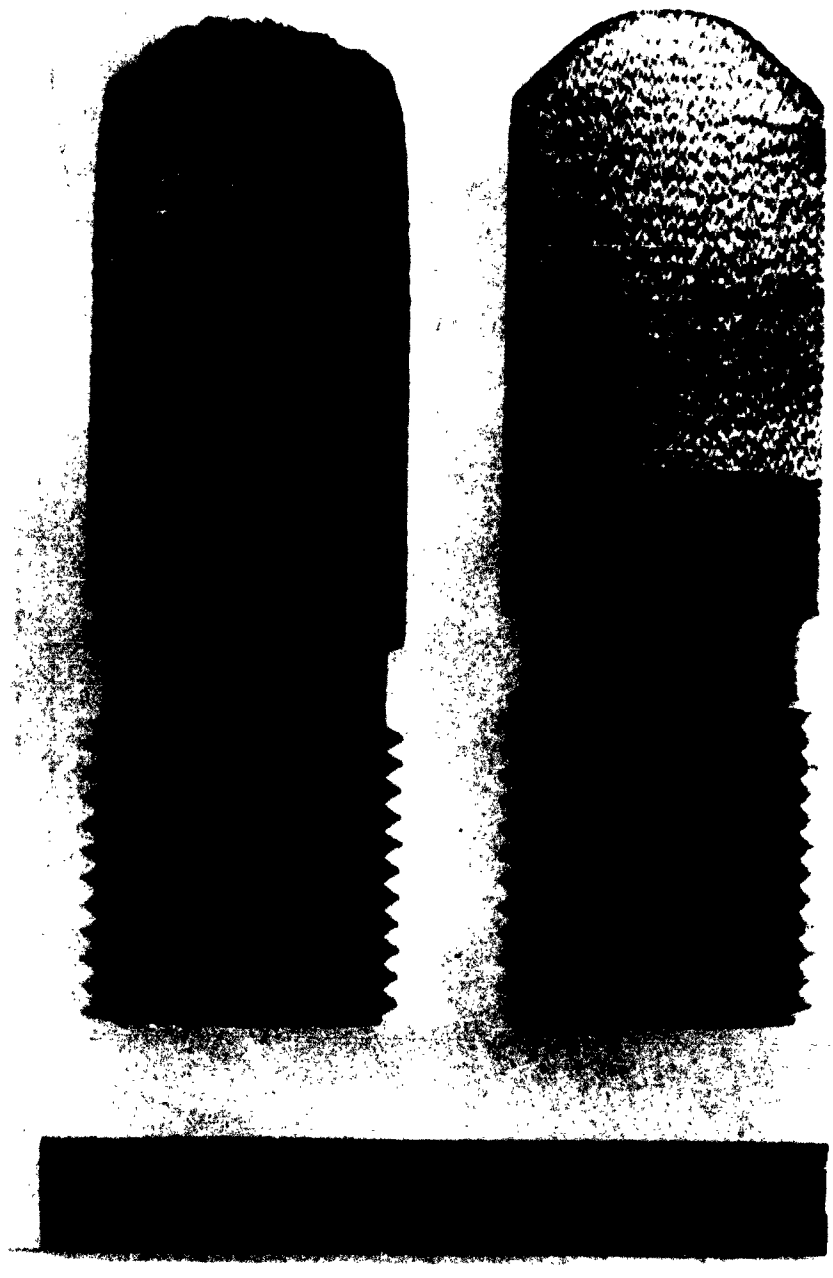

TEST CONDITIONS

$h_e/RT_o = 175$

$Q = 60$ BTU/FT^2 SEC; $t = 120$ SEC

$Q_{TOTAL} = 7200$ BTU/FT^2

$h_e/RT_o = 175$

$Q = 830$ BTU/FT SEC; $t = 10$ SEC

$Q_{TOTAL} = 8300$ BTU/FT^2

Figure IV-5.1 Comparison of Material Behavior at High and Low Ablation Rates

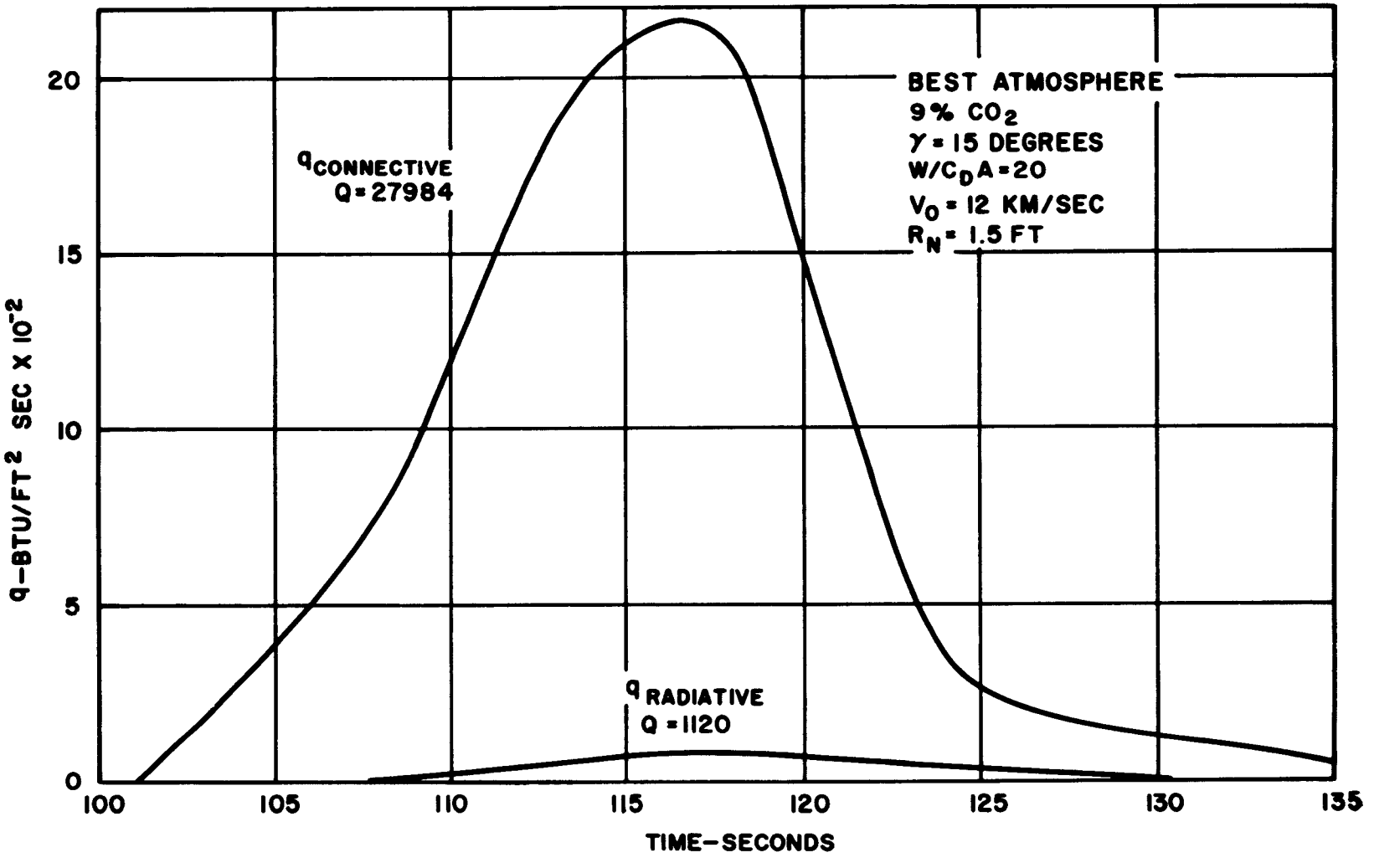

Figure IV-5.2 Stagnation Point Heat Transfer

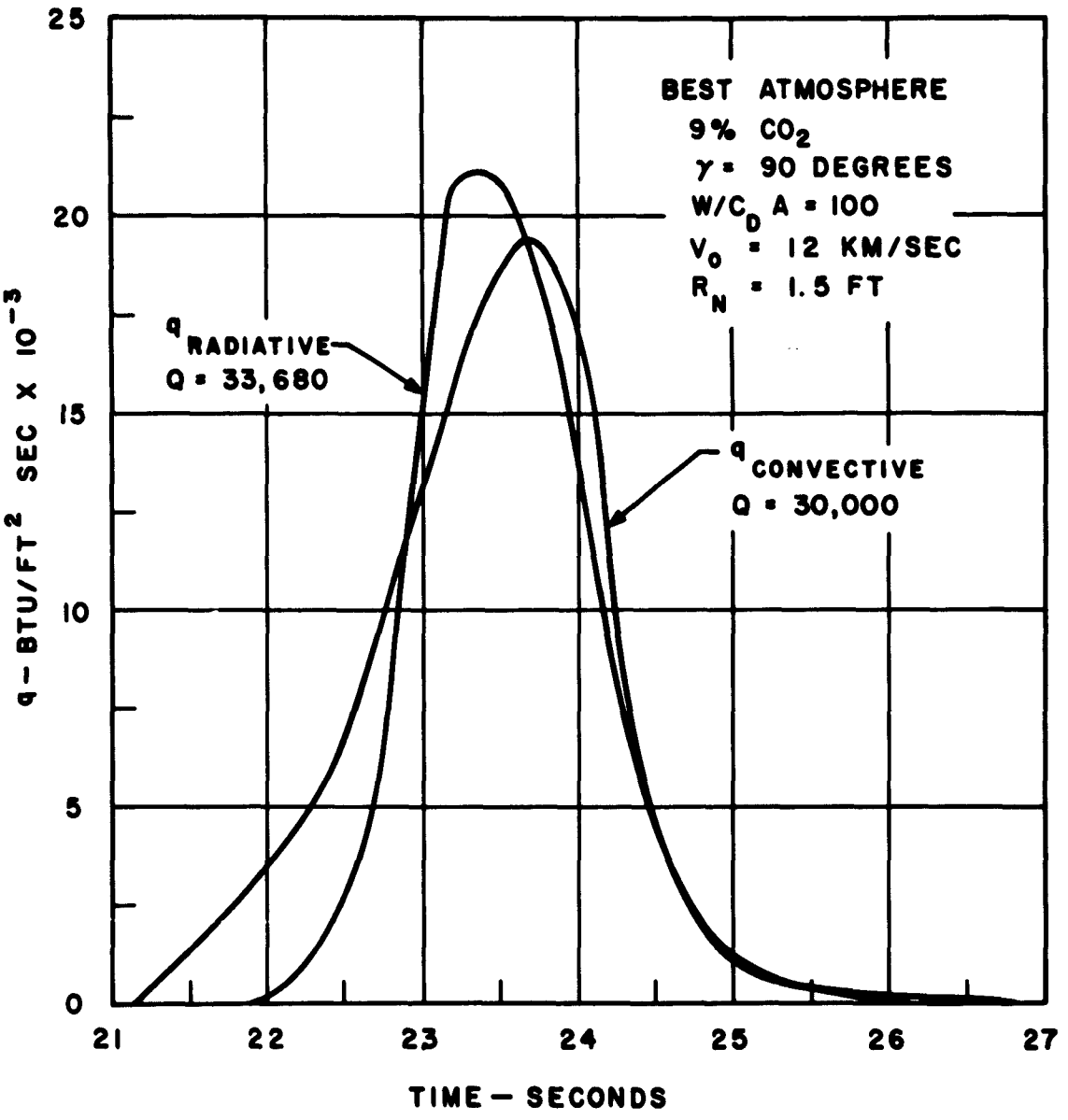

Figure IV-5.3 Stagnation Point Heat Transfer

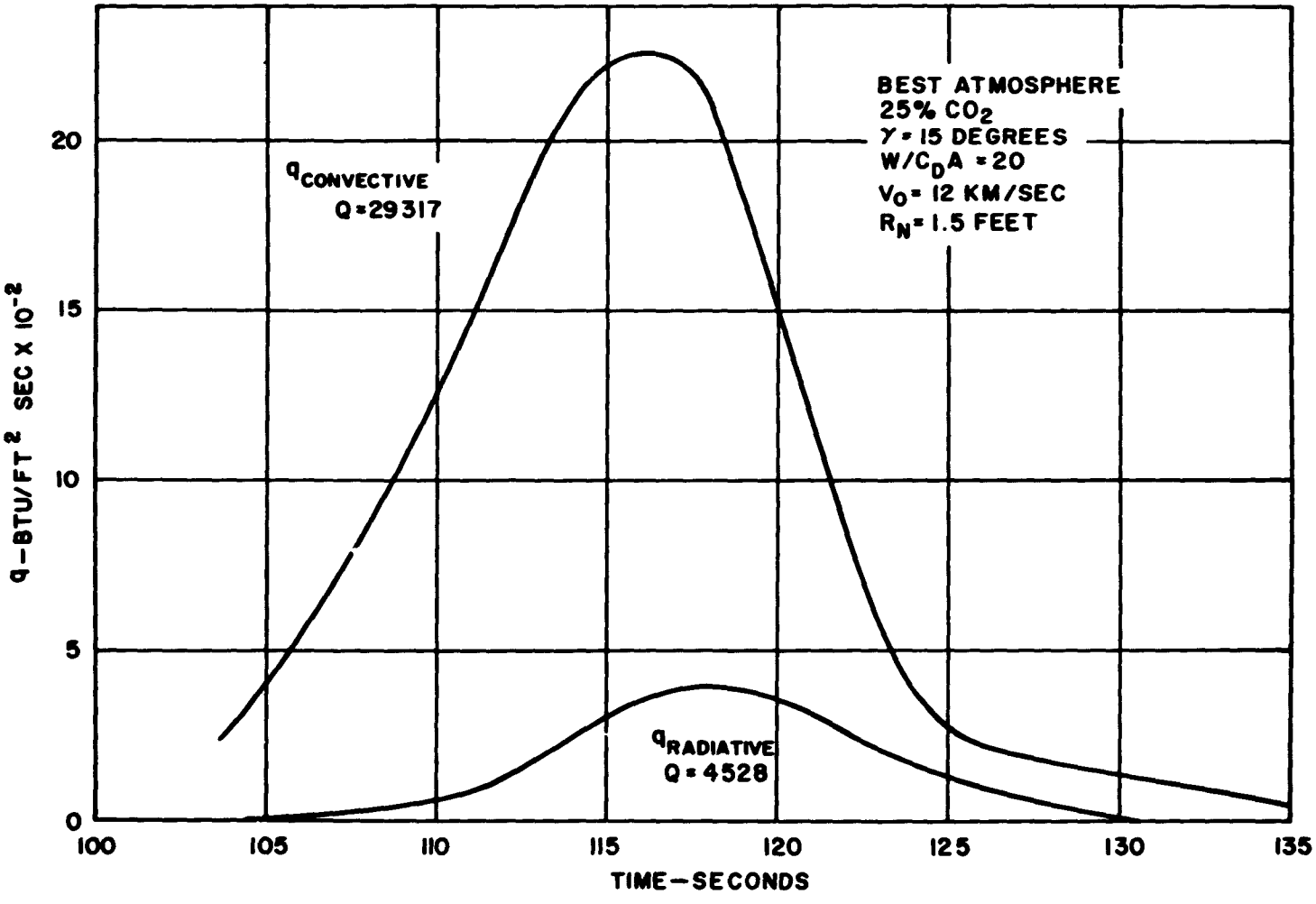

Figure IV-5.4 Stagnation Point Heat Transfer

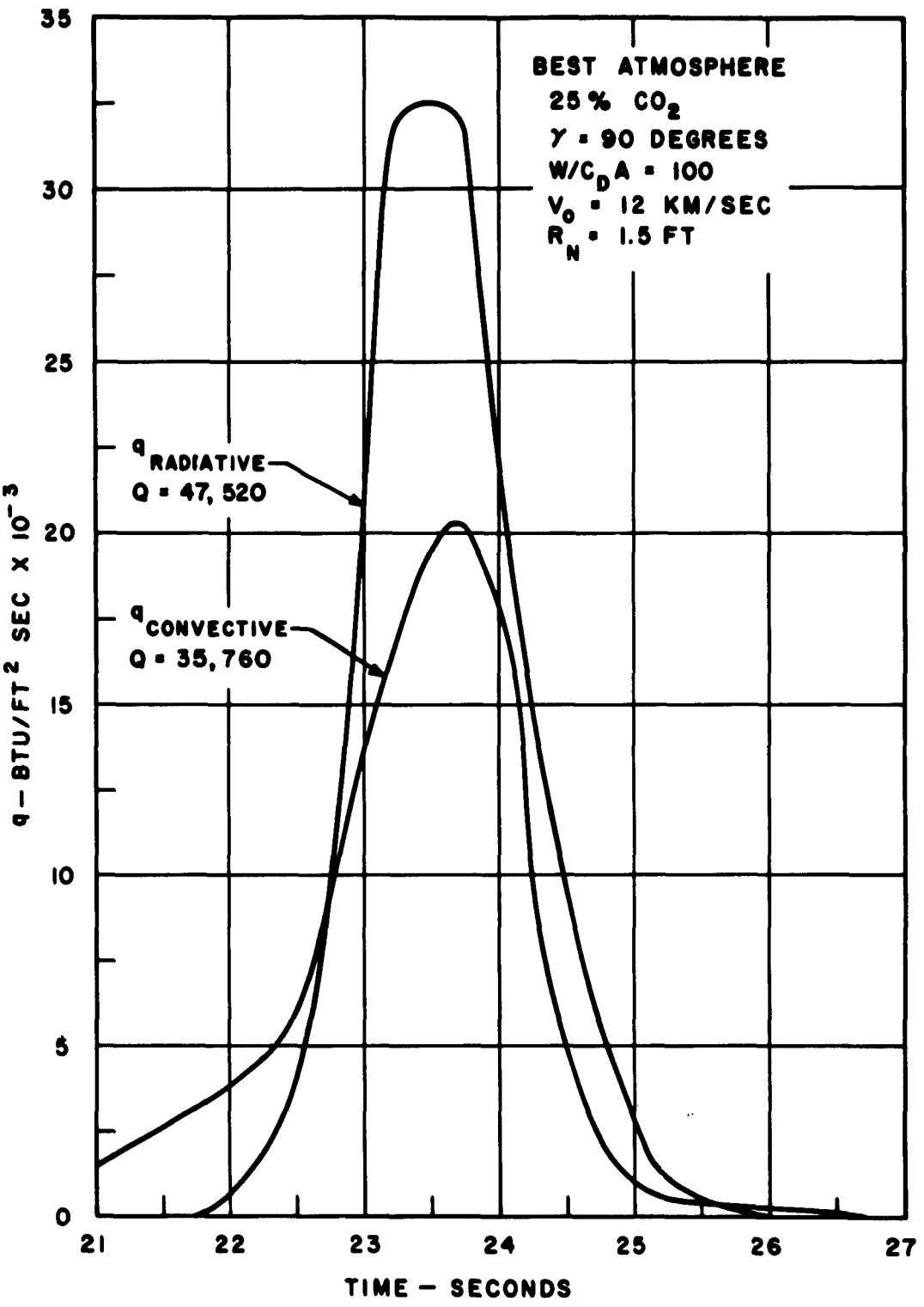

Figure IV-5.5 Stagnation Point Heat Transfer

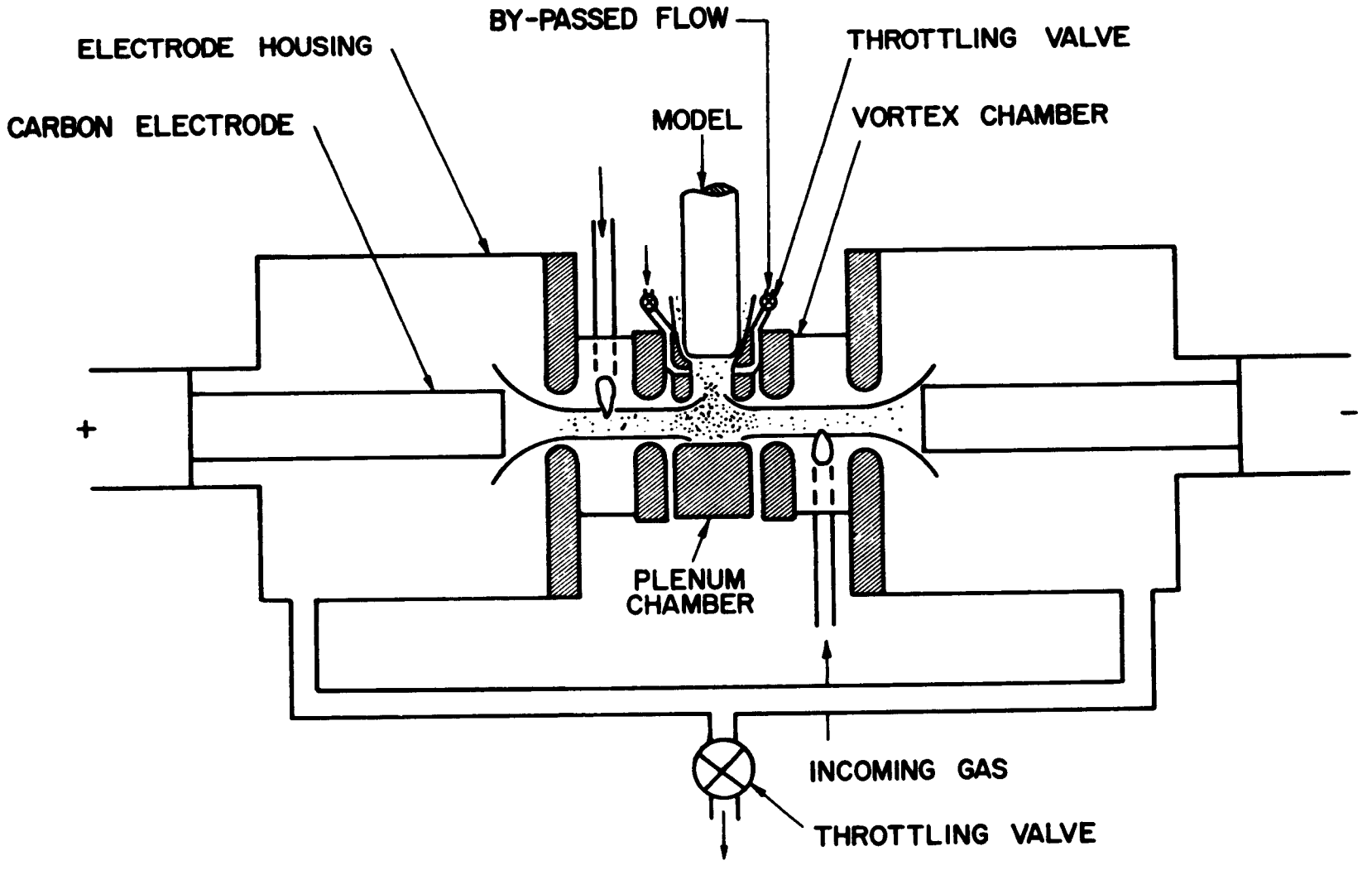

Figure IV-5.6 Tandem Gerdien Shroud Arc for Material Radiation Studies

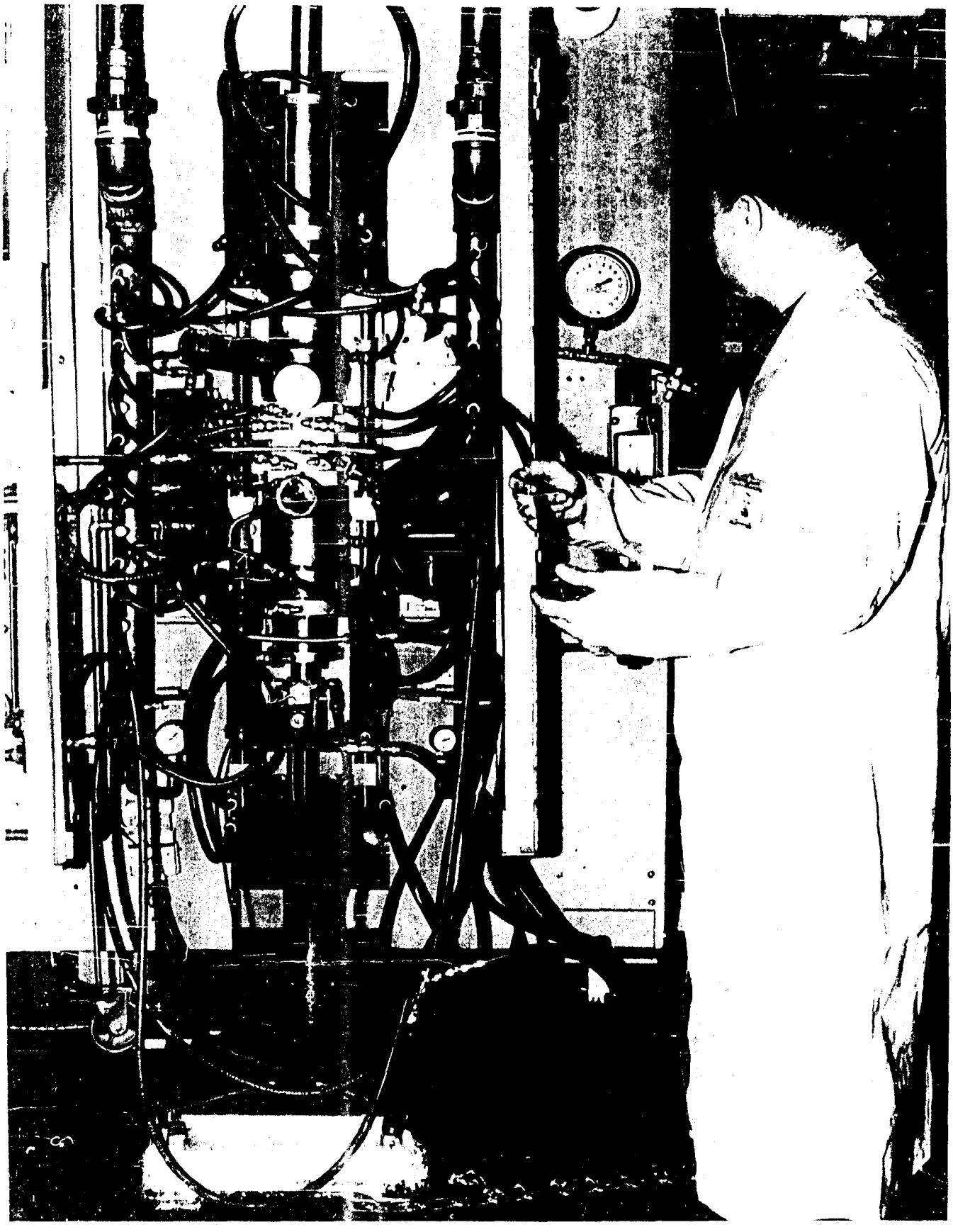

Figure IV-5.7 Radiation Arc

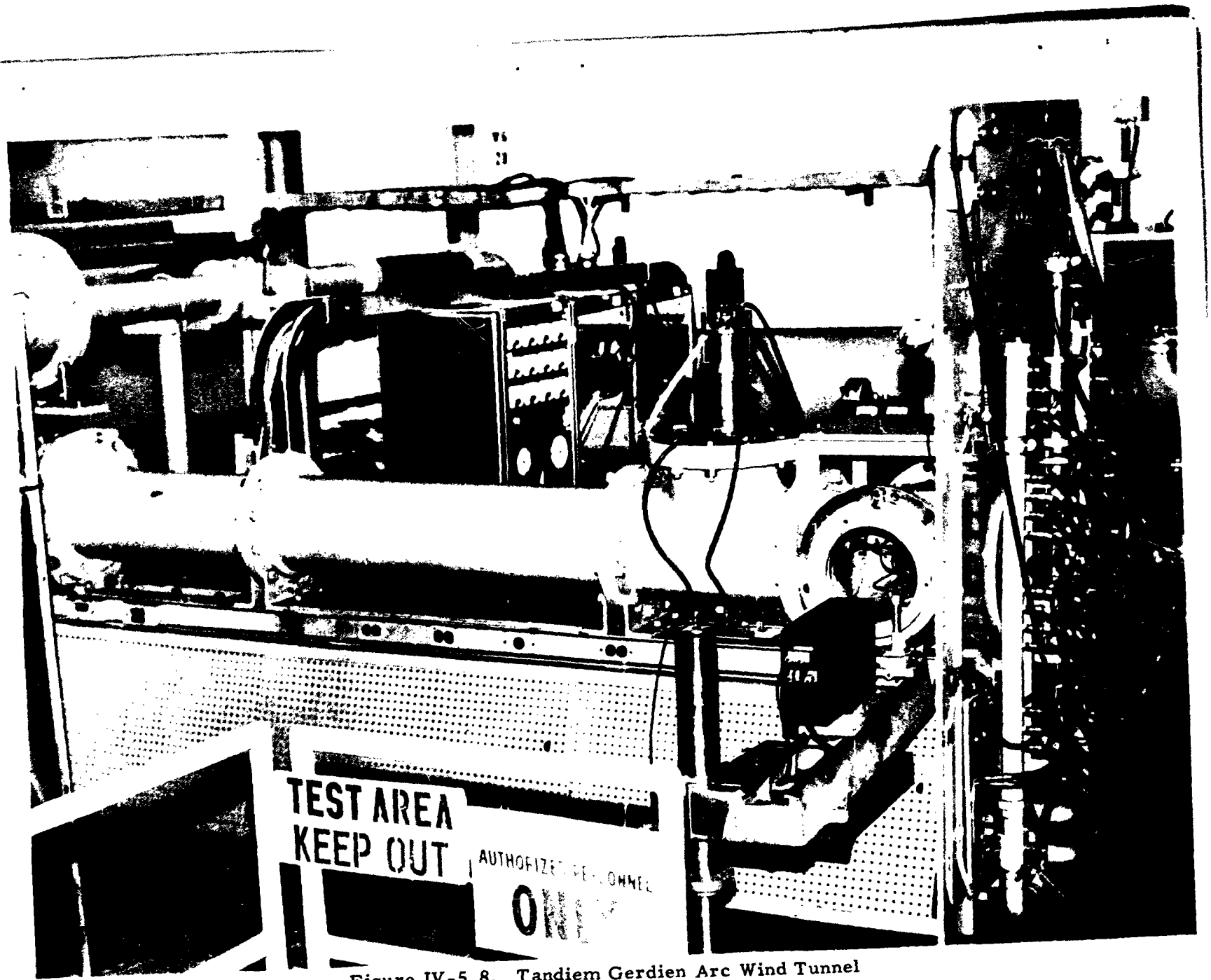

Figure IV-5.8. Tandiem Gerdien Arc Wind Tunnel

IV-6 HEAT SHIELD MATERIALS

6.1 Introduction

The choice of thermal protection materials for Venus-Mars entry is made difficult by the extremely high heating rates and shear forces which will be encountered. For a 90° entry into Venus with a 250 lb. capsule ($W/C_dA = 60$) the peak heating rates expected are 21,700 to 32,300 BTU/ft.^{2} sec. Preliminary estimates (Ref. 18) indicate that as a consequence of these heating rates, 81 lbs. of phenolic-nylon for heat protection would be required in the 250 lb. vehicle if phenolic-nylon were the heat shield choice. With the heat shield weight being such a high percentage of the total weight, any reduction in weight will have a strong influence on payload capability. Added to the heating rate problem is the fact that peak shear forces can be expected to reach 60 to 70 lbs./ft.^{2}. Thus, the heat shield material must have great mechanical integrity and must not lose excess surface material as a result of shear forces during the heat flux accompanying entry. A still further complication is the difference in Venus atmosphere from that of the Earth, i.e., greater percentage of CO_2 on Venus.

These conditions are vastly different from those for which present day heat shield materials have been developed. Therefore new approaches are required which may include not only modification of present materials but also synthesis of completely new heat shield materials or composites. The two requirements which appear to be most prominent are: (1) the need for a material with an extremely high heat of ablation, and (2) the need for a reinforced or very strong material. The material must also have good

physical properties, and an attempt should be made to reduce or eliminate any physical incompatibility between the heat shield and the vehicle substructure.

6.2 Materials Classes

Based on the foregoing requirements four classes of materials should be studied which either alone or in combination appear to hold the most promise for success. These are:

(1) New organic resins with high heats of ablation.

(2) Reinforced organic ablation materials.

(3) New silicone polymers.

(4) Refractory materials such as pyrolytic graphite.

These classes of materials are discussed briefly in the following paragraphs.

The 200 Series material, which is a quartz fiber reinforced resin, has been tested in a pebble bed heater jet ($4000^{o}F$, 300 $BTU/ft^2/sec$, 900 psia). The weight loss was found to be markedly less than that of phenolic nylon and the linear erosion rate about 15 times less than that of PN. The latter difference is due partially to the intumescent character of the Century material as it ablates.

A second ablation condidate has shown a very high heat of ablation, approximately three times that of Series 100 Resin and six times that of PN. This material involves the use of a radically new curing system with an epoxy resin. Such material could be reinforced by high melting, high strength fibers. Modifications might include the synthesis of graft polymers using

this material as a backbone. Prominent consideration should be given to organometallic grafts such as silicones.

A third candidate material as a highly crosslinked low siloxane resin silicone. Recent data indicate that this material has a higher heat of ablation than the Century Series or PN. Again these materials could be strengthened by reinforcing agents and by altering the molecular structure.

A fourth possibility is the use of pyrolytic-graphite either by itself or in a composite. As a first approximation it is estimated that the weight of PG required for the vehicle mentioned earlier might be one half that for PN. The insulating properties of PG coupled with the ablation properties of materials mentioned before should result in composites of great reliability. Such a composite might take the form of a graphite-resin laminate.

Vacuum aging experiments with PN and Century Resins are relevant to this problem since a Venus-Mars entry vehicle will spend considerable time in high vacuum before entry. These materials have been exposed to high vacuum and elevated temperatures for extended periods of time. Under these conditions no effect on the heat of ablation of PN was noticed. However, a slight improvement in the heat of ablation of the Century material was recorded.

The effect of particle radiation on heat protection materials for a Mars-Venus type mission have not been explored. It is possible that the radiation encountered would have an adverse effect on ablation performance. In going to Venus the outside of the vehicle would receive 10^5 to 10^6 rads

from solar emission. Inside of the first gm/cm^2 the dose should be reduced to 10^2 to 10^3 rads.

The above considerations should form an integral part of a materials development program. The problems to be encountered are such that present materials can not be expected to perform efficiently and hence additional research is a necessity.

6.3 Materials Development and Evaluation Program

A proposed program of materials development would concentrate on producing a heat shield material having a high heat of ablation and a high resistance to shear forces. Good physical properties would also be emphasized and an attempt would be made to reduce or eliminate any physical incompatibility between the heat shield and the vehicle structure.

The program would consist essentially of three tasks to run concurrently during the course of the study. These are: (1) Resin synthesis and development, (2) Formulations and reinforcement, and (3) Materials evaluation and characterization.

In the materials evaluation and characterization portion of the program a complete range of physical and thermal evaluations will be included. Screening tests will be run to indicate the more promising formulations and composites and these will then be tested further in the arc facilities described in previous sections of this report. As this testing would be conducted under conditions of heating (i.e., radiative/convective) and in atmosphere pertinent to Venus entry, the results would provide direct inputs to design calculations

of heat shield weights as well as provide guidelines for further materials improvement.

The characterization of these materials would be accomplished by rigorous examination of newly developed materials as well as determination of the products of decomposition brought about by ablation testing. It is important to know the physical characteristics of the heat shield material over a wide temperature range in order to determine design criteria as well as to determine physicochemical interactions which might affect ablation performance. The gaseous and liquid decomposition products of the ablating material determine the efficiency with which the shield will perform, and must be correlated with the entry environment anticipated. The structure of the char is also of paramount importance, since char stability will determine the extent to which the plasma will erode the virgin plastic - char interface.

Vacuum aging experiments with the more promising materials should be carried out since a Venus-Mars entry vehicle will spend considerable time in high vacuum before entry. The materials will be exposed to high vacuum and elevated temperatures for extended periods of time to determine the effect on material degradation or on the thermal properties such as that of heat of ablation.

The foregoing considerations of synthesis, evaluation and characterization from an integral part of a materials development program. The problems to be encountered in Venus-Mars entry are such that present materials cannot be expected to perform adequately, and further research is a necessity.

IV-7 VENUS IONOSPHERE PROPAGATION

A problem associated with the determination of Venusian ionospheric attenuation is that of the effective electron collision cross section. Even if an assumed model atmosphere is correct there is considerable uncertainty in the values of the cross section. For the expected electron energies well below a volt, the available data is very sparse (Ref. 30). The uncertainty appears to be of the order of one magnitude.

Another factor is that if any new data becomes available (from such as a Venus Flyby showing higher concentrations of CO_2 on Venus), the whole picture could change and possible attenuation estimates would be much higher and would necessitate an experimental program to better determine the effective collision cross section for the Venus model atmosphere (in the energy range of 0.001 to 1 ev). Another factor that should be investigated is the effect of ionosphere electron concentration estimate. The present study used an estimate of 10^6 electrons/cc. This is JPL's "best model" estimate; their high extreme model has an estimate of 10^8 electrons/cc. This model will make conditions much less favorable and a short study is here indicated to determine what attenuation could be expected at this limit.

V. REFERENCES

1. G. Schilling, "Extreme Model Atmospheres of Mars", Rand Report RM 2782, JPL, June 22, 1961.

2. Browne, W. G., "Thermodynamic Properties of Some Diatomic and Linear Polyatomic Molecules", Engineering Physics TM #3; GE-MSVD.

3. Brinkly, S. R., J. Chem. Physics 14, 563-564, 686 (1946) and 15, 107-110 (1947) et al.

4. Browne, W. G., "Equilibrium Thermodynamic Properties of the Environment of Mars", Advanced Aerospace Physics Tech. Memo No. 2, March 26, 1962.

5. Browne, W. G., "Thermodynamic Properties of the Venusian Atmosphere", Advanced Aerospace Physics Tech. Memo No. 13, (Three Parts), June 11, 1962.

6. Cary, B., "High Altitude Shock Wave Structure", Part II, AFOSR Document 1494, May 1962.

7. Byron, W., "Interferometric Measurement in a Shock Tube of Dissociation Rates for Air and its Component Gases", Proceedings of the Ninth General Assembly of AGARD, NATO, Aachen, Germany, Sept. 1959.

8. Eckerman, J., "A Study of the Relaxation Time for Thermal Dissociation of Nitrogen Using Free-Flight Techniques", NAVORD Report No. 5704, Vol. 1, May 1958.

9 Camm, J. and Keck, J., "Experimental Studies of Shock Waves in Nitrogen", AVCO Laboratory Report No. 140, June 1959.

10. Allen, R. et al, "Non-Equilibrium Radiation from Shock Heated N_2 and a Determination of the Recombination Rates", AVCO Laboratory Report No. 110, June 1961.

11. Herron, J. et al, "Kinetics of N_2 Recombination", J. Chem. Phys. Vol. 29, p. 230, 1958.

12. Wentinck, T. et al., "Nitrogen Atom Recombination at Room Temperature", J. Chem. Phys., 29, 231, (1958).

13. Harteck, P. et al, "Rate of Recombination of N_2 Atoms", J. Chem. Phys., 29, 608, (1958).

14. Resler, E.L., Lin, S.C., and Kantrowitz, A., "The Production of High Temperature Gases in Shock Tubes", JAP 23, No. 12 (1952) December.

15. Rose, P.H., and Stark, W.I., "Stagnation Point Heat Transfer Measurements in Dissociated Air", JAS 25, No. 2 (1958) February.

16. Hollyer, R.N., Hunting, A.C., Laporte, O., and Turner, E.B., "Luminosity Generated by Shock Waves", Nature 171, 395 (1953).

17. Warren, W.R., Rogers, D.A., and Harris, C.J., "The Development of an Electrically Heated Shock Driven Test Facility", 2nd Symposium on Hypervelocity Techniques, University of Denver, Denver, Colorado, March 1962.

18. GE-MSD: Venus-Mars Capcule Study, JPL Contract 950250, (Two Volumes) July 30, 1962.

19. Rose, P.H., "Development of the Colonimeter Heat Transfer Gage for Use in Shock Tubes", AVCO Research Report 17, February 1958.

20. Rutowski, R.W., and Chan, K.K., "Shock Tube Experiments Simulating Entry Into Planetary Atmospheres", LSMD-288139, January 1960.

21. Scala, S.M., and Baulknight, C.W., "Transport and Thermodynamic Properties in a Hypersonic Laminar Boundary Layer -- Part 2, Applications", ARS Jour. 30, No. 4, (1960) April.

22. Scala, S.M., Private Communication.

23. Scala, S.M., "The Ablation of Graphite in Dissociated Air: Part I, Theory", Nat'l Summer Meeting, Inst. of Aero/Space Sciences, Los Angeles, Calif., June 19-22, 1962.

24. Diaconis, N.S., Gorsuch, P.D., and Sheridan, R.A., "The Ablation of Graphite in Dissociated Air, Part II, Experimental", Nat'l Summer Meeting, Inst. of Aero/Space Sciences, Los Angeles, Calif., June 19-22, 1962.

25. Scala, S.M., "A Study of Hypersonic Ablation", 10th Int'l Astronautical Congress, London, 29 Aug. - 5 Sept., 1959.

26. Diaconis, N.S., Fanucci, J.B., and Sutton, G.W., "The Heat Protection Potential of Several Ablation Materials for Satellite and Ballistic Re-Entry into the Earth's Atmosphere", Ballistic Missiles and Space Technology Vol. II, Pergamon Press, 1961.

27. Metzger, J.W., "Ablation Data on Molded Phenolic Nylon Tested in the Shroud Nozzle Air Stabilized Arc", Advanced Aerodynamics TM 92, Sept. 1959.

28. Drummond, J.E., Plasma Physics, McGraw-Hill Company, 1961.

29. Massey, H.S.M. and Burhop, E.H.S., Electronic and Ionic Impact Phenomena, Oxford University Press, London, 1952.

30. Brown, S.C., Basic Data on Plasma Physics, Wiley, 1959.

31. Opik, E., "The Atmosphere and Haze of Mars", J. Geophys. Res. (USA), Vol. 65, No. 10, p. 3057, 1960.

32. Mahon, B., "The Photolysis of CO_2," J. Chem. Phys., Vol. 33, p. 959, 1960.

33. Byron, S., "Measurements of the Rate of Dissociation of Oxygen", J. Chem. Phys. 30, No. 6, 1380 (1959).

34. Rink, J. et al., "Shock Tube Determination of Dissociation Rates of Oxygen", J. Chem. Phys. 34, No. 6, 1942 (1961).

35. Bortner, M., "Electromagnetic Effects Associated with Hypersonic Vehicles", Aero Sciences Laboratory Report, May 15, 1959.

36. Warren, W.R., and Diaconis, N.S., "The Performance of Ablation Materials as Heat Protection for Re-Entering Satellites", IAS Paper 60-49, IAS 28th Annual Meeting, New York, N.Y., January, 1960; Also WADD TR 60-58, May 1960.

37. Warren, W.R. et al, "The Development of an Electrically Heated Shock Driven Test Facility," pres. 2nd Hypervelocity Symp., Denver, Colo., March, 1962.

38. Camm, J., "Escape Velocity Shock Tube With Arc Heated Driver, Avco-Everett Res. Lab., Res. Rpt., pres. at 2nd Hypervelocity Symp., Denver, Colo.,March, 1962.

39. Diaconis, N.S., "Combined Radiative and Convective Heat Transfer Effects on Ablation Materials", ARVP Doc. No. 62SD655 (Conf.) August 6, 1962.

40. McGinn, J.H.,"Arc Development", GE-MSD TIS No. R61SD201, December, 1961.

DISTRIBUTION LIST FOR TIS R62SD84

EXTERNAL

Air Force Ballistic Missiles Division
Hdqs. Air Research & Development Command
AF Unit Post Office
Los Angeles 45, California
Attn: WDTVR (1)
Note: All reports directed to the above should be forwarded to G. Persh, Room 5211, Chestnut St. for transmittal.

Air Force Cambridge Research Center
Hdqs. Air Research & Development Command
Laurence G. Hanscom Field, Massachusetts
Attn: Technical Library (1)
Dr. J. M. Howard (1)
Dr. Max Nagel (1)
Mr. W. Rothman (1)

Air Force Cambridge Research Center
Geophysics Division
Laurence G. Hanscom Field
Bedford, Mass.
Attn: Technical Library (1)
Lt. John W. Salisbury (1)

Air Force Office of Scientific Research
Technical Information & Intelligence
Washington 25, D.C.
Attn: Technical Library (1)

Commander
Air Force Office of Scientific Research
Washington 25, D.C.
Attn: Mechanics Division (1)

Commander
Arnold Engineering Development Center
Air Research & Development Command
Tullahoma, Tennessee
Attn: AEOIM (1)
J. Lukasiewiiz (1)

DISTRIBUTION LIST FOR TIS R62SD84 (Cont'd)

Dr. Frank Wattendorf, Director
AGARD, APO 230
c/o Postmaster
New York, New York (1)

Commander
USAF Institute of Technology
Wright-Patterson Air Force Base, Ohio
Attn: Technical Library, MCLI (1)

Commander
Wright Air Development Division
Wright-Patterson Air Force Base, Ohio
Attn: Dr. B. L. Landrum (1)
J. I. Wittebort (1)
L. Salzberg (1)
Dr. R. Mills, WCLJD (1)
F. L. Daum (1)
R. D. Neumann (1)
WCOSI - Distribution (2)
WWFEA - Reports Unit (1)

Commander
Air Materiel Command
Wright-Patterson Air Force Base, Ohio
Attn: Technical Library (1)

National Aeronautics & Space Administration
Marshall Space Flight Center
Huntsville, Alabama
Attn: Dr. E. W. Adams/M-AERO-A (1)

Aberdeen Proving Ground
Ballistics Research Laboratories
Aberdeen, Maryland
Attn: Dr. C. L. Poor (1)
Dr. J. H. Frazer (1)
Technical Library (1)

Army Engineer Research & Development Labs.
Technical Reference & Analysis Branch
Fort Belvoir, Virginia
Attn: Mr. Goldberg (1)

Commander
Army Rocket & Guided Missile Agency
Redstone Arsenal, Alabama
Attn: Research & Development Division

W. H. Ewart, ARDXR-REM	(1)
R. Easley	(1)
Dr. C.F. Bjork, Future Concepts Branch, Building 5687	(1)
J. E. Norman, Ordnance Miss. Lab	(1)
Dr. E. W. King	(1)
Frank Vann/Lt. W.J. Schultiss, ORDXR-RFE	(1)
Technical Library	(1)

Army Ballistic Missile Agency
Redstone Arsenal, Alabama

Attn: W. A. Mrazek, ORDAB-DS	(1)
Dr. E. Geissler	(1)
W. K. Dahm, Aero Analysis Br.	(1)
Technical Documents Library	(1)

Office of the Chief of Ordnance
Department of the Army
Washington 25, D.C.
Attn: ORDTB (1)

Office of the Chief of R & D
Department of the Army
Washington 25, D.C.
Attn: Scientific Information (1)

*Dr. Walter Haeussermann
1607 Sandlin Avenue, S.E.
Huntsville, Alabama (1)

Signal Corps Engineering Laboratory
Fort Monmouth, New Jersey
Attn: SIGFMIEL - RPO (1)

David Taylor Model Basin
Aerodynamics Laboratory
Washington 7, D.C.
Attn: Library (1)

*of ABMA. Requested reports be sent to private office address.

NASA
Manned Spacecraft Center
Houston, Texas
Attn: J. Kotanchik (1)
K. Weston (1)
Technical Library (1)

NASA
Goddard Space Flight Center
Greenbelt, Md.
Attn: L. G. Stroud (1)
L. E. Richtmyer (1)
Technical Library (1)

National Aeronautics & Space Administration
1520 H Street, N. W.
Washington 25, D.C.
Attn: Director of Research (1)
Dr. R. Horner (1)
Dr. R. Jastrow (1)
Document Library (1)

National Aeronautics & Space Administration
Langley Research Center
Langley Field, Virginia
Attn: Dr. J. Shortal (1)
Technical Library (1)
E. Love (1)
W. A. Brooks (1)

National Aeronautics & Space Administration
Ames Aeronautical Laboratory
Moffett Field, California
Attn: H. Julian Allen (1)
A. Eggers (1)
R. Savin (1)
Technical Library (1)
G. Goodwin (1)
V. Stevens (1)

National Aeronautics & Space Administration
Lewis Aeronautical Laboratory
21000 Brookpark Road
Cleveland 25, Ohio
Attn: J. H. Discher (1)
Technical Library (1)

National Aeronautics & Space Administration
Western Coordination Office
7660 Beverly Boulevard
Los Angeles, California
Attn: Technical Library (1)

National Aeronautics & Space Administration
Redstone Arsenal, Alabama
Attn: Dr. E. Stuhlinger (1)
Technical Library (1)

J. P. L.
Pasadena, Calif.
E. Freeman (1)
J. Spiegal (1)
R. Nagler (1)
L. Sola (1)
T. Pounder (1)
Technical Library (1)

Office of Technical Services
Department of Commerce
Washington 25, D.C. (1)

Institute for Defense Analyses
Research & Engineering Support Div.
1825 Connecticut Ave., N. W.
Washington 9, D. C.
Attn: Technical Library (1)

Director
National Bureau of Standards
Washington 25, D. C.
Attn: Fluid Mechanics Section (1)
Electron Physics Section (1)
Thermodynamics Section (1)
Technical Library (1)

U. S. Atomic Energy Commission
1901 Constitution Avenue, N. W.
Washington 25, D. C.
Attn: Technical Library (1)

U.S. Atomic Energy Commission
Technical Information Extension
P.O. Box 62
Oak Ridge, Tennessee (1)

DISTRIBUTION LIST FOR TIS R62SD84 (Cont'd)

Armed Services Technical Information Agency
Arlington Hall Station
Arlington 12, Virginia
Attn: TIPCR (10)

Aeronautical Research Laboratory
Wright-Patterson Air Force Base
Dayton, Ohio
Attn: Mr. E. C. Callan/RRLO (1)

National Science Foundation
1951 Constitution Avenue, N.W.
Washington 25, D.C.
Attn: Engineering Sciences Division (1)

Armour Research Foundation
Illinois Institute of Technology
Chicago 16, Illinois
Attn: Dr. D. Hacker (1)
Technical Library (1)

Auburn University
Department of Mechanical Engineering
Auburn, Alabama
Attn: Technical Library (1)

Battelle Memorial Institute
505 King Avenue
Columbus 1, Ohio
Attn: Technical Library (1)

Brown University
Division of Engineering
Providence 12, Rhode Island
Attn: Dr. F. Maeder (1)
Aeronautical Laboratory (1)
Technical Library (1)
Prof. R. F. Probstein (1)

California Institute of Technology
Jet Propulsion Laboratory
4800 Oak Grove Drive
Pasadena 4, California
Attn: Technical Library (1)

California Institute of Technology
Pasadena 4, California
Attn: Department of Physics (1)
Technical Library (1)

California Institute of Technology
Guggenheim Aeronautical Laboratory
1201 East California Avenue
Pasadena 4, California
Attn: Prof. C. Millikan (1)
Prof. L. Lees (1)
Prof. J. Cole (1)
Technical Library (1)

Case Institute of Technology
Department of Aerodynamics
Cleveland 6, Ohio
Attn: Prof. G. Kuerti (1)
Technical Library (1)

Case Institute of Technology
Department of Electrical Engineering
University Circle
Cleveland 6, Ohio
Attn: Prof. O.K. Mawardi (1)

Colorado State University
Department of Civil Engineering
Fort Collins, Colorado
Attn: Technical Library (1)

Columbia University
Dept. of Civil Engineering & Eng. Mechanics
New York 27, New York
Attn: Technical Library (1)

Cornell University
School of Aeronautical Engineering
Ithaca, New York
Attn: Prof. W. Sears (1)
Prof. E. Resler, Jr. (1)
Technical Library (1)

Cornell University
Department of Physics
Ithaca, New York
Attn: Dr. Hans Bethe (1)

Cornell Aeronautical Laboratory
4455 Genesee Street
Buffalo 21, New York
Attn: Dr. F. Moore (1)
Dr. I. G. Ross (1)
Dr. R. Kell (1)
Technical Library (1)

Drexel Institute of Technology
32nd & Chestnut Streets
Philadelphia 4, Pennsylvania
Attn: Technical Library (1)

Harvard University
Department of Engineering Sciences
Cambridge 38, Massachusetts
Attn: Prof. G. Carrier (1)
Prof. H. Emmons (1)
Technical Library (1)

Harvard University
Harvard Observatory
Cambridge, Massachusetts
Attn: Prof. F. Whipple (1)

Illinois Institute of Technology
Physics Research Department
3440 South State Street
Chicago 16, Illinois
Attn: Technical Library (1)

Institute of the Aeronautical Sciences
2 East Sixty-Fourth Street
New York 21, New York (1)

John Crerar Library
86 E. Randolph Street
Chicago 1, Illinois (1)

Johns Hopkins University
Department of Mathematics
Baltimore 18, Maryland
Attn: Dr. F. Clauser (1)
Dr. S. Corrsin (1)
Technical Library (1)

Johns Hopkins University
Applied Physics Laboratory
8621 Georgia Avenue
Silver Spring, Maryland
Attn: Dr. Gibson, Director (1)
Technical Library (1)

Lehigh University
Department of Physics
Bethlehem, Pennsylvania
Attn: Technical Library (1)

Massachusetts Institute of Technology
Cambridge 39, Massachusetts
Attn: Dr. J. Killian (1)
Prof. H. Woodson (1)
Prof. H. Allis (1)
Technical Library (1)

Massachusetts Institute of Technology
Department of Aeronautical Engineering
Cambridge 39, Massachusetts
Attn: Prof. H. Stever (1)
Prof. L. Trilling (1)

Massachusetts Institute of Technology
Department of Mathematics
Cambridge 39, Massachusetts
Attn: Prof. C. Lin (1)
Prof. J. Fay (1)
Prof. M. Finston (1)

Massachusetts Institute of Technology
Department of Mechanical Engineering
Cambridge 39, Massachusetts
Attn: Prof. F. Kaye (1)

Massachusetts Institute of Technology
Lincoln Laboratory
Cambridge 39, Massachusetts
Attn: Dr. G. F. Pippert (1)
Technical Library (1)
Dr. R. E. Slattery (1)

Massachusetts Institute of Technology
Naval Supersonic Laboratory
Cambridge 39, Massachusetts
Attn: Technical Library (1)

Midwest Research Institute
425 Volker Blvd.
Kansas City 10, Missouri
Attn: Library (1)

New York University
Guggenheim School of Aeronautics
New York 53, New York
Attn: Prof. J. Ludloff (1)
Technical Library (1)

New York University
Institute of Mathematical Sciences
25 Waverly Place
New York 3, New York
Attn: Prof. H. Grad (1)
Technical Library (1)

North Carolina State College
Division of Engineering Research
Raleigh, North Carolina
Attn: Technical Library (1)

National Research Laboratories
Division of Mechanical Engineering
Ottawa, Canada
Attn: K. Orlik-Ruckerman (1)
Technical Library (1)

Northwestern Universtiy
Department of Mechanical Engineering
Evanston, Illinois
Attn: Technical Library (1)
Ali Balent Cambel (1)

Ohio State University
Rocket Research Laboratory
2240 Olentangy River Road
Columbus 10, Ohio
Attn: Technical Library (1)

Ohio State University
Department of Aeronautical Engineering
Columbus, Ohio
Attn: Technical Library (1)

Pennsylvania State University
University Park, Pennsylvania
Attn: Technical Library (1)

Polytechnic Institute of Brooklyn
Aerodynamics Laboratory
527 Atlantic Avenue
Freeport, Long Island, New York
Attn: Dr. A. Ferri (1)
Dr. P. Libby (1)
Dr. M. Bloom (1)
Dr. K. P. Chopra (1)
Technical Library (1)

Polytechnic Institute of Brooklyn
333 Jay Street
Brooklyn 1, New York
Attn: Technical Library (1)

Agricultural & Mechanical College of Texas
Dept. of Aeronautical Eng.
College Station, Texas
Attn: A. E. Cronk, Prof. & Head (1)

Princeton University
Palmer Physical Laboratory
Princeton, New Jersey
Attn: Prof. W. Bleakney (1)

Princeton Universtiy
Department of Aeronautical Engineering
Princeton, New Jersey
Attn: Prof. S. Bogdonoff (1)
Prof. W. Hayes (1)

Princeton University
Princeton Observatory
Princeton, New Jersey
Attn: Prof. L. Spitzer, Jr. (1)

Princeton University
The James Forrestall Research Center
Princeton, New Jersey
Attn: M. H. Smith, Associate Editor,
ARS Journal (1)
Technical Library (1)

Purdue University
Department of Aero. & Engineering Sciences
Lafayette, Indiana
Attn: Prof. R. Goulard (1)
Technical Library (1)

Rennselaer Polytechnic Institute
Department of Aeronautical Engineering
Troy, New York
Attn: Prof. T. Y. Li (1)
Technical Library (1)

Southern Methodist University
Department of Mechanical Engineering
3548 Southwestern Blvd.
Dallas 5, Texas
Attn: Prof. J. E. Denton (1)

Stevens Institute of Technology
Hoboken, New Jersey
Attn: Technical Library (1)

State University of New York
Oyster Bay, New York
Attn: Prof. W. S. Bradfield (1)
Prof. S. Levine (1)
Prof. T. Irvine (1)

Temple University
Research Institute
4150 Henry Avenue
Philadelphia 44, Pennsylvania (1)

Temple University
Broad & Montgomery
Philadelphia, Pennsylvania
Attn: Technical Library (1)

United States Air Force Academy
Department of Aeronautics
Colorado (1)

University of California
Los Alamos Scientific Laboratory
P.O. Box 1663
Los Alamos, New Mexico
Attn: Theoretical Division (1)
Technical Library (1)

University of California
Lawrence Radiation Laboratory
P.O. Box 808
Livermore, California
Attn: Dr. S. Colgate (1)
Dr. R. Post (1)
H. P. Furth (1)
Space Physics Research Group
Dr. C. D. Schrader
Room 235, Bldg. 152 (1)

University of California
Berkeley, California
Attn: Dr. S. Schaaf (1)
Dr. Edward Teller (1)
Technical Library (1)

University of California
Los Angeles Division
Los Angeles 24, California
Attn: Dept. of Engineering,
Publications Group, TEB-2B (1)
Department of Physics (1)

University of Chicago
Yerkes Observatory
Williams Bay, Wisconsin
Attn: Dr. S. Chandrasekhar (1)
Technical Library (1)

University of Chicago
Chicago, Illinois
Attn: Technical Library (1)

University of Illinois
Department of Aeronautical Engineering
Urbana, Illinois
Attn: Technical Library (1)

University of Maryland
Institute of Fluid Mechanics & Applied Math.
College Park, Maryland
Attn: Dr. S. Pai (1)
Dr. A. Sherwood (1)
Technical Library (1)

University of Maryland
Glenn L. Martin Institute of Technology
College Park, Maryland
Attn: Prof. G.S.S. Ludford, Dept. of
Aeronautical Engineering (1)

University of Michigan
Department of Aeronautical Engineering
Ann Arbor, Michigan
Attn: Prof. A. Kuethe (1)

University of Michigan
Department of Engineering Research
Ann Arbor, Michigan
Attn: Prof. O. LaPorte (1)
Prof. G. Uhlenbeck (1)

University of Michigan
Engineering Research Institute
201 Catherine Street
Ann Arbor, Michigan
Attn: Dr. Keeve Siegel (1)

University of Michigan
Willow Run Laboratories
P.O. Box 2008
Ann Arbor, Michigan
Attn: Mr. William Wolfe - IRIA (1)

University of Michigan
Willow Run Laboratories
P. O. Box 618
Ann Arbor, Michigan
Attn: Dr. George Zissis (1)

Ballistic Missile Radiation Analysis Center
University of Michigan
Willow Run Laboratories
P.O. Box 2008
Ann Arbor, Michigan
Attn: BAMIRAC Library (1)

University of Minnesota
Department of Aeronautical Engineering
Minneapolis, Minnesota
Attn: Prof. J. Akerman (1)
Technical Library (1)

University of Minnesota
Rosemount Aeronautical Laboratories
Minneapolis, Minnesota
Attn: Technical Library (1)

University of Pennsylvania
Department of Physics
Norman, Oklahoma
Attn: Technical Library (1)

University of Pennsylvania
34th & Walnut Street
Philadelphia 4, Pennsylvania
Attn: Technical Library (1)

University of Pennsylvania
Towne School
33rd & Locust Streets
Philadelphia 4, Pennsylvania
Attn: Dr. H. Yeh (1)

University of Southern California
University Park
Los Angeles 7, California
Attn: Engineering Center - Library (1)

University of Texas
Defense Research Laboratory
P.O. Box 8029
Austin, Texas
Attn: Technical Library (1)

University of Toronto
Institute of Aerophysics
Toronto 5, Canada
Attn: Dr. G. Patterson, Director (1)
Technical Library (1)

University of Utah
Experimental Research Laboratory
Salt Lake City, Utah
Attn: Technical Library (1)

University of Virginia
Ordnance Research Laboratory
Charlottsville, Virginia
Attn: Technical Library (1)

University of Washington
Department of Aeronautical Engineering
Seattle 5, Washington
Attn: Technical Library (1)

University of Wisconsin
Department of Chemistry
P.O. Box 2127
Madison 5, Wisonsin
Attn: Prof. J. Hirschfelder (1)
Prof. C. Curtiss (1)

Yale University
Department of Mechanical Engineering
New Haven 10, Connecticut
Attn: Technical Library (1)

Yale University
Sterling Chemistry Laboratory
New Haven, Connecticut
Attn: Technical Library (1)

Aeroject - General Nucleonics
P. O. Box 77
San Ramon, Calif.
Attn: S. T. Friedman (1)

AeroChem Research Laboratories, Inc.
P.O. Box 12
Princeton, New Jersey
Attn: Dr. H. F. Calcote (1)

Aerojet Engineering Corporation
6352 North Irwindale Avenue
Box 296
Azusa, California
Attn: Technical Library (1)

Aerospace Corporation
Box 95085
Los Angeles 45, California
Attn: Dr. Joseph Logan (1)
Technical Information Center (2)

Argonne National Laboratories
Box 299
Lemont, Illinois
Attn: Technical Library (1)

Atlantic Research Corporation
Alexandria, Virginia
Attn: Technical Library (1)

AVCO-Everett Research Laboratory
2385 Revere Beach Parkway
Everett 49, Massachusetts
Attn: Dr. M. Adams (1)
Dr. A. Kantrowitz (1)
Dr. J. Keck (1)
Dr. B. Kivel (1)
Peter Rose (1)
Technical Library (1)

AVCO Research Laboratories
201 Lowell Street
Wilmington, Massachusetts
Attn: Technical Library (1)
R. John (1)

Barnes Engineering Company
30 Commerce Road
Stamford, Connecticut
Attn: Dr. Eric Wormser (1)
Technical Library (1)

Bell Aircraft Corporation
P.O. Box 1
Buffalo 5, New York
Attn: Technical Library (1)

Bell Telephone Laboratories
Whippany, New Jersey
Attn: V. O. Mowery (1)
R. Sinclair (1)
Dr. Hoover (1)
Technical Reports Librarian,
Technical Information Libraries (1)

Bendix Aviation Corporation
Research Laboratory Division
Box 5115
Detroit 35, Michigan
Attn: Technical Library (1)

Bendix Systems Division
3300 Plymouth Road
Ann Arbor, Michigan
Attn: Technical Library (1)

Boeing Airplane Company
Aero-Space Division
Box 3707
Seattle 24, Washington
Attn: Dr. S. Chen (1)
Technical Library (1)
W. K. Kluse (1)
W. G. Harris (1)
Gordon Davison (1)

Defense Research Corp.
Santa Barbara, Calif.
Attn: B. Alexander (1)

Borg Warner Corporation
Des Plaines, Illinois
Attn: Technical Library (1)

Chance Vought Aircraft Corporation
Dallas, Texas
Attn: H. B. Gibbons (1)
Technical Library (1)

Convair
Division of General Dynamics
Pomona, California
Attn: Mr. J. J. Marcinek (Mail zone 6-96)
(1)

General Dynamics/Astronautics
P.O. Box 1128
San Diego 12, California
Attn: Dr. H. Dunholter (1)
Dr. A. Greene (1)

Convair Scientific Research Laboratory
Division of General Dynamics
5001 Kearney Villa Road
San Diego 11, California
Attn: Technical Library (1)

Convair
Fort Worth Division
Fort Work 1, Texas
Attn: Technical Library (1)

Convair General
Division of General Dynamics
3303 Pacific Highway
San Diego 12, California
Attn: F. Stephenson (1)
Technical Library (1)

Chicago Midway Laboratories
6220 S. Drexel Avenue
Chicago, Illinois
Attn: Mr. L. M. Biberman (1)

Douglas Aircraft Company, Inc.
3000 Ocean Park Boulevard
Santa Monica, California
Attn: Chief Missiles Engineer (1)
Technical Library (1)

Douglas Aircraft Company, Inc.
827 Lapham Street
El Segundo, California
Attn: Technical Library (1)

E. I. DuPont de Nemours & Company, Inc.
Research & Development Division
Wilmington 98, Delaware
Attn: Technical Library (1)

Electro-Optical Systems, Inc.
170 N. Daisy Avenue
Pasadena, California
Attn: Dr. A. Zarem (1)
Technical Library (1)
Dr. R. Buhler (1)

Experiment, Inc.
Richmond 2, Virginia
Attn: Technical Library (1)

Flight Sciences Laboratory, Inc.
1965 Sheridan Drive
Buffalo 23, New York
Attn: Dr. J. Isenberg (1)
Technical Library (1)

General Applied Science Laboratories
Meadowbrook National Bank Building
60 Hempstead Avenue
Attn: Technical Library (1)

General Motors Corp.
Defense Systems Division
Box T
Santa Barbara, Calif.
Attn: Henry M. Musal, Jr.,
Staff Scientist (1)
Technical Library (1)
C. F. Hansen (1)
Allen Charters (1)

General Applied Sciences Laboratories, Inc.
Merrick & Stewart Roads
Hempstead, N. Y.
Attn: Technical Library (1)

General Atomic
Division of General Dynamics Corporation
P.O. Box 608
San Diego 12, California
Attn: Technical Library (1)

Geophysics Corporation of America
Burlington Road
Bedford, Massachusetts
Attn: Dr. M. Zellikof, Dir. of Res. (1)
Technical Library (1)
Dr. J. I. F. King (1)

Giannini Plasmadyne Corporation
18400 South Main Street
Santa Ana, California
Attn: Technical Library (1)

Gruman Aircraft Engineering Corporation
Bethpage, Long Island, New York
Attn: Technical Library (1)

Gruman Aircraft Engineering Corporation
69-21 266 Street
Floral Park, Long Island, New York
Attn: Dr. Theodore Baurer,
Research Scientist (1)

Hughes Aircraft Company
Research & Development Laboratory
Culver City, California
Attn: Technical Library (1)

Linde Company
Speedway Laboratories
1500 Polco Street
Indianapolis 24, Indiana
Attn: Technical Library (1)

Litton Industries
336 N. Foothill Road
Beverly Hills, California
Attn: Technical Library (1)

Lockheed Aircraft Corporation
Missile & Space Division
Palo Alto, California
Attn: Dr. D. Bershader (1)
Dr. D. Tellep (1)
Dr. W. Griffith (1)
Dr. R. Meyerott, 53-22 Dept. (1)
Technical Library (1)

Lockheed Aircraft Corporation
Missile & Space Division
Box 504
Sunnyvale, California
Attn: Director of Research (1)
Technical Library (1)

Lockheed Aircraft Corporation
P.O. Box 551
Burbank, California
Attn: Technical Library (1)

MacDonald Engineering Company
22 West Madison Street
Chicago 1, Illinois
Attn: Technical Library (1)

McDonnell Aircraft Corporation
Lambert-Saint Louis Airport
Box 516
St. Louis, Missouri
Attn: Technical Library (1)

Marquardt Aircraft Corporation
16555 Saticoy Street
Van Nuys, California
Attn: Technical Library (1)

The Glenn L. Martin Company
Baltimore 3, Maryland
Attn: Dr. M. Morkovin (1)
Technical Library (1)

The Glenn L. Martin Company
Box 179
Denver, Colorado
Attn: Technical Library (1)

The Glenn L. Martin Company
Orlando, Florida
Attn: E. Noey (1)
G. Sprague (1)

National Carbon Research Laboratory
Box 6116
Celeveland 1, Ohio
Attn: Dr. Breckenridge (1)
Technical Library (1)

National Research Corporation
70 Memorial Drive
Cambridge 42, Massachusetts
Attn: Technical Library (1)

North American Aviation, Inc.
12214 Lakewood Boulevard
Downey, California
Attn: Dr. E. van Driest (1)
Technical Library (1)

Northrop Aircraft Company
Box 1525
9756 Wilshire Boulevard
Beverly Hills, California
Attn: Technical Library (1)

Northrop Aircraft, Inc.
Hawthorne, California
Attn: Technical Library (1)

Radio Corporation of America
Moorestown, New Jersey
Attn: Mr. A. Gold (1)
Technical Library (1)

Ramo-Wooldridge Inc.
R W Division
8433 Fallbrook Ave.
Canoga Park, Calif.
Attn: Technical Library (2)

Rand Corporation
1700 Main Street
Santa Monica, California
Attn: Dr. C. Gazley, Jr. (1)
Dr. D. Masson (1)
Mr. S. Passman (1)
Technical Library (1)

Reaction Motors Division
Thiokol Chemical Corporation
Denville, New Jersey
Attn: Technical Library (1)

Republic Aviation Corporation
Missile Systems Division
223 Jericho Turnpike
Mineola, Long Island
Attn: Technical Library (1)

Republic Aviation Corporation
Plasma Propulsion Laboratory
Farmingdale, Long Island, New York
Attn: Dr. Philip M. Mostov, Bldg. 55 (1)

Rocketdyne, Inc.
6633 Canoga Avenue
Canoga Park, California
Attn: Technical Library (1)

Sandia Corporation
Sandia Base, Box 5800
Albuquerque, New Mexico
Attn: Technical Library (1)

Stanford Research Institute
Department of Chemistry
Menlo Park, California
Attn: Dr. D. E. Van Sickle,
Organic Chemistry Section (1)

Stanford Research Institute
Menlo Park, California
Attn: Dr. Myles Berg (1)
Technical Library (1)

Thompson Ramo-Wooldridge Corporation
7209 Platt Avenue
Cleveland 4, Ohio
Attn: S. H. Fairweather (1)

Thompson Ramo-Wooldridge Corporation
Los Angeles 45, California
Attn: Technical Library (1)

Thompson Products, Inc.
23555 Euclid Avenue
Cleveland 17, Ohio
Attn: Technical Library (1)

Unified Science Associates
826 S. Arroyo Parkway
Pasadena, California
Attn: Dr. S. Naiditch, President (1)

Union Carbide Corporation
30 East Forty-Second Street
New York, New York
Attn: H. Babcock (1)
Technical Library (1)

United Aircraft Corporation
Research Department
362 Main Street
East Hartford 8, Connecticut
Attn: Technical Library (1)

Vidya, Inc.
2626 Hanover Street
Stanford Industrial Park
Palo Alto, California
Attn: Technical Library (1)

Vitro Corporation
261 Madison Avenue
New York, New York
Attn: Technical Library (1)

Vitro Laboratories
East Orange, New Jersey
Attn: Technical Library (1)

DISTRIBUTION LIST FOR TIS R62SD84 (Cont'd)

Westinghouse Electric Corporation
306 4th Avenue
Pittsburgh, Pennsylvania
Attn: Technical Library (1)

Young & Rubicam, Inc.
285 Madison Avenue
New York, New York (17)
Attn: Gerald A. Siesfield (1)

INTERNAL*

Aircraft Nuclear Propulsion Department
Box 132
Cincinnati 15, Ohio
Attn: Dr. G. Newton
Technical Library (1)

Defense Systems Department
Defense Evaluation Operation
425 Thirteenth Street, N. W.
Washington 4, D. C.
Attn: H. S. Hansell

Defense Systems Department
Technical Military Planning Operation
735 State Street
Santa Barbara, California
Attn: Dr. R. Henrick, Jr.
Dr. A. Knaas
Dr. B. Levine
Dr. R. Raymond
J. F. Sears
D. P. Wilkinson
Technical Library (4)

Flight Propulsion Laboratory Department
Cincinnati 15, Ohio
Attn: Dr. S. Suciu
Dr. M. Ghai
Dr. W. Cornell
Dr. Nietzel
Technical Library (1)

Gas Turbine Division
Cincinnati 15, Ohio
Attn: Technical Library (1)

*With the exceptionof underlined names, all G. E. Department addresses will receive TIS page only.

General Engineering Laboratory
1 River Road
Schenectady 5, New York
Attn: Dr. G. Dunlap
Dr. R. Fehr
Dr. H. Holloman
Dr. R. Norris
Dr. H. Poritsky
L. L. Stahl
Dr. B. Sternlight
Dr. D. Wilcock
Technical Library (1)
Dr. J. K. Wolfe, Bldg. 36, Room 520

Hanford Laboratories Operation
Hanford Atomic Products
Richland, Washington
Attn: H. M. Parker
L. P. Bupp
P. F. Gast
Technical Library (1)

Heavy Military Electronics Department
Industrial Park
Syracuse, New York
Attn: E. F. Herzog
R. M. Gilmore
R. C. Jensen
C. R. Wayne
T. I. Paganelli
B. P. Brown, Jr.
Technical Library (1)

Industrial Electronics Division
Communications Products Department
Mountain View Road
Lynchburg, Virginia
Attn: R. P. Gifford

Light Military Electronics Department
French Road
Utica, New York
Attn: Technical Library (1)

Light Military Electronics Department
Advanced Electronics Center
Cornell University
Ithaca, New York
Attn: H. F. Mayer
I. R. Howland
H. L. Heydt
Technical Library (1)

Electronics Park Library
Building 3, Room 143
Syracuse, New York
Attn: Miss C. Lukens, Librarian (3 TIS pages)

Microwave Laboratory
Stanford University
601 South California Avenue
Palo Alto, California
Attn: Dr. A. Ryan
Dr. W. Edson

Missile & Spave Div.
3198 Chestnut Street
Philadelphia 4, Pennsylvania
Attn: M. Fthenakis, Room 6074A
Robert Wallace 3124
G. Persh 5211
O. Klima 5101
Dr. J. Stewart 5501A
T. Shaw 5120A

Missile & Space Div.
Space Sciences Laboratory
P.O. Box 8555
Philadelphia, Pennsylvania
Attn: T. K. Pugmire, Room 1322M (30)
Dr. K. L. Coulson 9503L (1)
Dr. M. Dank 9511M (1)
Dr. Joseph Farber 9539M (1)
Mr. A. Harrison 1240U (2)*
Dr. H. G. Lew 9551L (1)
Dr. F. A. Lucy 9169A-M (1)
Mr. C. Mannal 9537M (1)
Mr. L. R. McCreight 9531M (1)
Dr. T. R. Riethof 9503L (1)
Dr. S. M. Scala 7023A-M (1)
Dr. Leo Steg 9551M (1)

*Plus reproducible tissue master copy

Dr. G. W. Sutton	9161L	(1)
Dr. V. G. Szebehely	9545M	(1)
Dr. W. R. Warren	1338M	(1)
Dr. H. E. Weber	1326M	(1)
Document Library	1343L	(1)
H. Bousman	1308M	(1)
B. B. Cary	1316M	(1)
N. S. Diaconis	1332M	(1)
D. G. Flom	9157M	(1)
J. S. Gruszczynski	1334M	(1)
R. S. Harner	1308M	(1)
C. J. Harris	1334M	(1)
W. G. King	Bldg. 5	(1)
M. J. Linevsky	9539L	(1)
D. A. Rogers	1308M	(1)
H. Sadjian	1308M	(1)
R. A. Sheridan	1326M	(1)
M. Solomon	9110M	(1)
S. Visvanathan	1310M	(1)
H. Y. Wachman	1316M	(1)

Ordnance Department
100 Plastics Avenue
Pittsfield, Massachusetts
Attn: R. C. Berendsen
Technical Library (1)

Power Tube Department
1 River Road
Schenectady 5, New York
Attn: C. M. Young
Technical Library (1)

Missile & Space Div.
Valley Forge Space Technology Center
Philadelphia 1, Pennsylvania

Attn: Dr. S. R. Hurst	3140M	
P. Thome	7211M	
R. Reid	7217M	
D. Mullen	3128M	
Dr. P. J. Friel	3217M	
Dr. W. Raithel	3230M	
H. Wittner	3020M	

Missile & Space Div.
Valley Forge Space Technology Center
Cabot, Cabot and Forbes
Philadelphia 1, Pennsylvania
Attn: L. B. Cowles Bldg. 5, Room 5004
R. J. Kirby Bldg. 6, Room 6305

Research Laboratory
P.O. Box 1088
Schenectady, New York
Attn: Chemistry Research Department:
Dr. A. Marshall
Dr. H. Liebhafsky
A. J. Nerad
Dr. R. Alpher
Dr. R. Johnson
Dr. H. Nagamatsu
Dr. D. White
Dr. C. Muckenfuss
Dr. W. Hooker

Attn: Electron Physics Department
Dr. J. Lawson
Dr. H. Hurwitz, Jr.
Dr. V. Stout
Dr. P. Pashler
Dr. R. Shuey

Attn: General Physics Research Department
Dr. M. Hebb
Dr. J. Lafferty

Attn: Metallurgy & Ceramics Research Department
Dr. D. Turnbull
Dr. R. Schmitt
Dr. R. Fullman

Attn: Technical Library (2)

DISTRIBUTION FOR TIS R62SD84 (Cont'd)

Technical Data Center
One River Road
Building 5-120
Schenectady, New York (2)*

Technical Products Operation
Electronics Park
Syracuse, New York
Attn: H. G. Towlson

Mr. Fred Baum
G.E. Field Representative
333 West First Street
Dayton 2, Ohio

*Plus 6 copies of TIS page

GENERAL ELECTRIC

SPACE SCIENCES LABORATORY
MISSILE AND SPACE DIVISION

TECHNICAL INFORMATION SERIES

AUTHOR	SUBJECT CLASSIFICATION	NO.
T. K. Pugmire	Planetary Entry Research	R62SD84
		DATE: October 1962
TITLE: Experimental Planetary Entry Research for Mars and Venus - 1962		G. E. CLASS: I
		GOV. CLASS: None
REPRODUCIBLE COPY FILED AT MSD LIBRARY, DOCUMENTS LIBRARY UNIT, VALLEY FORGE SPACE TECHNOLOGY CENTER, KING OF PRUSSIA, PA.		NO. PAGES: 204

SUMMARY

1. Prediction of stagnation point heat transfer for Mars and Venus ballistic entry based on high enthalpy shock tube studies.
2. The development of an experimental facility, 6 inch arc driven helium shock tube, capable of simulating planetary entry velocities up to 45,000 ft/sec.
3. The performance of several "class" ablation materials relative to air in simulated atmospheres of Mars and Venus at gas enthalpies proportional to entry velocities of 22,000 to 28,000 ft/sec.
4. The relative efficiency of nitrogen atoms and molecules in producing dissociation as determined by studies of combustion generated shock structures.
5. Development of a versatile equilibrium thermochemistry computer program for planetary atmospheres.
6. Assessment of effect of Venus ionosphere on communication attenuation.
7. Recommended future experimental studies.

By cutting out this rectangle and folding on the center line, the above information can be fitted into a standard card file.

AUTHOR T K Pugmire

COUNTERSIGNED C Donnal